

# **Process-based characterisation of flow and transport in karst aquifers at catchment scale**

Dissertation  
zur Erlangung des Doktorgrades  
der Mathematisch-Naturwissenschaftlichen Fakultäten  
der Georg-August-Universität zu Göttingen

vorgelegt von

**Tobias Geyer**

aus Zeulenroda

Göttingen 2008

D 7

Referent: Prof. Dr. Martin Sauter (Georg-August-Universität Göttingen)

Korreferent: Prof. Dr. Rudolf Liedl (Technische Universität Dresden)

Tag der mündlichen Prüfung: 5. Mai 2008

# Abstract

The main objective of the present dissertation is the development of methods for quantification of flow and transport processes in karst aquifers. It deals with both detailed parameter studies and the evaluation of collected field data using mathematical models.

Due to the presence of large-scale heterogeneities (karst conduits) in the hydraulic parameter field of karst aquifers, regulation and sustainable management of karst water resources require specific methods to characterise these systems on catchment scale. Evaluation of spring responses provides an appropriate method to obtain integral hydraulic and geometric parameters of karst aquifers but is associated with some uncertainties because of the unknown temporal distribution of recharge in these systems.

This work provides a time-continuous numerical approach for the estimation of inflow into the conduit system of karst aquifers. It is demonstrated that this function can be used to determine the temporal distribution of direct recharge into the conduit system. The presented approach employs the first time derivative of a spring hydrograph together with the recession coefficient of the conduit system. The first time derivative of a karst spring hydrograph reflects the temporal change of inflow to and outflow from the conduit system. The recession coefficient controls the velocity of transmission of a hydraulic signal. The methodology has been applied to quantify direct recharge into the conduit system of the Gallusquelle catchment (Swabian Alb, Germany) after a rainstorm event. The result is in agreement with information obtained from an independent isotope study reported in literature. In a further example, the introduced approach has been applied to a recharge event initiated by snowmelt. A clearly diurnal cycle of inflow into the conduit system was calculated and is attributed to a diurnal cycle of the melting process resulting from variations of air temperature (day/night). The recession coefficient of the conduit system was obtained by spring hydrograph analysis. It corresponds to the reciprocal of the mean tracer travel time determined from an artificial tracer test covering the extent of the catchment. The calculated inflow into the conduit system and interpretation of temporal distribution of recharge are therefore based on a plausible and measurable parameter.

The second part of this study deals with the quantification of reactive transport of artificial tracers and the determination of geometrical conduit parameters from multitracer tests. Therefore a large-scale multitracer test was performed and a strategy for calibration of reactive transport parameters developed applying the two-region nonequilibrium model CXTFIT2.1. The ambiguity of the reactive model was reduced by the introduction of specific ranges in which reactive calibration parameters have to fit in. The model succeeds in calibrating conservative (with uranine) and reactive transport parameters (with sulforhodamine G), and verifies that tracer/rock interactions preferably occur in the immobile fluid region of the conduit system that comprises, however, only a small part of the total conduit volume. Artificial multitracer tests are therefore a useful tool in characterising fast transport in karst aquifers and may play an important role for the characterisation of conduit surfaces in the future.

Additionally, environmental tracers provide valuable information on slow transport processes through the fissured matrix of karst aquifers. The analyses of data from spring Gallusquelle has shown that simulated mean ages for the following tracers differ in the order:  $^3\text{H} \gg ^{85}\text{Kr} = \text{SF}_6 > ^3\text{H}/^3\text{He}$ . The result indicates a slow percolation of water through the thick unsaturated zone. The interpretation is supported by distributive parameter modelling (FEFLOW5.3) of flow and transport in a fissured matrix block that comprises a thick unsaturated zone. The simulations show that the unsaturated zone of karst aquifers may provide an important water storage and indicate the existence of quasi-stagnant zones in the saturated porous matrix of karst aquifers. The presence of such zones in the Gallusquelle karst aquifer was verified by a large amount of radiogenic  $^4\text{He}$  in water samples from wells within the catchment area. However, the unambiguous interpretation of isotopic data requires further research, for example, to quantify the influence of diffusive transfer between the fissures and the porous matrix for the specific tracers.





# Zusammenfassung

Ziel der vorliegenden Dissertation ist die Entwicklung von Methoden zur Quantifizierung von Strömungs- und Transportprozessen in Karstgrundwasserleitern. Die Arbeit beschäftigt sich sowohl mit Parameterstudien wie auch mit der Auswertung von erhobenen Geländedaten anhand mathematischer Modelle.

Aufgrund großskaliger Heterogenitäten (Karströhren) im hydraulischen Parameterfeld von Karstgrundwasserleitern stellt die Nutzung und nachhaltige Bewirtschaftung von Karstwasserressourcen eine große Herausforderung dar und erfordert spezielle Methoden zur Charakterisierung dieser Systeme auf der Einzugsgebietsskala. Einen vielsprechenden Ansatz hierfür liefert die Auswertung von Quellsignalen, wie z.B. einer Abflussganglinie. Dieser Ansatz beinhaltet allerdings, wegen fehlender Informationen über die zeitliche Verteilung der Grundwasserneubildung, große Unsicherheiten.

Die vorliegende Arbeit präsentiert einen numerischen Ansatz zur zeitkontinuierlichen Berechnung des Zuflusses in das Röhrensystem eines Karstgrundwasserleiters. Es wird gezeigt, dass hieraus auf den zeitlichen Verlauf der direkten Grundwasserneubildung in einem Karströhrensystem geschlossen werden kann. Den Kern des Ansatzes bilden die erste Zeitableitung der Abflussganglinie einer Karstquelle und der Leerlaufkoeffizient des Röhrensystems. Die erste Zeitableitung der Abflussganglinie beschreibt das Verhältnis von Zuflüssen in das und Abflüssen aus dem Röhrensystem. Der Leerlaufkoeffizient des Röhrensystems kontrolliert die Geschwindigkeit der Übertragung eines hydraulischen Signals durch das System. Die entwickelte Methode wurde zur Berechnung der direkten Grundwasserneubildung in dem Einzugsgebiet der Gallusquelle (Schwäbische Alb) nach einem Starkregenereignis eingesetzt. Das Ergebnis der Auswertung wird durch eine in der Literatur dokumentierte Isotopenstudie bestätigt. In einem zweiten Beispiel wurde der Ansatz zur Berechnung der direkten Grundwasserneubildung nach einem Schneeschmelzereignis verwendet. Die berechnete Zuflusskurve weist einen deutlichen Tagesgang auf, welcher auf einen täglichen Zyklus des Abschmelzprozesses durch Variationen der Lufttemperatur (Tag/Nacht) schließen lässt. Der Leerlaufkoeffizient des Röhrensystems wurde aus dem Leerlaufvorgang an der Karstquelle ermittelt. Das Ergebnis stimmt mit dem Reziproken der mittleren Transportzeit im Röhrensystem überein. Die mittlere Transportzeit konnte aus einem künstlichen Tracerversuch bestimmt werden, welcher die gesamte Ausdehnung des Einzugsgebietes der Gallusquelle berücksichtigt. Die berechnete Zuflussfunktion und die Interpretation der direkten Grundwasserneubildung basieren somit auf einem plausiblen und messbaren Parameter.

Der zweite Teil der Arbeit beschäftigt sich mit der Quantifizierung des reaktiven Transportes von künstlichen Tracern (Markierungsstoffen) und der Bestimmung geometrischer Parameter von Karströhrensystemen anhand von Multitracerversuchen. Hierzu wurde ein großskaliger Multitracerversuch durchgeführt und eine Strategie zur Kalibrierung reaktiver Transportparameter unter Verwendung des Nichtgleichgewichtsmodells CXTFIT2.1 entwickelt. Die Mehrdeutigkeit des Modells konnte durch die Einführung von Grenzwerten für die reaktiven Transportparameter verringert werden. Die Modellstrategie konnte erfolgreich zur Kalibrierung von konservativen (anhand von Uranin) und reaktiven Stofftransportparametern (anhand von Sulforhodamin G) verwendet werden und zeigte, dass Reaktionen zwischen der Röhrenoberfläche und Tracern insbesondere in immobilen Zonen auftreten, welche jedoch nur einen geringen Teil des Gesamtröhrenvolumens ausmachen. Künstliche Multitracerversuche stellen somit eine geeignete Methode zur Charakterisierung des schnellen Transportes in Karstgrundwasserleitern dar und könnten in Zukunft eine wichtige Rolle bei der Charakterisierung von Röhrenoberflächen spielen.

Weiterhin können Umwelttracer wertvolle Informationen über den langsamen Transport durch die geklüftete Matrix eines Karstgrundwasserleiters liefern. An der Gallusquelle wurden mittlere Transportzeiten für verschiedene Umwelttracer in der folgenden Reihenfolge ermittelt:  $^3\text{H} \gg ^{85}\text{Kr} = \text{SF}_6 > ^3\text{H}/^3\text{He}$ . Dieses Resultat kann durch die langsame Perkolations von Wasser durch die ungesättigte Zone erklärt werden. Die Interpretation wird unterstützt durch die Simulation der Strömung und des Transportes (FEFLOW5.3) durch einen geklüfteten Matrixblock, welcher eine mächtige ungesättigte Zone aufweist. Die Simulation zeigt, dass die ungesättigte Zone von Karstgrundwasserleitern einen großen Wasserspeicher darstellen kann und die gesättigte poröse Matrix quasi-stagnante Zonen beinhaltet. Die Existenz solcher Zonen konnte durch hohe Konzentrationen von radiogenem  $^4\text{He}$  in Wasserproben aus Bohrlöchern auf dem Einzugsgebiet der Gallusquelle nachgewiesen werden. Die eindeutige Interpretation der Isotopenergebnisse erfordert jedoch weitere Forschungsarbeiten, z.B. um den Einfluss der Diffusion zwischen Matrix- und Feinkluftsystem auf den Transport der verwendeten Umwelttracer zu quantifizieren.



# Danksagung

An erster Stelle möchte ich mich bei Prof. Martin Sauter bedanken. Er unterstützte meine Arbeit zu jeder Zeit und gab mir die Freiheit eigene Ideen zu entwickeln und umzusetzen. Hierfür spielten intensive Diskussionen mit ihm eine bedeutende Rolle, wobei seine langjährige Erfahrung in der Karsthydrogeologie eine wichtige Stütze darstellte.

Mein besonderer Dank gilt zudem Prof. Rudolf Liedl und Prof. Steffen Birk. Das Gelingen der vorliegenden Arbeit ist ebenfalls ein Resultat der intensiven und fruchtbaren Kooperation mit beiden in einem gemeinsamen Forschungsprojekt. Ich hoffe, dass diese Art des wissenschaftlichen Austauschs auch in Zukunft anhält und weitere Fragestellungen zusammen gelöst werden können. Das Forschungsprojekt wurde finanziert von der Deutschen Forschungsgemeinschaft (DFG).

Weiterhin möchte ich mich bei dem Zweckverband Wasserversorgung Zollernalb und insbesondere bei den Mitarbeitern des Wasserwerkes Hermentingen Peter Knaus, Thomas Wessner und Hubert Schaarschmidt bedanken. Aufgrund der technischen Unterstützung konnten großskalige Experimente erst durchgeführt werden. Zudem habe ich mich immer über die freundschaftliche Atmosphäre vor Ort gefreut. Hierbei möchte ich mich gleichzeitig auch bei Birgit Heinz und Marisa Molinari bedanken. Sie halfen zuverlässig dabei, langjährige Datenreihen zu erheben und unterstützten mich bei der Betreuung der Geländegeräte an der Gallusquelle. Birgit Heinz hatte zudem im Rahmen ihrer Diplomarbeit wertvolle Kenntnisse über den mikrobiellen Transport in Karstgrundwasserleitern gewonnen.

Dr. Tobias Licha möchte ich für die vielen anregenden Diskussionen über den Stofftransport in Karstgrundwasserleitern danken. Diskussionen mit Dr. Iulia Ghergut und Dr. Thomas Graf boten immer wieder neue Anstöße in Bezug auf die Modellierung dieser Systeme. Maria Herold und Dr. Till Heinrichs möchte ich ausdrücklich für das Korrekturlesen von Teilen der Arbeit danken.

Dr. Jürgen Sültenfuß und der Firma Hydroisotop/Schweitenkirchen gilt mein besonderer Dank für die Messung der He/Ne - Isotope bzw. von Krypton-85 und für die Unterstützung bei der Auswertung der Messwerte. Ebenso danke ich Dr. Harald Oster für die Messung der FCKWs und von SF<sub>6</sub>. Weitere wertvolle Informationen über frühere Isotopenmessungen an der Gallusquelle wurden mir vom Landesamt für Geologie, Rohstoffe und Bergbau (LGRB) Baden-Württemberg zur Verfügung gestellt. Auch hierfür meinen ausdrücklichen Dank! Beim Bundesamt für Strahlenschutz (BFS) und dem Global Network of Isotopes in Precipitation (GNIP/IAEA) möchte ich mich für die zur Verfügung gestellten Zeitreihen von Krypton-85 in der Atmosphäre und Tritium im Niederschlag bedanken.

Zudem möchte ich mich bei meinen französischen Kooperationspartnern des BRGM - EAU/RMD, Nathalie Dörfliger und Bernard Ladouche, für die Unterstützung bei der Datenerhebung bedanken. Auch wenn die erhobenen Messreihen für das Einzugsgebiet Cent Fonts/Südfrankreich noch nicht in der vorliegenden Arbeit dokumentiert sind, waren diese doch wertvoll für den Vergleich mit an der Gallusquelle gewonnenen Daten. Ich freue mich auf unsere weitere Zusammenarbeit.

Weiterer Dank gilt meiner Familie und meinen Freunden, deren Unterstützung ich mir jeder Zeit während der Dissertation sicher sein konnte, sowie Karolin für die außerordentliche Geduld und ihr großes Verständnis während der Arbeitsphase.



# Table of Contents

1	Introduction.....	1
1.1	Motivation and background.....	1
1.2	Objectives and approaches.....	2
1.3	Format of the thesis.....	4
1.4	References.....	5
2	General overview of karst hydrogeology.....	6
2.1	Conceptual model of a karst system.....	6
2.2	Modelling approaches in karst aquifers.....	10
2.3	Methods for characterisation of karst aquifers.....	12
2.3.1	Spring hydrograph analysis.....	15
2.3.2	Analysis of chemical and isotopic spring responses.....	17
2.3.3	Artificial tracer tests.....	19
2.4	References.....	20
3	Quantification of temporal distribution of recharge in karst systems from spring hydrographs.....	26
3.1	Introduction.....	28
3.2	Method.....	29
3.2.1	Analytical solution.....	30
3.2.2	Numerical solution.....	31
3.3	Parameter studies.....	32
3.4	Results from the parameter studies.....	33
3.5	Case study.....	37
3.6	Determination of the recession coefficient for the conduit system.....	38
3.7	Temporal recharge distribution from discharge events.....	39
3.8	Discussion and conclusions.....	41
3.9	Appendix A.....	43
3.10	References.....	47

4	Multitracer test approach to characterise reactive transport in karst aquifers .....	49
4.1	Introduction.....	51
4.2	Methodology .....	52
4.3	Field site .....	55
4.4	Tracer selection .....	56
4.5	Multitracer experiment.....	57
4.6	Modelling results.....	59
4.7	Sensitivity analyses .....	62
4.8	Discussion and conclusions .....	65
4.9	References .....	67
5	Analysing transport of the environmental tracers $^3\text{H}$ , $^{85}\text{Kr}$ , $\text{SF}_6$ , and He in a karst system with a thick unsaturated zone.....	69
5.1	Introduction.....	71
5.2	Methods.....	72
5.2.1	Environmental tracers applied in this study.....	72
5.2.2	Lumped parameter modelling.....	75
5.3	Field site .....	76
5.4	Environmental tracer data in precipitation, atmosphere, and groundwater .....	79
5.5	Interpretation of environmental tracers using the lumped parameter approach .....	82
5.6	Simulation of life expectancy of water in a fissured matrix block .....	85
5.7	Results of numerical flow and transport simulation .....	86
5.8	Discussion and conclusions .....	88
5.9	Appendix B .....	90
5.10	References .....	92
6	General conclusions and perspectives .....	95
6.1	References .....	101
	Appendix C .....	102

# List of Figures

- Figure 1.1: Distribution of major outcrops of carbonate rocks (COST 65 1995, in Goldscheider 2002).
- Figure 2.1: Conceptual model of a karst system with typical karst features such as sinkholes, dry valleys, and a conduit system draining groundwater from fissured matrix blocks towards a karst spring (modified from Liedl and Sauter 2000).
- Figure 2.2: Effects of spatial scale on the hydraulic conductivity (modified from Kiraly 1978).
- Figure 2.3: Conceptualisation of the epikarst (modified from Mangin 1975).
- Figure 2.4: Examples of different patterns of conduit systems in karst aquifers (top view).
- Figure 2.5: Effects of the duality of recharge, storage, and flow processes in karst aquifers (from Smart and Hobbs 1986).
- Figure 2.6: Classification scheme of distributive parameter models for karst aquifers (SCPE, "Single Continuum Porous Equivalent", DCPE "Double Continuum Porous Equivalent", HM, "Hybrid Model", DSFS "Discrete Single Fracture Set", DMFS "Discrete Multiple Fracture Set") (Teutsch and Sauter 1991).
- Figure 2.7: Relationship between investigation methods, scale of investigation, and hydraulic conductivity in a karst aquifer (Sauter 1992).
- Figure 2.8: Methods for characterisation of flow and transport within karst aquifers on local scale and catchment scale.
- Figure 2.9: Event spring hydrograph after a recharge event (Kiraly 1998, in Kovács et al. 2005).
- Figure 2.10: Two conceptual models with different hydraulic parameter fields suitable for the quantitative interpretation of karst aquifers.
- Figure 2.11: Conceptual models of tracer transport in karst aquifers; a) multi-dispersion flow; b) diffusion between fissures (or conduits) and the porous matrix (from Maloszewski et al. 1992).
- Figure 3.1: A two-reservoir model, which allows the simulation of the hydraulic behaviour of karst aquifers in principle.  $R_l$  recharge into the low permeability reservoir,  $R_h$  recharge into the highly permeable reservoir,  $Q_l$  flow from the low permeability reservoir into the highly permeable reservoir,  $Q_h$  outflow from the highly permeable reservoir (spring discharge).
- Figure 3.2: Replenishment of the highly permeable reservoir  $V_h$  and recession behaviour of the two-reservoir model. Parameter studies commence on  $t = 50$  d.
- Figure 3.3: Simulation results with recharge into the highly permeable reservoir only.
- Figure 3.4: Influence of the recession coefficient  $\alpha_h$  on the spring hydrograph  $Q_h$  and its first derivative if recharge is into the highly permeable reservoir only. The corresponding recharge function is shown in Figure 3.3.
- Figure 3.5: Simulation results with recharge into the low permeability reservoir only.
- Figure 3.6: Influence of the recession coefficient  $\alpha_h$  on the first and second derivative of the spring hydrograph  $Q_h$  if recharge is into the highly permeable reservoir only. The corresponding recharge function is shown in Figure 3.5.
- Figure 3.7: Simulation results with dual recharge function. The portion of the total recharge that is applied directly to the highly permeable reservoir amounts to 50% in a) and to 5% in b).
- Figure 3.8: a) Location of Gallusquelle catchment (delineation according to Sauter (1992)); b) Distribution of dry valleys and sinkholes as features of direct recharge.
- Figure 3.9: Estimation of first derivative of spring discharge  $Q_s$  and total inflow into the conduit system after a recharge event caused by an intensive storm event.

- Figure 3.10: Estimation of first derivative of spring discharge  $Q_s$  and total inflow into the conduit system after a recharge event initiated by a snowmelt.
- Figure 3.11: Comparison of analytical and numerical solution for the two-reservoir model.
- Figure 4.1: Conceptual model of the geometry and the flow within a karst conduit.
- Figure 4.2: General map of Gallusquelle catchment showing the tracer injection point (sinkhole) (from Birk et al. 2005).
- Figure 4.3: Tracer recovery with time.
- Figure 4.4: TBCs resulting from transport simulations based on the physical non-equilibrium model. The diamonds for observed data represent every twentieth measurement point. Residuals represent observed minus inversely fitted data. Note that for tinopal CBS-X the grey curve was fitted by manual calibration taking into account the completely recovered mass and the black curve was fitted under consideration of the recovered mass after 65 hours (see chapter modelling results).
- Figure 4.5: Sensitivity analysis of the conservative transport model. The respective calibration parameter (Table 4.2) was varied between  $-90\%$  and  $90\%$ . Please note the different scales of the ordinates. The variations of  $\nu$  and  $\theta_m$  yield the largest root mean square error (RMSE). Model results are least sensitive to changes in the mass transfer coefficient  $\alpha$ . Because  $\theta_m$  is allowed to vary only between 0 and 1 the range of positive variations of this parameter is limited.
- Figure 4.6: Diagrams illustrating the effect of parameter variation for the conservative transport parameters. The illustrated steps of variations are  $-90$ ,  $-30$ ,  $-10$ ,  $10$ ,  $30$ , and  $90\%$  of the calibrated value ( $0\%$ ) (compare with Figure 4.5). Note that diagrams for the non-equilibrium parameters are plotted logarithmically on the ordinate to clarify the importance of the parameters with respect to the tail of the TBC.
- Figure 4.7: Sensitivity analysis of the reactive transport model for sulforhodamine G and tinopal CBS-X. Because  $\beta$  is allowed to vary only between 0 and 1 the range of positive variations of this parameter is limited. Please note the different scales of the ordinates. The grey boxes in diagrams b and d indicate the possible range of  $\beta$  to accomplish the requirement for physically reasonable values of  $f$  (eq. 4.6).
- Figure 4.8: Diagrams that illustrate the effect of parameter variations by sensitivity analysis to the reactive TBCs. The steps of variations are  $-90$ ,  $-30$ ,  $-10$ ,  $10$ ,  $30$ , and  $90\%$  of the calibrated value ( $0\%$ ) (compare with Figure 4.7). Note that diagrams for  $\beta$  are plotted logarithmically on the ordinate to clarify the importance of the parameters with respect to the tail of the TBC.
- Figure 5.1: a) Location of the Gallusquelle catchment (delineation according to Sauter (1992)); b) Geological map and stratigraphical overview of the Upper Jurassic in the area of investigation.
- Figure 5.2: Dynamics of spring discharge, recharge, and precipitation on a) long-term scale and b) seasonal time scale.
- Figure 5.3: Input functions of environmental tracers used in this study.
- Figure 5.4: Mean residence times for a)  $^3\text{H}$ , b)  $^{85}\text{Kr}$ , and c)  $\text{SF}_6$  estimated by various lumped parameter models.
- Figure 5.5: Separation of  $^3\text{He}$  and  $^4\text{He}$  components from measured He concentrations for different locations (Table 1).
- Figure 5.6: Flow and transport simulation (2D vertical model) in a fissured matrix block with diffuse recharge and a drainage point (e.g. conduit system). a) Model geometry, model boundaries, and hydraulic parameters ( $K_{\max}$ ,  $K_{\min}$  = hydraulic conductivity (maximum, minimum),  $S_c$  = confined storage coefficient,  $\varepsilon$  = porosity,  $n$  and  $\alpha$  = Van Genuchten parameters); b) Hydraulic heads and flow velocities; c) Saturation ( $\psi$  = pressure head,  $\psi > 0$  saturated medium,  $\psi < 0$  unsaturated medium); d) Distribution of life expectancy of water in the model domain.
- Figure 5.7: Water balance model for calculation of recharge (modified from Sauter 1992).
- Figure 6.1: Concept for characterisation of karst aquifers by large-scale pumping tests.



## List of Tables

- Table 4.1: Chemical structure of the selected fluorescent dyes (modified after Behrens 1986, Field 2002).
- Table 4.2: Parameter estimates resulting from physical non-equilibrium modelling. Results of model calibration are displayed in italics, fixed model parameters are underlined. Note that for tinopal CBS-X the values in parentheses are obtained by truncation of the long flat tailing after 65 h of tracer observation.  $K_s$  and  $f$  are estimated from the modelling parameters according to eqs. 4.5 and 4.7.
- Table 5.1: Measured tracer concentrations at sampling sites in the Gallusquelle catchment area.
- Table 5.2: Characteristics of sampling sites in the Gallusquelle catchment area.
- Table 5.3: Calculated  $^3\text{H}/^3\text{He}$  ages and  $^3\text{H} + ^3\text{He}_{\text{trit}}$  in water samples at the sampling sites in the Gallusquelle catchment area.



# Chapter 1

## Introduction

### 1.1 Motivation and background

Karst aquifers develop where solution enlargement of fissures and bedding planes creates a third type of aquifer porosity, the highly permeable conduit system. The development of a conduit system introduces a large heterogeneity in the hydraulic parameter field of aquifers and leads to complex flow and transport phenomena that markedly differ from those in porous and fissured aquifers. Typical features of karst hydrogeology are, for example, fast and concentrated flow and transport through the saturated and unsaturated zone of karst systems causing rapid fluctuations in discharge of karst springs and a high vulnerability of karst aquifers to contamination.



**Figure 1.1:** Distribution of major outcrops of carbonate rocks (COST 65 1995, in Goldscheider 2002).

Generally, outcrops of soluble rocks are dominated by carbonate rocks. In Europe, for example, 35% of the ice-free land surface is covered by carbonate rocks (Figure 1.1). Thus, it is not astonishing that in some European countries 50% of drinking water is supplied by carbonate aquifers (COST 65 1995). Worldwide roughly 20-25% of the population depend largely or entirely on groundwater obtained from carbonate aquifers which show to a large extent karst groundwater

circulation (Ford and Williams 2007). The sustainable management of karst water resources and conservation of their quality is therefore essential for drinking water supply worldwide.

In general, sustainable management of groundwater resources must be based on reliable information on flow and transport processes in hydrogeological systems. It depends to a large degree on the ability to make predictions, e.g., on the impact of climatic changes to discharge of springs or on the transport of pollutants in aquifer systems. As a tool for simulation of flow and transport processes, mathematical models are frequently employed. Depending on their capability to describe spatial heterogeneities, they range from lumped parameter models to distributive parameter models. Lumped parameter models treat a hydrogeological system as an entity and are therefore useful for interpreting field data when there is only limited knowledge of the hydrogeological system investigated. Especially in strongly heterogeneous aquifers, this approach is not capable of reproducing the physics of flow and transport and therefore it carries only limited predictive power. On the other hand, distributed parameter models are capable of simulating flow and transport at different scales for various sets of parameters and boundary conditions, and so permit the replication of complex geometric settings. The major difficulty with distributed models lies in finding appropriate data to describe the hydrogeological problem completely. This is especially true for karst aquifers, where groundwater flow is focused in the highly permeable conduit system, which comprises, however, only a small percentage of the total aquifer volume. The majority of the aquifer porosity is provided by low permeability fissured matrix blocks. Consequently, most boreholes in karst aquifers are located between karst conduits and aquifer characterisation is not easily achieved by hydrogeological standard investigation techniques, such as pumping tests. In fact, characterisation of karst aquifers requires further techniques, which provide information on the geometry, hydraulic parameters and boundary conditions of the highly permeable conduit system.

## 1.2. Objectives and approaches

This thesis aims to fill the gap between model requirements for simulation of karst aquifers and field data provision to a certain extent. It deals with the identification and quantification of flow and transport processes in karst aquifers, which is necessary for the interpretation of field data and the development of methods for aquifer characterisation.

As a result of their genetic history, karst springs are connected to highly permeable conduit systems, which drain the low permeability fissured matrix blocks. Analysis of hydraulic and chemical responses of karst springs, for example the recession behaviour of spring discharge, therefore provide the possibility for an integral characterisation of karst aquifers on catchment

scale. Building on that, this work will employ variations of spring discharge after precipitation events for the quantification of the temporal distribution of recharge in karst aquifers. The temporal distribution of recharge is an important boundary condition especially for transient flow and transport models.

Artificial tracer tests are familiar characterisation techniques in karst hydrogeology, for example, to determine point to point connections and flow velocities in the karst conduit system. They may also provide information on the total conduit volume between a sinkhole and a karst spring. However, only limited information is gained about the conduit geometry. In this work, the potential of artificial tests is investigated to determine geometric conduit parameters from the tracer transport. For this purpose, a multitracer test with three simultaneously injected different reactive tracers is conducted in a well characterised karst system. The tracer breakthrough curves (TBCs) will be analysed using the two-region non-equilibrium model CXTFIT2.1 (Toride et al. 1999).

In addition to artificial tracer tests, this work deals with the evaluation of environmental tracers in order to characterise slow and diffuse flow in karst aquifers with a thick unsaturated zone. In general, mean ages obtained from various environmental tracers can substantially differ from each other depending on the tracer input function and the transport behaviour of a specific tracer. Simultaneous measurement of various tracers is therefore recommended in order to enhance the information gained. In this work the following environmental tracers were collected: tritium, helium-3, helium-4, neon, krypton-85, and sulfurhexafluoride. The evaluation of the tracers is based on lumped parameter modelling. A distributive modelling study (FEFLOW5.3, Diersch 2006) is performed to identify important flow and transport processes in the saturated and unsaturated zone of karst systems, and to verify conclusions made from the interpretation of environmental tracers applying lumped parameter models.

All data were collected in the groundwater catchment of the Gallusquelle spring (Swabian Alb). The catchment is geologically and hydrogeologically well studied including borehole investigations, piezometric surface mapping and ground water tracing. A detailed review is provided by Sauter (1992). Additionally the author presented approaches to characterise of hydraulic properties of the karst aquifer Gallusquelle on local scale (borehole tests) and catchment scale (spring recession analysis). Details of this previous work are presented in this work in the chapters dealing with current research activities.

In addition to the topics above, further co-authored research contributions in peer-reviewed scientific journals exist (Appendix C), which consider (1) the evaluation of artificial tracer tests in karst aquifers using lumped parameter and distributive parameter models (Birk et al. 2005) and (2) the vulnerability of karst aquifers to pollutants. At this, Heinz et al. (2006) investigated the

consequences of overflows at a storm-water tank spillway basin to the raw water quality in a karst aquifer by the analysis of chemical and microbiological parameters at a karst spring. Brosig et al. (2007) studied the distribution of travel times in the catchment area of a karst spring in Jordan applying GIS (Geographical Information System) for the determination of zones with a high vulnerability.

### 1.3 Format of the thesis

An introduction to karst hydrogeology will be presented in Chapter 2. It comprises a conceptual model of a karst system as well as modelling approaches for simulation of flow and transport in these systems. Next, a short review of field methods for parameterisation and/or calibration of mathematical models is given. The main research work is presented in chapters 3, 4, and 5, which are written as manuscripts for presentation in scientific journals.

Chapter 3 provides a method for quantification of temporal distribution of recharge in karst systems from spring hydrographs. Additionally, the chapter delivers a link between hydraulic spring responses and conduit volumes calculated from the evaluation of artificial tracer tests. *The research work, i.e. the relationship between temporal distribution of recharge and a spring hydrograph, is based on the numerical solution of a two-reservoir model. The respective numerical solutions (eqs. 3.5 - 3.10) together with parameter studies, case studies, determination of the recession coefficients, and discussion of the results was provided by myself. The numerical solution of the two-reservoir model was verified by the analytical solution for a specific recharge event. This analytical solution is presented in the appendix of chapter 3 and was provided by Prof. Dr. Rudolf Liedl.*

Chapter 4 presents a multitracer approach to characterise reactive transport in karst aquifers and to estimate geometric conduit parameters.

Chapter 5 deals with the slow transport in the karst aquifer Gallusquelle (Swabian Alb) using the evaluation of environmental tracers and numerical modelling.

Chapter 6 summarises the conclusions with respect to the objectives of this thesis and provides suggestions for further research.

Appendix C includes a list of all publications authored or co-authored by me and directly related to the presented work.

*Please note that as a result of the cumulative nature of this thesis a reference list is provided at the end of every chapter.*

## 1.4 References

- Birk, S., Geyer, T., Liedl, R., Sauter, M., 2005. Process-based interpretation of tracer tests in carbonate aquifers. *Ground Water* 43 (3), 381-388.
- Brosig, K., Geyer, T., Subah, A., Sauter, M., 2007. Travel time based approach for the assessment of vulnerability of karst groundwater: the transit time method. *Environmental Geology* 54 (5), 905-911.
- COST 65, 1995. Hydrogeological aspects of groundwater protection in karstic areas, Final report (COST action 65). European Commission, Directorate-General XII Science, Research and Development, Report EUR 16547 EN, 446 pp.
- Diersch, H.-J., G., 2006. FEFLOW5.3 - Finite element subsurface flow and transport simulation - User's manual. WASY GmbH, 200 pp.
- Ford, D., Williams, P., 2007. *Karst hydrogeology and Geomorphology*. John Wiley & Sons Ltd., West Sussex, 562 pp.
- Goldscheider, N., 2002. Hydrogeology and vulnerability of karst systems: examples from the Northern Alps and Swabian Alb. Ph.D thesis, Universität Karlsruhe, 236 pp.
- Heinz, B., Birk, S., Liedl, R., Geyer, T., Straub, K.L., Bester, K., Kappler, A., 2006. Vulnerability of a karst spring to wastewater infiltration (Gallusquelle, Southwest Germany). *Austrian Journal of Earth Sciences* 99, 11-17.
- Sauter, M., 1992. Quantification and forecasting of regional groundwater flow and transport in a karst aquifer (Gallusquelle, Malm, SW. Germany). *Tübinger Geowissenschaftliche Arbeiten*, C13, 150 pp.
- Toride, N., Leij, F.J., van Genuchten, M.T., 1999. The CXTFIT code (version 2.1) for estimating transport parameters from laboratory or field tracer experiments. U.S. Salinity Laboratory Agricultural Research Service, U.S. Department of Agriculture Riverside, California. Research Report, 137, 119 pp.

## Chapter 2

# General overview of karst hydrogeology

### 2.1 Conceptual model of a karst system

According to Ford and Williams (2007), the term karst refers to a terrain with distinctive hydrology and landforms that arise from a combination of particularly soluble rocks, and a well developed effective porosity. With a view to hydrogeology, a karst system may be described as a set of interacting components, which show to a certain extent karst features and form an integrated hydrogeological system (Figure 2.1). Karst features mainly occur in carbonate rocks but also evaporite formations (gypsum and anhydrite), and sometimes quartzite, when special chemical conditions prevail, are subject to karst phenomena (Bakalowitz 2005). Here, only karst hydrology in carbonate aquifers will be considered.

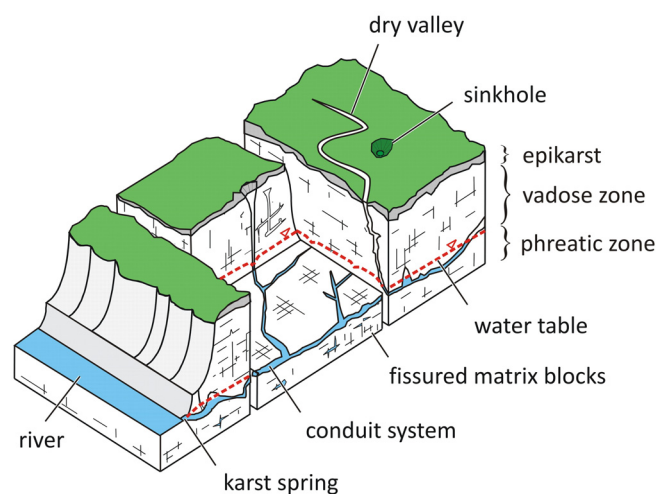


**Figure 2.1: Conceptual model of a karst system with typical karst features such as sinkholes, dry valleys, and a conduit system draining groundwater from fissured matrix blocks towards a karst spring (modified from Liedl et al. 2003).**

The development of highly conductive flow paths by solution enlargement of fissures is what sets karst aquifers apart from other aquifer systems, i.e. karst aquifers are characterised by a triple porosity that includes intergranular pores (matrix porosity), fissures and bedding partings (fissure porosity), and solution enlarged voids (conduit porosity). On the one hand, the development of the conduit porosity depends on the chemical composition of the rock and of water. On the other hand, the relative karstification of, for example, various fissure sets, is governed by the direction



and rate of groundwater flow. This relationship leads to a positive feedback loop of the karstification process due to the following: (1) the groundwater flow rate depends on the hydraulic conductivity and the hydraulic gradient, (2) the hydraulic conductivity depends on the opening of voids, and (3) the opening depends on the direction and magnitude of the groundwater flow rate. Thus, solution enlargement is enhanced in fissures which are sub-parallel to the local hydraulic gradient. The competition for drainage between highly conductive zones leads to the capture of slower developing branches and contributes to the unification of a karst conduit system (Király 2002). Consequently, the structure of a karst aquifer results not only from the geological history of the rock but also from the evolution of the flow system. Karst aquifers can therefore be considered as partly self-regulated systems (Király 1975).

The development of karst conduit systems introduces an extreme heterogeneity with a strong anisotropic character in the hydraulic parameter field of karst aquifers. This leads to scaling issues, which have to be considered when characterising karst aquifers. Király (1978) demonstrated that the hydraulic conductivity of carbonate aquifers changes with the considered aquifer volume by several orders of magnitude (Figure 2.2).

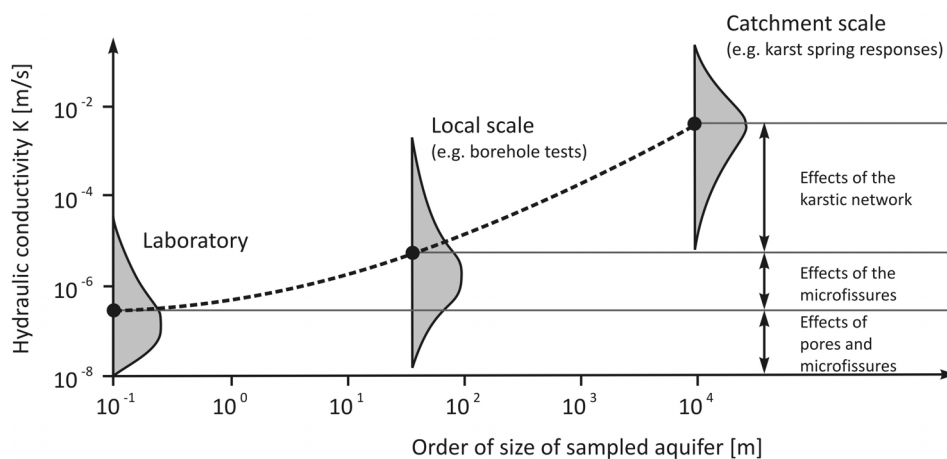


**Figure 2.2: Effects of spatial scale on the hydraulic conductivity (modified from Király 1978).**

On laboratory scale, the hydraulic conductivity is extremely low and dominated by the properties of the porous matrix. However, at larger scales the hydraulic conductivity increases. This is plausible because of the added effect of higher permeability features, i.e. interconnected fissures on the local scale and the conduit system on the catchment scale. Over large volumes (catchment scale) the spatial distribution of the matrix porosity and the fissure porosity may be statistically interpreted as isotropic and flow in fissured matrix blocks can be described similar to a porous medium, i.e. a representative elementary volume (REV, the smallest volume over which averaged material parameters are representative for the whole, Bear 1972) can be defined. However, because of the presence of a conduit system, it may not be possible to obtain one REV for an

entire karst aquifer. Flow in well developed karst aquifers can therefore be considered to be (1) slow and diffuse through low permeability fissured matrix blocks and (2) rapid and concentrated through highly conductive flow paths (Atkinson 1977, Shuster and White 1971, White 1969).

In general, karst systems can be vertically classified in three zones: the epikarst, the vadose (unsaturated) zone, and the phreatic (saturated) zone (Figure 2.1). The epikarst is the upper weathered layer of a carbonate platform with significant fracturing and solution enlargement (Mangin 1975). Because of its high permeability in comparison to the underlying rock, the epikarst may produce localised saturated zones (perched aquifer) and acts therefore as a temporal storage element. It distributes water as either a concentrated or a diffuse recharge component towards the vadose zone (Figure 2.3) (Aquilina et al. 2006, Dörfliger et al. 1999, Field 1993, Kiraly 2002, Klimchouk 2004, Perrin et al. 2003, Sauter 1992, Williams 1983).

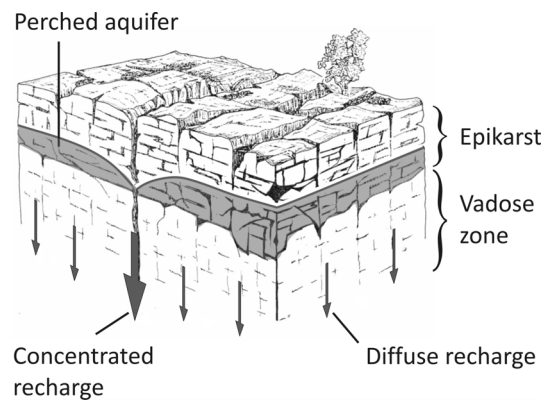


**Figure 2.3: Conceptualisation of the epikarst (modified from Mangin 1975).**

Within the vadose zone water is transmitted vertically from the epikarst to the phreatic zone either concentrated and rapidly, e.g. via vertical shafts, or diffuse and slowly through fissured matrix blocks. The thickness of the vadose zone in karst systems may be several hundreds of meters resulting from the lowering of the outflow boundary (e.g. a karst spring) by valley deepening and the development of underground drainage systems (conduit systems).

Groundwater flow in the phreatic zone is concentrated in highly conductive conduits. Turbulent flow arises in those openings that have been sufficiently enlarged by solution. Depending on the distribution of the hydraulic heads, the conduits exchange water with the surrounding rock. During low flow conditions, heads in fissured matrix blocks are higher than in conduits, and the conduits drain groundwater from fissured matrix blocks towards some point of discharge, i.e. a karst spring. However, following precipitation events, the hydraulic gradient between conduits and fissured matrix blocks may reverse, particularly where conduits are directly recharged, and conduits may feed fissured matrix blocks (Drogue 1992, Grasso and Jeannin 2002). Conduit systems in well developed karst aquifers extend over large distances and may show different

network patterns (or a combination of patterns) depending on their development history (Palmer 1991, Ford 1999) (Figure 2.4). However, the majority of groundwater storage in karst aquifers is usually provided by low permeability fissured matrix blocks. Flow within fissured matrix blocks occurs along highly interconnected bedding planes, joints, and fissures. The porous matrix is often considered to be a quasi-stagnant reservoir referring to its extreme low hydraulic conductivity (e.g. Maloszewski et al. 2002). While porous storage is of limited significance to the flow signal of karst aquifers, it may have an important role for the transport of solutes, e.g. diffusion between fissures and the porous matrix (Foster 1975).

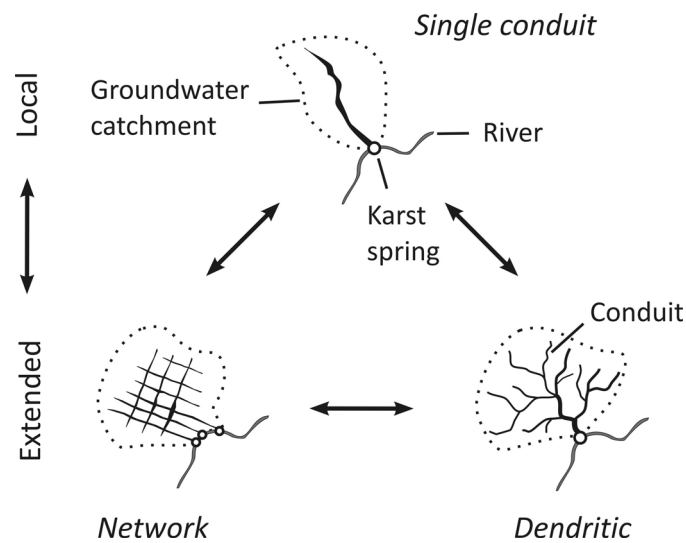


Figure 2.4: Examples of different patterns of conduit systems in karst aquifers (top view).

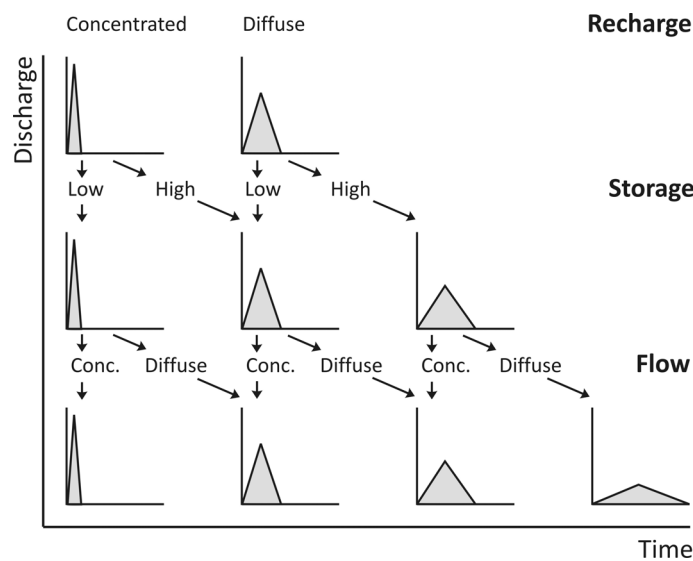


Figure 2.5: Effects of the duality of recharge, storage, and flow processes in karst aquifers (from Smart and Hobbs 1986).

The complex structure of karst aquifers has a direct consequence for the transmission of flow in these systems. An important attempt to combine the duality of flow, storage, and recharge in karst aquifers was proposed by Smart and Hobbs (1986) (Figure 2.5). All three processes are ranged between end members giving a three-dimensional field into which a karst aquifer may be plotted. Low storage and conduit flow, for example, are assumed to allow the unmodified propagation of a recharge signal to a karst spring but high storage and diffuse flow results in a reduction of the peak signal.

## 2.2 Modelling approaches in karst aquifers

Prediction and characterisation of flow and transport in aquifers is an integral part of sustainable management and protection of groundwater resources. It requires the development and application of mathematical models. Detailed and recent reviews of different approaches for modelling of karst aquifers are presented by Kiraly (2002), Kovács and Sauter (2007), and Sauter et al. (2006).

A mathematical model can be described as the realisation of a schematic representation (conceptual model) of nature using mathematical terms. The schematic representation of a groundwater flow model includes: the model geometry, the hydraulic parameter field, appropriate flow equations, the boundary conditions, and initial conditions for every point of the model domain. In principle, mathematical models in hydrogeology can be distinguished by their description of spatial heterogeneities into (1) lumped parameter models (LPM) and (2) distributed parameter models (DPM). Lumped parameter models treat the flow system as a whole, i.e. dependent variables are not a function of spatial position. Single parameters, a group of parameters or a function are used to reproduce an observed system response from a given input function. Due to their simplicity, LPMs are particularly useful for the interpretation of data when it is neither possible nor justified to use distributed parameter models. Distributed parameter models possess the possibility to describe heterogeneities in aquifer systems and therefore require more detailed knowledge of an investigated system which is, however, often unavailable. They are usually based on partial differential equations. Stochastic models arise when the model contains elements that are probabilistic in nature. In contrast deterministic models are characterised by clear cause-effect relationships (Hangos and Cameron 2001). Teutsch and Sauter (1991) provide a classification scheme of numerous variations of distributive parameter models for the simulation of fractured and karstified aquifers. The models are classified according to (1) their capability to represent heterogeneities, (2) their practical applicability, and (3) the investigation effort required (Figure 2.6). Single continuum porous medium models (SCPE) do not describe the dual nature of karst aquifers. They require that the representative elementary volume (REV) is constant over the

whole model domain, which is not realistic in karst aquifers. Simulation of dual flow systems without detailed information about aquifer geometry is possible with double continuum models (DCPE). The conduit system and fissured matrix blocks of a karst aquifer are both represented by continuum formulations. Flow within the continua is described by Darcy's law and the exchange of water between the continua is calculated via the head difference and a linear exchange term (Barenblatt et al. 1960, Teutsch 1988, Mohrlok 1996, Mohrlok and Teutsch 1997). The double continuum concept comprises the duality of flow in karst aquifers. The approach was successfully applied for simulation of discharge of karst springs, for example, by Sauter (1992). However, because the conduit system is considered as one continuum, the geometry of the hydraulic parameter field is not adequately described.

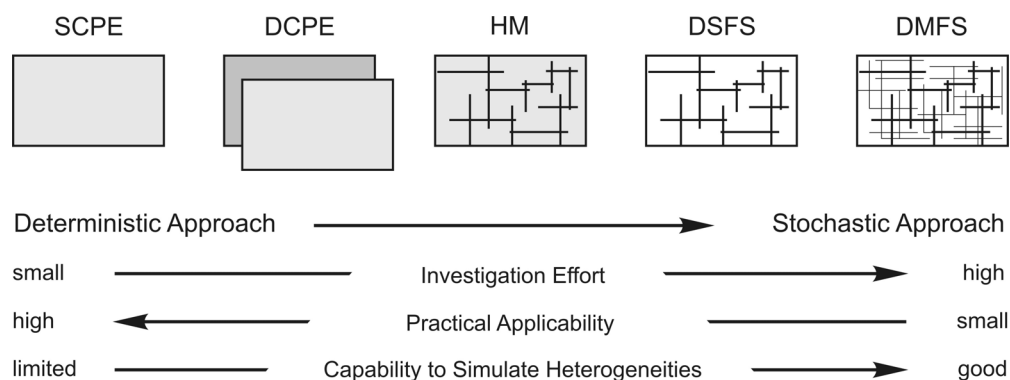


**Figure 2.6: Classification scheme of distributive parameter models for karst aquifers (SCPE, "Single Continuum Porous Equivalent", DCPE "Double Continuum Porous Equivalent", HM, "Hybrid Model", DSFS "Discrete Single Fracture Set", DMFS "Discrete Multiple Fracture Set") (Teutsch and Sauter 1991).**

A much better representation of the geometry of a karst system can be achieved by the representation of discrete networks of highly permeable structures (DSFS "Discrete Singular Fracture Set", DMFS "Discrete Multiple Fracture Set") (Andersson and Dverstorp 1987, Long et al. 1982). Different laws of flow motion can be defined within such discrete features, e.g. Hagen-Poiseuille or Darcy-Weißbach, in order to simulate turbulent or laminar flow conditions. A disadvantage of the application of purely discrete models is that the geometry of all individual discontinuities (fissures, conduits) must either be exactly known, or has to be described using statistical parameters. Therefore, discrete models are rarely applied in field studies (Jeannin and Maréchal 1995, Jeannin 2001) and are mainly used for the simulation of small-scale problems to explain specific types of flow and transport phenomena (Hauns et al. 2001). A compromise between discrete network and continuum models are hybrid models (HM) (Király and Morel 1976, Liedl et al. 2003). They are capable of considering the geometry of highly permeable structures, such as karst conduits, but do not require the detailed information to describe the fissured system, which is considered as a continuum. The hybrid approach facilitates the application of

observed aquifer geometry and measured hydraulic parameters. It was successfully employed to study flow and transport processes between conduits and fissured matrix blocks (Birk et al. 2005, Birk et al. 2006) and is the basic type of models for simulation of karst genesis on regional scale (Liedl et al. 2003).

### 2.3 Methods for characterisation of karst aquifers

Due to strong local heterogeneities caused by the presence of karst conduits, the assemblage of aquifer geometry, the generation of a valid parameter field and the definition of boundary conditions for mathematical modelling of karst aquifers is associated with some difficulties. The framework and geometry of aquifers is usually obtained by geological methods, such as geological mapping and drilling techniques. They provide an initial indication of the rock formation in an area together with stratigraphic and structural interrelationships. Based on this information, some assumptions about hydraulic parameters and the boundaries of an aquifer can be made (Butscher and Huggenberger 2007). However, in karst systems the karstification of rocks must not be related to their stratigraphical boundaries (e.g. Sauter 1992) and the geometry of conduit systems is not only coupled to the presence of fissures but rather to the evolution of the groundwater flow system (Dreybrodt 1988, Dreybrodt et al. 2005, Kiraly 2002). Speleological exploration of conduits may provide detailed information about the geometry of a conduit system (e.g. Jeannin 2001, Jeannin et al. 2007). But, this technique is limited to conduit diameters corresponding to the size of the human body and even more difficult to perform in the case of phreatic conduits. Therefore, only a small and perhaps unrepresentative part of a karst aquifer is likely to be accessible. Surface geophysical methods may supply spatial-high resolution information but these methods are limited to a penetration depth of some tens of meters, and the greater the depth, the lower the resolution (e.g. Bechtel et al. 2005). The application of these methods is therefore difficult in aquifer systems with a deep unsaturated zone and strong local features as can be found in karst aquifers.

The hydraulic parameter field of mathematical models is typically obtained by interpolation or extrapolation of measured data provided from standard investigation techniques such as borehole tests. In karst aquifers, boreholes are usually located between karst conduits, and the radius of influence of borehole tests is typically limited from a few meters to hundreds of meters (local scale) depending on the injection or withdrawal rate of water (Figure 2.7). Small-scale slug-tests and pumping tests provide therefore information about the properties of the fissured matrix blocks but are of limited use for the hydraulic characterisation of conduits. However, parameters obtained from hydraulic borehole testing are crucial to parameterise, for example, the continuum of hybrid models.

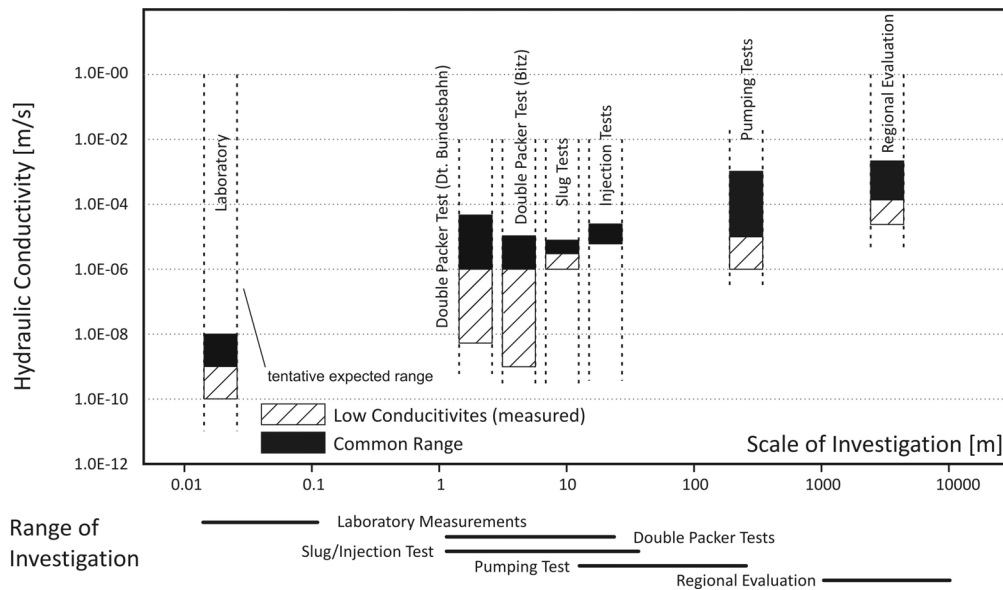


**Figure 2.7: Relationship between investigation methods, scale of investigation, and hydraulic conductivity in a karst aquifer (Sauter 1992).**

Promising tools for the characterisation of conduit systems are quantitative artificial tracer tests (Goldscheider et al. 2008). If the point of tracer injection is a sinkhole, transport parameters can be calculated and used for estimation of integral hydraulic conduit parameters (Field and Pinsky 2000). However, only little information is gained about the geometry of a conduit system.

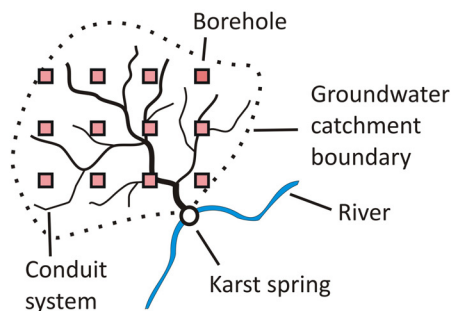
Besides to the geometry of the conduit system the definition of meaningful model boundary conditions is a challenge for simulation of karst aquifers. Modelling of spring catchment areas facilitates the application of mass balance concepts because it is assumed that the whole flow converges to a single spring, and can therefore be measured. Artificial tracer tests are useful to define lateral catchment boundaries and simple water balance approaches (recharge vs. discharge) are capable to estimate the area of a groundwater catchment. However, spring catchments may overlap depending on groundwater levels within karst aquifers. Additionally, transient simulation of flow and transport in karst aquifers is complicated because transient boundary conditions (e.g. recharge) are highly variable in time and space (Figure 2.3). Standard techniques such as water balance approaches are useful to estimate the amount of recharge (Rushton and Ward 1979, Sauter 1992) but, they are not capable to separate recharge into a diffuse component and a component recharging directly the conduit system. However, typical karst spring hydrographs can not be simulated without direct recharge into the conduit system (Geyer et al. 2008).

Therefore, a number of further investigation techniques were developed in karst hydrogeology. These techniques are mainly based on global signals, resulting from the hydraulic and physico-chemical response of karst springs to recharge events. In contrast to borehole tests where only a small part of an aquifer is considered, and artificial tracer tests, which usually refer to the conduit

system, global methods include the whole groundwater catchment of a karst spring (catchment scale). The evaluation of global signals is mainly based on lumped parameter models. Distributed parameter models were particularly applied for the verification of global approaches (e.g. Birk et al. 2006, Eisenlohr 1997a, 1997b, Kovács et al. 2005). A short review about evaluation of spring responses and artificial tracer tests is given in the following (Figure 2.8). Continuative research work considering these approaches is presented in chapters 3, 4, and 5.

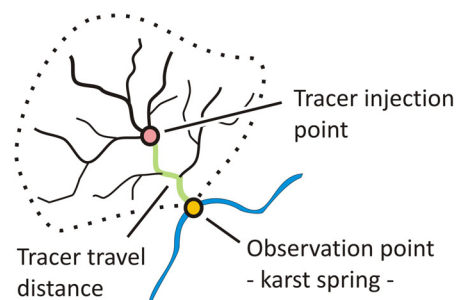
## Artificial tests

### Borehole tests



**Methods:** slug tests, pumping tests, injection tests, ...  
**Input:** borehole  
**Observation point:** borehole(s)  
**Scale:** typically local scale (depends on pumping rate)  
**Investigated system:** typically fissured matrix blocks (depends on location of borehole)

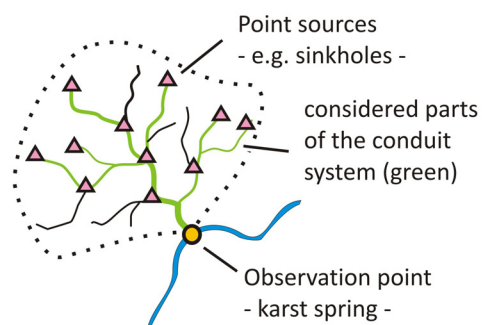
### Artificial tracer tests



**Methods:** single tracer tests, multi tracer tests  
**Tracer injection:** sinkhole, sinking stream, borehole connected to the conduit system  
**Observation point:** karst spring  
**Scale:** catchment scale  
**Investigated system:** part of the conduit system

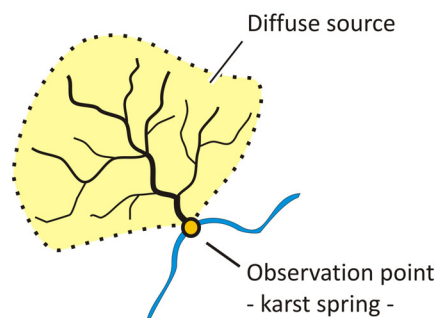
## Global approaches

### Concentrated flow and transport



**Methods:**  
**Flow:** spring hydrograph analysis (event analysis),  
**Transport:** analysis of environmental tracers during discharge events  
**Input:**  
**Flow:** concentrated recharge of water via sinkholes, dry valleys, sinking streams, fractures  
**Transport:** water (oxygen 18, deuterium), solute content, turbidity, temperature  
**Observation point:** karst spring  
**Scale:** catchment scale  
**Investigated system:** conduit system, highly permeable fractures

### Diffuse flow and transport



**Methods:**  
**Flow:** spring hydrograph analysis (baseflow recession),  
**Transport:** analysis of environmental tracers with long-term input function  
**Input:**  
**Flow:** diffuse recharge of water via fissured matrix blocks  
**Transport:** water (e.g. tritium), atmospheric deposition (e.g. krypton 85), agricultural activity (e.g. pesticides), in-situ production (e.g. radioactive decay)  
**Observation point:** karst spring  
**Scale:** catchment scale  
**Investigated system:** fissured matrix blocks

**Figure 2.8: Methods for characterisation of flow and transport within karst aquifers on local scale and catchment scale.**



### 2.3.1 Spring hydrograph analysis

The only signals activating volumes of water in an aquifer system on a regional scale are recharge events (Sauter 1992). As a result of their genetic history, flow from the total catchment of a karst aquifer is often focused to one single spring (Jeannin and Sauter 1998). The response of a karst spring to a recharge event contains therefore integral information about the characteristics of a karst aquifer. In general, spring hydrograph analysis can be distinguished into single event approaches and time series analysis. Single event models deal with the response of a karst spring after a recharge event (Figure 2.9). They are mostly based on simple, or sometimes on a combination of reservoirs, and involve physical phenomena. An event spring hydrograph can be separated in a rising limb and a falling limb. The latter includes the flood recession and the baseflow recession. According to Kiraly (1998, in Kovács et al. 2005), the increase in discharge reflects the commencement of the recharge at the groundwater table. The point of inflection on the rising limb of the hydrograph represents the maximum of recharge, and recharge ceases at the point of inflection on the falling limb. After the cessation of recharge, the shape of a spring hydrograph is only influenced by the drainage of an aquifer. Based on the work of Kiraly (1998), chapter 3 of this work provides a time-continuous approach for the quantification of recharge in karst aquifers from spring hydrographs.

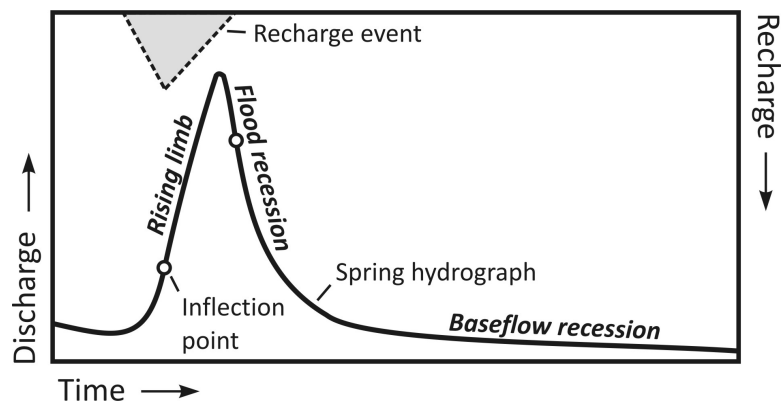


**Figure 2.9: Event spring hydrograph after a recharge event (Kiraly 1998, in Kovács et al. 2005).**

The mathematical realisation of the recession behaviour of a single linear reservoir (recession behaviour is described by an exponential function) was already provided by Maillet (1905). To account for different aquifer components (e.g. conduit system, fissured system, mixed systems), Forkasiewicz and Paloc (1967) proposed that the recession curve of a karst aquifer can be represented by the sum of three or more exponential functions. The exponential function with the highest recession coefficient would represent the recession of the conduits and the exponential curve with the lowest recession coefficient the low permeability fissured matrix blocks. Intermediate exponential functions are assumed to be mixed systems. However, Kiraly and Morel

(1976) and later Eisenlohr et al. (1997a) showed by numerical modelling (hybrid model) that the intermediate exponential can simply be explained by transient phenomena in the vicinity of the conduit system. Other analytical models applied for simulation of karst spring recession distinguish the recession curve of a spring hydrograph into a linear and a non-linear part in order to account for contributions from the unsaturated zone and the saturated zone (Mangin 1975) or suggest the simulation of the whole recession process by one single hyperbolic formula (Drogue 1972).

In addition to the simulation of the recession process, spring hydrograph analyses are important tools to infer integral geometric and hydraulic parameters of karst aquifers. An analytical solution, which relates the recession coefficient of Maillet (1905) to hydraulic parameters of a homogeneous aquifer, was already presented by Rorabaugh (1964) for the estimation of water released from bank storage to a stream flow. This approach was transferred for estimation of hydraulic parameters of karst aquifers by Atkinson (1977), Sauter (1992), Shevenell (1996) and Baedke and Krothe (2001).

In recent studies, Kovács (2003) and Kovács et al. (2005) provided analytical solutions for the recession process of a heterogeneous aquifer consisting of a regular network of high-conductivity karst conduits embedded in a low permeability fissured rock matrix (Figure 2.10). In contrast to other methods, their approach takes into account conduit network characteristics, namely conduit spacing and conduit conductivity. Furthermore, the authors could identify two fundamentally different flow domains, which depend on the state of karstification of an aquifer. In a mature karst aquifer (well developed conduit system) the recession process is influenced by the storage and transmissivity of the fissured matrix blocks and conduit spacing ("matrix-restrained flow regime"). In contrast, recession of an early karst system depends on the storage of the fissured matrix blocks, the spacing and conductivity of the conduits, and the extent of the aquifer ("conduit-influenced flow regime"). While the approach of Kovács et al. (2005) is based on a rectangular network of conduits, Hergarten and Birk (2007) provided an analytical solution to simulate the recession process of a fractal network. This approach considers highly permeable conduits/large fractures, which drain fissured matrix blocks of different sizes with identical shapes (Figure 2.10).

Time series analysis of the whole spring hydrograph and analysis of transfer functions between input and output time series include, for example, cross correlations (e.g. Dreiss 1989, Mangin 1984), spectral analysis (e.g. Labat et al. 2000), cross-spectral analysis (e.g. Padilla and Pulido-Bosch 1995) and multifractal analysis (e.g. Majone et al. 2004). These methods focus on process identification, prediction and data compilation. A critical review of some methods is provided by Jeannin and Sauter (1998) and Kovács and Sauter (2007).

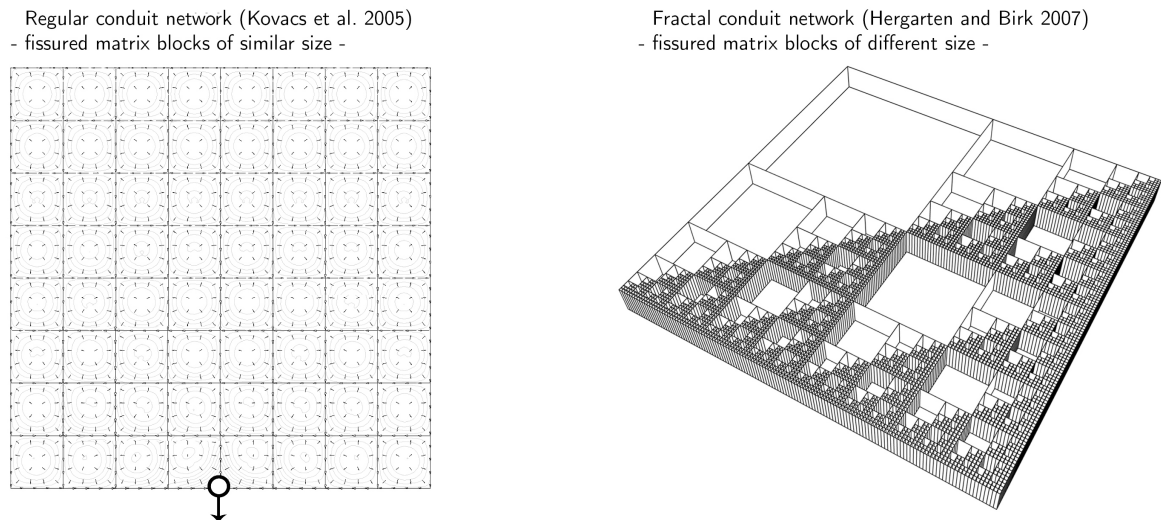


**Figure 2.10: Two conceptual models with different hydraulic parameter fields suitable for the quantitative interpretation of karst aquifers.**

### 2.3.2 Analysis of chemical and isotopic spring responses

The analysis of spring hydrographs may be complemented by chemical and isotopic analyses of spring water (e.g. Aquilina et al. 2005, Birk et al. 2004, Winston and Criss 2004). On karst springs, it is typically observed that after recharge events the solute content in spring water decreases shortly after the rise of spring discharge. The rise of discharge may occur only a few hours after a storm event although the unsaturated zone comprises more than 100 m. The rapid response of spring discharge indicates that there must be a substantial concentrated recharge component. This results from the transmission of a pressure signal induced by the arrival of concentrated recharged water at the groundwater table. In contrast, the decrease of solute content in spring water denotes the arrival of recharged water at a karst spring. The water discharged in-between the hydraulic and the transport response refers to the water filled conduit volume displaced by concentrated recharge. This simple estimation of the conduit volume of a karst aquifer was already established by Ashton (1966) and later applied by e.g. Atkinson (1977), and Desmaris and Rojstaczer (2002). However, several authors showed that the estimated conduit volume should be regarded as an upper bound on the actual conduit volume due to the fact that it neglects water from the epikarst storage (Williams 1983, Sauter 1992). Additionally, Birk et al. (2006) demonstrated by distributive modelling (hybrid model) the dependence of Ashton's method on the duration and intensity of a recharge pulse and on the conduit geometry.

The rapid transport of fresh water through the unsaturated zone leads to the dilution of groundwater. On the basis of end-member mixing, the dilution observed in spring water after recharge events may be calculated in order to obtain the percentage of the concentrated recharge

component (Dreiss 1989). As pointed out by Kiraly (2002), this approach could lead to misinterpretation because end-members of concentration and discharge are not necessarily related to each other. Additionally it has to be considered that the application of end-member mixing requires the evaluation of a conservative tracer such as stable isotopes (oxygen-18 and deuterium) (Lakey and Krothe 1996, Sauter 1997).

After the drop of solute content, it recovers typically to the pre-event value. This behaviour may be explained by mixing processes of recharged water with groundwater as well as by dissolution processes (Grasso and Jeannin 2002). Grasso et al. (2003) provided a deterministic approach where they relate the recovery process to calcite dissolution, and apply this method to evaluate geometric dimensions (openings and aperture) of conduit networks of real karst systems. The variation of solute content in spring water after storm events is often accompanied by a change in spring water temperature. This feature is, just like the variation of solute content, caused by fast and direct recharge entering the conduit system, whereas the direct recharge possesses a certain temperature difference to the pre-event groundwater temperature. When recharge enters the aquifer, the temperature of the recharged water will change due to mixing with groundwater and the heat exchange at the water-rock-interface. Renner and Sauter (1997) and Liedl et al. (1998) provide a numerical approach in which the heat exchange is related to the geometric properties of a conduit system.

The short-term variations of solute content in spring water after recharge events attenuates typically within a few days or weeks. However, groundwater may carry an imprint of environmental tracers correlating with long-term variations (several decades) in atmosphere/precipitation (e.g. tritium, krypton-85) or originating from in-situ production (e.g. helium-3, helium-4) within an aquifer, e.g. radioactive decay (Kaufmann and Libby 1954, Rózański and Florkowski 1979, Torgersen et al. 1979). Measured concentrations of environmental tracers at karst springs are often used to estimate the mean residence time of a tracer in a karst system, and to evaluate mean values of hydraulic parameters over the whole catchment area of a karst spring (Einsiedl 2003, Maloszewski and Zuber 2002). Evaluation of environmental tracers is usually based on lumped parameter models, which solve simple transit time distributions, such as exponential mixing or dispersive mixing, and fit the model on measured data (Eriksson 1958, Nir 1964, Maloszewski and Zuber 1982, Amin and Campana 1996). More elaborated transit time distributions, which consider the structure of a hydrogeological system, can be found by distributive parameter modelling as described by Cornaton and Perrochet (2006) and Kazemi et al. (2006). In this work both lumped parameter models as well as distributed parameter models are used for interpretation of environmental tracers measured at a karst spring (Chapter 5).

The analysis of chemical and isotopic spring responses reveals averaged information for the whole catchment area of a spring. However, in some cases detailed information on mass transport

between a point in the catchment area and a karst spring may be requested. For example, rapid infiltration via sinking streams or sinkholes into karst conduits may lead to a low natural attenuation and short residence time of pollutants within karst aquifers (e.g. Heinz et al. 2006). The identification of controlling transport processes as well as the quantification of the associated parameters is therefore essential for vulnerability assessment (Dörfliger et al. 1999, Brosig et al. 2007) of these systems. Approaches to find more accurate parameters for flow and transport in the conduit system provide artificial tracer tests.

### 2.3.3 Artificial tracer tests

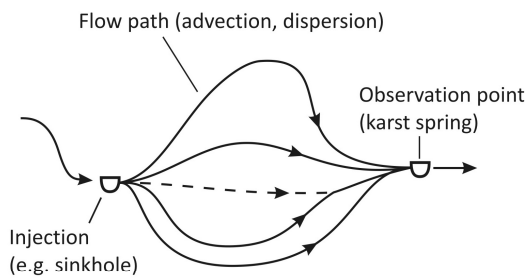
Artificial tracer tests in karst hydrogeology are typically based on the injection of a tracer into boreholes or karst surface features, such as sinkholes and sinking streams (Figure 2.1), and the observation of the tracer at a karst spring. In comparison to the evaluation of environmental tracers, artificial tracer tests lead to more unambiguous results because the tracer mass and the point of injection are exactly known. On the other hand, non-detection of an artificial tracer at an observation point does not necessarily indicate the absence of a hydraulic connection because the tracer concentration at an observation point might be less than the detection limit or the transit time of a tracer might be longer than expected (Long et al. 2008). However, artificial tracer tests were successfully applied in karst hydrogeology for: (1) identification of point-to-point connections, e.g. for the delineation of groundwater catchments, (2) characterisation of the type of a conduit system (Brown and Ford 1971, Atkinson 1973, Smart 1988), (3) determination of flow and transport parameters (Seiler et al. 1989, Maloszewski et al. 1992, Geyer et al. 2007), and (4) estimation of hydraulic aquifer parameters (Field and Pinsky 2000, Birk et al. 2005).

Jakowski and Ebhard (1997), for example, evaluated more than 700 artificial tracer tests carried out in the aquifers of the Triassic and Jurassic hard rocks in Baden Württemberg. The determined flow velocities in karst aquifers ranged between 0.2 and 250 m/h and averaged 72 m/h. The maximum distance between an injection and an observation point was 21 km.

Estimation of transport parameters from artificial tracer tests is usually based on lumped parameter modelling. In some cases the average tracer velocity and dispersivity are calculated from the centre of mass and the time-variance of a tracer breakthrough curve (TBC) observed on a karst spring (Field and Nash 1997). However, this approach is only valid if the tracer transport is described by the one-dimensional dispersion-advection equation. But, TBCs observed at karst springs often display strong tailings, which suggest the presence of additional processes affecting the tracer transport through karst aquifers. Therefore, modelling approaches which consider, to a certain extent, the physics of flow and tracer transport were developed: (1) diffusion between

fissures and the matrix (Maloszewski and Zuber 1985, Seiler et al. 1989) (Figure 2.11), (2) multi-dispersion flow by several individual flow paths (Maloszewski et al. 1992, Käss et al. 1996), and (3) the development of eddies and vortices within a conduit (Raven et al. 1988, Field and Pinsky 2000, Hauns et al. 2001).

a) *Multidispersion model*



b) *Diffusion model*

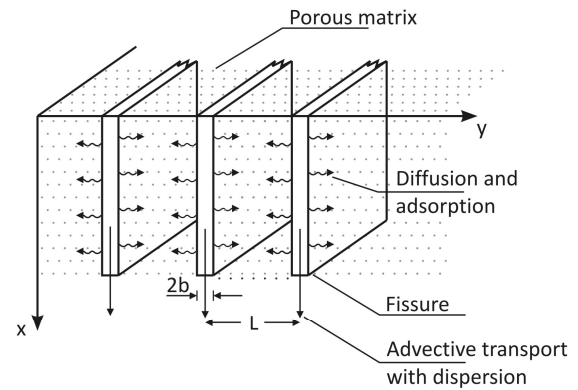


**Figure 2.11: Conceptual models of tracer transport in karst aquifers; a) multi-dispersion flow, b) diffusion between fissures (or conduits) and the porous matrix (from Maloszewski et al. 1992).**

Birk et al. (2005) simulated the tracer breakthrough curve obtained at a karst spring with the hybrid model CAVE. The dispersion of the breakthrough curve is attributed to mass transfer processes arising from velocity differences within the flow cross section (Taylor 1953, 1954), as well as mixing of water between the fissured matrix blocks and the conduit system. The model considers the dispersion coefficient as the product of the friction velocity and the conduit diameter, and therefore provides a direct link between solute transport in a conduit and geometric conduit parameters.

In addition to the conservative tracer transport, Geyer et al. (2007) introduced an approach to determine reactive transport parameters in karst conduits. This approach is presented in chapter 4 of this work.

## 2.4 References

- Amin, I.E., Campana, M.E., 1996. A general lumped parameter model for the interpretation of tracer data and transit time calculation in hydrologic systems. *Journal of Hydrology* 179 (1-4), 1-21.
- Aquilina, L., Ladouche, B., Dörfliker, N., 2005. Recharge processes in karstic systems investigated through the correlation of chemical and isotopic composition of rain and spring-waters. *Applied Geochemistry* 20, 2189–2206.
- Aquilina, L., Ladouche, B., Dörfliker, N., 2006. Water storage and transfer in the epikarst of karstic systems during high flow periods. *Journal of Hydrology* 327 (3-4), 472-485.

- Ashton, K., 1966. The analysis of flow data from karst drainage systems. *Transactions of the Cave Research Group of Great Britain* 7 (2), 161-203.
- Atkinson, T.C., 1977. Diffuse and conduit flow in limestone terrain in the Mendip Hills, Somerset (Great Britain). *Journal of Hydrology* 35, 93-110.
- Atkinson, T.C., Smith, D.I., Lavis, J.J., Whitaker, R.J., 1973. Experiments in tracing underground waters in limestones. *Journal of Hydrology* 19, 323-349.
- Anderson, J., Dverstorp, B., 1987. Conditional simulations of fluid flow in three-dimensional networks of discrete fractures. *Water Resources Research* 23 (10), 1876-1886.
- Baedke, S.J., Krothe, N.C., 2001. Derivation of effective hydraulic parameters of a karst aquifer from discharge hydrograph analysis. *Water Resources Research* 37 (1), 13-19.
- Bakalowicz, M., 2005. Karst groundwater: a challenge for new resources. *Hydrogeology Journal* 13, 148-160.
- Barenblatt, G.I., Zheltov, I.P., Kochina, I.N., 1960. Basic concepts in the theory of seepage of homogeneous liquids in fissured rocks. *Journal of Applied Mathematics and Mechanics* 24, 1286-1303.
- Bear, J., 1972. *Dynamics of fluids in porous media*. American Elsevier, New York, 764 pp.
- Bechtel, T.D., Bosch, F.P., Gurk, M., 2007. Modelling karst hydrodynamics. In: Goldscheider, N., Drew, D. (Eds.), *Methods in karst hydrogeology, International contributions to hydrogeology*, 171-199.
- Birk, S., Geyer, T., Liedl, R., Sauter, M., 2005. Process-based interpretation of tracer tests in carbonate aquifers. *Ground Water* 43 (3), 381-388.
- Birk, S., Liedl, R., Sauter, M., 2004. Identification of localised recharge and conduit flow by combined analysis of hydraulic and physico-chemical spring responses (Urenbrunnen, SW-Germany). *Journal of Hydrology* 286 (1-4), 179-193.
- Birk, S., Liedl, R., Sauter, M., 2006. Karst spring responses examined by process-based modeling. *Ground Water* 286 (1-4), 832-836.
- Brosig, K., Geyer, T., Subah, A., Sauter, M., 2007. Travel time based approach for the assessment of vulnerability of karst groundwater: the transit time method. *Environmental Geology* 54 (5), 905-911.
- Brown, M.C., Ford, D.C., 1971. Quantitative tracer methods for investigations of karst hydrology systems, with special reference to the Maligne Basin area, Canada. *Transactions of the Cave Research Group of Great Britain* 13 (1), 37-51.
- Butscher, C., Huggenberger, P., 2007. Implications for karst hydrology from 3D geological modeling using the aquifer base gradient approach. *Journal of Hydrology* 342 (1-2), 184-198.
- Cornaton, F., Perrochet, P., 2006. Groundwater age, life expectancy and transit time distributions in advective-dispersive systems: 1. Generalized reservoir theory. *Advances in Water Resources* 29 (9), 1267-1291.
- Desmarais, K., Rojstaczer, S., 2002. Inferring source waters from measurements of carbonate spring response to storms. *Journal of Hydrology* 260, 118-134.
- Dörfliger, N., Jeannin, P.-Y., Zwahlen, F., 1999. Water vulnerability assessment in karst environments: a new method of defining protection areas using a multi-attribute approach and GIS tools (EPIK method). *Environmental Geology* 39 (2), 165-176.
- Dreiss, S.Y., 1989. Regional scale transport in a karst aquifer - 1. Component separation of spring flow hydrographs. *Water Resources Research* 25 (1), 117-125.
- Dreybrodt, W., 1988. *Processes in karst systems, physics, chemistry and geology*. Springer series in physical environment, 288 pp.
- Dreybrodt, W., Gabrovsek, F., Romanov, D., 2005. *Processes of speleogenesis: a modeling approach*. *Carsologica* 4, ZRC Publishing, Ljubljana, 376 pp.
- Droge, C., 1972. Statistical analysis of hydrographs of karst springs. *Journal of Hydrology* 15, 49-69.
- Droge, C., 1992. *International Contribution to Hydrogeology* 13 Verlag Heinz Heise, Hannover, Germany, 133-149.

- Einsiedl, F., 2005. Flow system dynamics and water storage of a fissured-porous karst aquifer characterized by artificial and environmental tracers. *Journal of Hydrology* 312, 312-321.
- Eisenlohr, L., Kiraly, L., Bouzelboudjen, M., Rossier, Y., 1997a. Numerical simulation as a tool for checking the interpretation of karst spring hydrographs. *Journal of Hydrology* 193, 306-315.
- Eisenlohr, L., Bouzelboudjen, M., Kiraly, L., Rossier, Y., 1997b. Numeric versus hydrological and statistical modelling of natural response of a karst hydrogeological system. *Journal of Hydrology* 202, 244-262.
- Eriksson, E., 1958. The possible use of tritium for estimating groundwater storage. *Tellus X*, 472-478.
- Field, M.S., 1993. Karst hydrology and chemical contamination. *Journal of Environmental Systems* 22 (1), 1-26.
- Field, M.S., Nash, S.G., 1997. Risk assessment methodology for karst aquifers: (1) Estimating karst conduit-flow parameters. *Environmental Monitoring and Assessment* 47, 1-21.
- Field, M.S., Pinsky, P.F., 2000. A two-region nonequilibrium model for solute transport in solution conduits in karstic aquifers. *Journal of Contaminant Hydrology* 44, 329-351.
- Ford, D.C., 1999. Perspectives in karst hydrogeology and cavern genesis. In: Palmer, A.N., Palmer, V.P., Sasowsky, I.D. (Eds.), *Karst modelling, Special publications 5, Proceedings of the symposium held February 24 through 27, 1999, Charlottesville, Virginia*, 17-29.
- Ford, D.C., Williams, P., 2007. *Karst hydrogeology and Geomorphology*. John Wiley & Sons Ltd., West Sussex, 562 pp.
- Forkasiewicz, J., Paloc, H., 1967. Le régime de tarissement de la Foux de la Vis étude préliminaire. In: *Proceedings of the Dubrovnik Symposium, October 1965, Hydrology of fractured rocks* 1, 213-226.
- Foster, S.S.D., 1975. The chalk groundwater  $^3\text{H}$  anomaly—a possible explanation. *Journal of Hydrology* 25 (1-2), 159-165.
- Geyer, T., Birk, S., Licha, T., Liedl, R., Sauter, M., 2007. Multi-tracer test approach to characterize reactive transport in karst aquifers. *Ground Water* 45 (1), 36-45.
- Geyer, T., Birk, S., Liedl, R., Sauter, M., 2008. Quantification of temporal distribution of recharge in karst systems from spring hydrographs. *Journal of Hydrology* 348, 452-463.
- Goldscheider, N., Meiman, J., Pronk, M., Smart, C., 2008. Tracer tests in karst hydrogeology and speleology. *International Journal of Speleology* 37 (1), 27-40.
- Grasso, D.A., Jeannin, P.-Y., 2002. A global experimental system approach of karst springs' hydrographs and chemographs. *Ground Water* 40 (6), 608-617.
- Grasso, D.A., Jeannin, P.-Y., Zwahlen, Z., 2003. A deterministic approach to the coupled analysis of karst springs' hydrographs and chemographs. *Journal of Hydrology* 271, 65-76.
- Hangos, K., Cameron, I., 2001. *Process modelling and model analysis*. Process systems engineering 4. Academic Press, San Diego, 543 pp.
- Hauns, M., Jeannin, P.-Y., Atteia, O. 2001. Dispersion, retardation and scale effect in tracer breakthrough curves in karst conduits. *Journal of Hydrology* 241, 177-193.
- Heinz, B., Birk, S., Liedl, R., Geyer, T., Straub, K.L., Bester, K., Kappler, A., 2006. Vulnerability of a karst spring to wastewater infiltration (Gallusquelle, Southwest Germany). *Austrian Journal of Earth Sciences* 99, 11-17.
- Hergarten, S., Birk, S., 2007. A fractal approach to the recession of spring hydrographs. *Geophysical Research Letters* 34, L11401, doi:10.1029/2007GL030097.
- Jakowski, A.E., Ehardt, G., 1997. Geohydraulic parameters in hard rocks of SW-Germany determined by tracer tests. In: *Tracer Hydrology* 97, Kranjc, A. (Ed.), 415-421. Rotterdam, Netherlands, Balkema.
- Jeannin, P.-Y., 2001. Modeling flow in phreatic and epiphreatic karst conduits in the Hölloch cave (Muotatal, Switzerland). *Water Resources Research* 37 (2), 191-200.
- Jeannin, P.-Y., Groves, C., Häuselmann, P., 2007. Speleological investigations. In: Goldscheider, N., Drew, D. (Eds.), *Methods in karst hydrogeology, International contributions to hydrogeology*, 25-44.
- Jeannin, P.-Y., Maréchal, J.-C., 1995. Lois de pertes de charge dans les conduits karstiques: base théorique et observations. *Bulletin d'Hydrogéologie (Neuchâtel)* 14, 149-176.



- Jeannin, P.-Y., Sauter, M., 1998. Analysis of karst hydrodynamic behaviour using global approach: a review. *Bulletin d'Hydrogéologie (Neuchâtel)* 16, 9-30.
- Käss, W., Löhnert, E.P., Werner, A., 1996. Der jüngste Markierungsversuch im Karst von Paderborn (Nordrhein-Westfalen). *Grundwasser* 2/96, 83-89.
- Kaufmann, S., Libby, W.F., 1954. The natural distribution of tritium. *Physical Reviews* 93, 1337-1344.
- Kazemi, G.A., Lehr, J.H., Perrochet, P., 2006. *Groundwater age*. New Jersey, USA: John Wiley and Sons, 325 pp.
- Kiraly, L., 1975. Rapport sur l'état actuel des connaissances dans les domaines des caractères physiques des roches karstiques. In: Burger A., Dubertret L. (Ed.), *Hydrogeology of karstic terrains*, Int. Union of Geol. Sciences B3, 53-67.
- Kiraly, L., 1978. La notion d'unité hydrogéologique dans le Jura (essai de définition). Ph.D. thesis, Université de Neuchâtel, 216 pp.
- Kiraly, L., 1998. Introduction à l'hydrogéologie des roches fissurées et karstiques, Bases théoriques à l'intention des hydrogéologues. Université de Neuchâtel, Manuscrit.
- Kiraly, L., 2002. Karstification and Groundwater Flow. In: *Proceedings of the Conference on Evolution of Karst: From Prekarst to Cessation*. Postojna-Ljubljana, 155-190.
- Kiraly, L., Morel, G., 1976. Etude de régularisation de l'Areuse par modèle mathématique. *Bulletin d'Hydrogéologie de l'Université de Neuchâtel* 1, 19-36.
- Klimchouk, A., 2004. Towards defining, delimiting and classifying epikarst: Its origin, processes and variants of geomorphic evolution. *Speleogenesis and Evolution of Karst Aquifers* 2 (1), 13 pp.
- Kovács, A., 2003. Geometry and hydraulic parameters of karst aquifers: A hydrodynamic modelling approach. Ph.D. thesis, Université de Neuchâtel, 131 pp.
- Kovács, A., Perrochet, P., Kiraly, L., Jeannin, P.-Y., 2005. A quantitative method for the characterisation of karst aquifers based on spring hydrograph analysis. *Journal of Hydrology* 303, 152-164.
- Kovács, A., Sauter, M., 2007. Modelling karst hydrodynamics. In: Goldscheider, N., Drew, D. (Eds.), *Methods in karst hydrogeology*, International contributions to hydrogeology, 201-222.
- Labat, D., Ababou, R., Mangin, A., 2000. Rainfall-runoff relations for karstic springs. Part I: convolution and spectral analyses. *Journal of Hydrology* 238 (3-4), 123-148.
- Lahey, B., Krothe, N.C., 1996. Stable isotopic variation of storm discharge from a perennial karst spring, Indiana. *Water Resources Research* 32 (3), 721-731.
- Liedl, R., Renner, S., Sauter, M., 1998. Obtaining information on fracture geometry from heat flow data in karst systems. *Bulletin d'Hydrogéologie (Neuchâtel)* 16, 143-153.
- Liedl, R., Sauter, M., Hückinghaus, D., Clemens, T., Teutsch, G., 2003. Simulation of the development of karst aquifers using a coupled continuum pipe flow model. *Water Resources Research* 39 (3), 1-11.
- Long, A.J., Sawyer, J.F., Putnam, L.D., 2008. Environmental tracers as indicators of karst conduits in groundwater in South Dakota, USA. *Hydrogeology Journal* 16, 263-280.
- Long, J.C.S., Remer, J.S., Wilson, C.R., Witherspoon, P.A., 1982. Porous media equivalents for networks of discontinuous fractures. *Water Resources Research* 18 (3), 645-658.
- Maillet, E., 1905. *Essais d'hydraulique souterraine et fluviale*. Paris, 218 pp.
- Majone, B., Bellin, A., Borsato, A., 2004. Runoff generation in karst catchments: multifractal analysis. *Journal of Hydrology* 294 (1-3), 176-195.
- Maloszewski, P., Harum, T., Benischke, R., 1992. Mathematical modelling of tracer experiments in the karst of Lurbach system. *Steirische Beiträge zur Hydrogeologie* 43, 116-136.
- Maloszewski, P., Stichler, W., Zuber, A., Rank, D., 2002. Identifying the flow systems in a karstic-fissured-porous aquifer, the Schneesalpe, Austria, by modelling of environmental  $^{18}\text{O}$  and  $^3\text{H}$  isotopes. *Journal of Hydrology* 256, 48-59.
- Maloszewski, P., Zuber, A., 1982. Determining the turnover time of groundwater systems with the aid of environmental tracers : 1. Models and their applicability. *Journal of Hydrology* 57, 207-231.

- Maloszewski, P., Zuber, A., 1985. On the theory of tracer experiments in fissured rocks with a porous matrix. *Journal of Hydrology* 79, 333-358.
- Maloszewski, P., Zuber, A., 2002. Manual on lumped-parameter models used for the interpretation of environmental tracer data in groundwaters. In: Yurtsever, Y. (ed.): Use of isotopes for analyses of flow and transport dynamics in groundwater systems. IAEA-UIAGS/CD 02-00131, IAEA Vienna. 2002, 1-50.
- Mangin, A., 1975. Contribution à l'étude hydrodynamique des aquifères karstiques. Ph.D thesis. Université de Dijon (*Annales de Spéléologie* 29 (3), 283-332; 29 (4), 495-601; 30 (1), 21-124).
- Mangin, A., 1984. Pour une meilleure connaissance des systèmes hydrologiques à partir des analyses corrélatoire et spectrale. *Journal of Hydrology* 67, 25-43.
- Mohrlok, U. 1996. Parameter-Identifikation in Doppel-Kontinuum-Modellen am Beispiel von Karstaquiferen. *Tübinger Geowissenschaftliche Arbeiten*, C31, 125 pp.
- Mohrlok, U., Teutsch, G., 1997. Double continuum porous equivalent (DCPE) versus discrete modeling in karst terranes. In: Günay, G., Johnson, A.I. (Eds.), *Karst Waters and Environmental Impacts*, 319-326.
- Nir, A., 1964. On the interpretation of tritium age measurements of groundwater. *Journal of Geophysical Research* 69 (12), 2589-2595.
- Padilla, A., Pulido-Bosch, A., 1995. Study of hydrographs of karstic aquifers by means of correlation and cross-spectral analysis (France, Spain). *Journal of Hydrology* 168, 73-89.
- Palmer, A.N., 1991. Origin and morphology of limestone caves: *Geological Society of American Bulletin* 103, 1-21.
- Perrin, J., Jeannin, P.-Y., Zwahlen, F., 2003. Epikarst storage in a karst aquifer: a conceptual model based on isotopic data, Milandre test site, Switzerland. *Journal of Hydrology* 279, 106-124.
- Raven, K.G., Novakowski, K.S., Lapcevic, P.A., 1988. Interpretation of field tracer tests of a single fracture using a transient solute storage model. *Water Resources Research* 24 (12), 2019-2032.
- Renner, S., Sauter, M., 1997. Heat as a natural tracer: Characterisation of a conduit network in a karst aquifer using temperature measurements of the spring water. In: Günay, G., Johnson, A.I. (Eds.), *Karst Waters and Environmental Impacts*, 319-326.
- Rorabaugh, M.I., 1964. Estimating changes in bank storage as ground-water contribution to streamflow. *International Association of Scientific Hydrology* 63, 432-441.
- Rózański, K., Florkowski, T., 1979. Krypton-85 dating of groundwater. IAEA-SM-228/51, 949-961.
- Rushton, K.R., Ward, C., 1979. The estimation of groundwater recharge. *Journal of Hydrology* 41, 345-361.
- Sauter, M., 1992. Quantification and forecasting of regional groundwater flow and transport in a karst aquifer (Gallusquelle, Malm, SW. Germany). *Tübinger Geowissenschaftliche Arbeiten*, C13, 150 pp.
- Sauter, M., 1997. Differentiation of fast and slow flow components in a karst aquifer using the  $\delta^{18}\text{O}$  signature - Data analysis and modeling. In: Kranjc, A. (Ed.), *Tracer Hydrology* 97, Balkema, 435-441.
- Sauter, M., Kovács, A., Geyer, T., Teutsch, G., 2006. Modellierung der Hydraulik von Karstgrundwasserleitern - Eine Übersicht. *Grundwasser* 3/2006, 143-153.
- Seiler, K.-P., Maloszewski, P., Behrens, H., 1989. Hydrodynamic dispersion in karstified limestones and dolomites in the upper jurassic of the franconian alb, F.R.G.. *Journal of Hydrology* 108, 235-247.
- Shevenell, L., 1996. Analysis of well hydrographs in a karst aquifer: estimates of specific yields and continuum transmissivities. *Journal of Hydrology* 174 (3-4), 331-355.
- Shuster, E.T., White, W.B., 1971. Seasonal fluctuations in the chemistry of limestone springs: A possible means for characterizing carbonate aquifers. *Journal of Hydrology* 14, 93-128.
- Smart, C.C., 1988. Artificial tracer techniques for the determination of the structure of conduit aquifers. *Ground Water* 26, 445-453.
- Smart, P.L., Hobbs, S.L., 1986. Characterisation of carbonate aquifers: A conceptual base. In: Graves, B.J., Lehr, J.H., Butcher, K., Crawford, N.C. (Eds.), *Proceedings of the Environmental Problems in Karst Terranes and their Solutions Conference*. Bowling Green, Kentucky, October, 28-30, 1986, 1-14.
- Taylor, G.I., 1953. Dispersion of soluble matter in solvent flowing slowly through a tube. *Proceedings of the Royal Society of London Series A* 219, 186-203.

- Taylor, G.I., 1954. The dispersion of matter in turbulent flow through a pipe. Proceedings of the Royal Society of London Series A 223, 446-468.
- Teutsch, G., 1988. Grundwassermodelle im Karst: Praktische Ansätze am Beispiel zweier Einzugsgebiete im Tiefen und Seichten Malmkarst der Schwäbischen Alb. Ph.D. thesis, University of Tübingen, 205 pp.
- Teutsch, G., Sauter, M., 1991. Groundwater modelling in karst terranes: Scale effects, data acquisition and field validation. Proc. 3<sup>rd</sup> Conf. on hydrogeology, ecology, monitoring and management of ground water in karst terranes. Nashville, 17-35.
- Torgersen, T., Clarke, W.B., Jenkins, W.J., 1979. The tritium/helium-3 method in hydrology. Isotope Hydrology 1978, IAEA-SM-228/49, Vienna, 917-930.
- White, W.B., 1969. Conceptual models for carbonate aquifers. Ground Water 7 (3), 15-21.
- Williams, P.W., 1983. The role of the subcutaneous zone in karst hydrology. Journal of Hydrology 61, 45-67.
- Winston, W.E., Criss, R.E., 2004. Dynamic hydrochemical and geochemical response in a perennial karst spring. Water Resources Research 40, W05106, doi:10.1029/2004WR003054.

## Chapter 3

# Quantification of temporal distribution of recharge in karst systems from spring hydrographs

Tobias Geyer<sup>1,4</sup>, Steffen Birk<sup>2</sup>, Rudolf Liedl<sup>3</sup>, Martin Sauter<sup>1</sup>

Citation: Geyer, T., Birk, S., Liedl, R., Sauter, M., 2008. Quantification of temporal distribution of recharge in karst systems from spring hydrographs. *Journal of Hydrology* 348, 452-463.

<sup>1</sup> Geoscientific Centre, University of Göttingen, Goldschmidtstr. 3, D-37077 Göttingen, Germany

<sup>2</sup> Institute for Earth Sciences, University of Graz, Heinrichstr. 26, A-8010 Graz, Austria

<sup>3</sup> Institute for Groundwater Management, Dresden University of Technology, Karcherallee 8, D-01277 Dresden, Germany

<sup>4</sup> Corresponding author - Phone: (49) 551 399398; Fax: (49) 551 399379; tgeyer@gwdg.de

## Abstract

The estimation of the temporal distribution of recharge in karst aquifers is a challenge due to large heterogeneities in geometric and hydraulic parameters of the vadose and phreatic zone. This article provides a time-continuous approach for the estimation of inflow into the conduit system of a karst aquifer which consists of the sum of direct recharge and flow from the fissured matrix blocks into the conduit system. The approach employs the first time derivative of the spring hydrograph and the recession coefficient of the conduit system for the determination of this function. The first time derivative of the hydrograph describes the rate of change in spring discharge. It reflects the ratio of inflow to and outflow from the conduit system. The recession coefficient depends on the hydraulic diffusivity, which controls the velocity of the signal transmission through the system. As shown in parameter studies with a simplified serial two-reservoir model, direct recharge into the conduit system clearly dominates the early hydrograph response during recharge events even if the fraction of direct recharge represents just a few percent of total recharge. This behaviour is caused by a large contrast in recession coefficients between conduit system and fissured matrix blocks. The direct recharge component can therefore be separated from the estimated total inflow into the conduit system. Estimation of inflow into the conduit system of the Gallusquelle spring (Swabian Alb, Germany) after a storm event yields similar results as those obtained from parameter studies. The separation of the direct recharge component is in agreement with information from an independent isotope study. The methodology has been further applied to a recharge event initiated by snowmelt. As a result of daily variations of the air temperature, a clearly diurnal cycle of inflow into the conduit system is estimated that is not easily recognisable from the spring hydrograph. The applicability of the proposed methodology requires knowledge about the magnitude of the recession coefficient of the conduit system. The characteristics of the conduit system become also apparent in the rapid transport of tracers. The recession coefficient of the conduit system can, for example, directly be estimated from the reciprocal of the mean tracer travel time. However, for this type of analysis, only tracer experiments covering the extent of the catchment should be taken into account. For the Gallusquelle catchment the recession coefficient obtained from the tracer experiment corresponds to that obtained from hydrograph recession analysis. The estimated inflow into the conduit system and interpretation of temporal distribution of recharge is therefore based on a plausible and physically based parameter.

### 3.1 Introduction

Time series of hydrological variables are often used for the identification of governing processes and for the quantification of the physical properties of aquifer systems. They represent a prerequisite for unsteady state groundwater modelling. Changes in the state of hydrogeological systems are commonly measured by recording water levels or discharge, e.g. at springs. Aquifer characterisation techniques based on the interpretation of spring hydrographs are of particular importance in karst aquifers because these systems are highly heterogeneous in terms of flow, storage, and groundwater recharge (Hobbs und Smart 1986, Király 2002). Since the length scale of karst features, such as conduit networks, can be very large, aquifer and process characterisation cannot adequately be assessed using standard borehole techniques that consider only relatively small aquifer volumes. In contrast, observations at karst springs provide information about the entire catchment, because the springs are usually connected to the highly permeable conduit system that acts as drainage channels for the low permeability fissured matrix blocks within the catchment (Jeannin and Sauter 1998).

In general, the interpretation of spring hydrographs may be based on the evaluation of their recession behaviour (e.g. Forkasiewicz and Paloc 1967, Kovács et al. 2005, Hergarten and Birk 2007) or on the statistical evaluation of the entire hydrograph and rainfall time series (e.g. Labat et al. 2000, Mangin 1984, Padilla and Pulido-Bosch 1995). In addition, numerical models were employed for simulation of spring hydrographs and spatially distributed karst aquifer hydraulics (e.g. Király and Morel 1976, Eisenlohr et al. 1997, Halihan and Wicks 1998, Jeannin 2001). One important uncertainty in the analysis of spring hydrographs is the spatial and temporal distribution of recharge. Karst systems are characterised by a duality of the recharge processes (e.g. Király 2002). On the one hand, direct recharge into the karst conduit system can be very rapid and highly localized. On the other hand, diffuse recharge into low permeability fissured matrix blocks is slow and distributed across the entire catchment area. In addition, a number of studies have shown the importance of the lateral redistribution of recharge within horizons close to the land surface, i.e. within the epikarst (e.g. Williams 1983, Perrin et al. 2003). This complexity of the recharge processes poses great challenges to the identification of the spatial and temporal distribution of recharge to karst aquifers. Soil-water balance methods involving a direct recharge component (Rushton and Ward 1979) are applied to estimate amount of recharge (Sauter 1992, Jocson et al. 2002). A frequency domain approach for parameterisation of a groundwater recharge model is introduced by Jukić and Denić-Jukić (2004). Chemical and isotopic spring signals can be used to determine direct and diffuse recharge components (e.g. Lakey and Krothe 1996, Sauter 1997). Similar to stream-flow hydrograph separation techniques some authors applied simple spring hydrograph separation to separate quick-flow from total karst spring discharge (Atkinson 1977, Dreiss 1983). Király (1998, in Kovács et al. 2005) provides one

method to infer temporal distribution of recharge by a triangular transfer function from an event spring hydrograph. There, the commencement of the recharge at the groundwater table coincides with the increase in spring discharge. The maximum of recharge is represented by the point of inflection on the rising limb of the hydrograph and the cessation of recharge by the point of inflection on the falling limb of the hydrograph.

The aim of this study is to provide a technique for the time-continuous identification of recharge to karst aquifers based on the analysis of spring hydrographs. The proposed methodology builds on the approach of cumulative storage accumulation (Ketchum et al. 2000). In the first part of this paper, the approach is examined theoretically for a dual flow system represented by a two-reservoir model. In the second part, the method is applied to and validated for the Gallusquelle karst catchment (Swabian Alb, Germany).

### 3.2 Method

The behaviour of karst spring hydrographs can, in principle, be simulated using a two-reservoir model (Figure 3.1). The low permeability reservoir represents the fissured matrix blocks of the aquifer and the highly permeable reservoir the karst conduits. The corresponding equations are (Király 2002):

$$\frac{dV_l}{dt} = R_l - Q_l = R_l - \alpha_l V_l \quad (3.1)$$

and

$$\frac{dV_h}{dt} = R_h + Q_l - Q_h = R_h + \alpha_l V_l - \alpha_h V_h \quad (3.2)$$

The subscripts in eqs. (3.1) and (3.2) refer to the low permeability reservoir (subscript  $l$ ) and the highly permeable reservoir (subscript  $h$ ). According to the base-flow recession concept of Maillet (1905), the discharge  $Q$  of each reservoir (= linear store) is a function of the volume of water held in storage  $V$  at time  $t$  and the recession coefficient  $\alpha$ . The recession coefficient depends on storage, permeability, and geometric properties of a reservoir (Kovács et al. 2005). Since the highly permeable conduits act as drainage channels for the fissured matrix blocks, the model assumes that discharge from the low permeability reservoir  $Q_l$  flows into the highly permeable reservoir  $V_h$ , while discharge from the highly permeable reservoir  $Q_h$  is equivalent to spring discharge. Recharge is represented by a dual recharge function, i.e. it might infiltrate into the low

permeability reservoir  $R_l$ , e.g. as result of diffuse recharge, and directly into the highly permeable reservoir  $Q_l$  via concentrated recharge, e.g. into sinkholes.

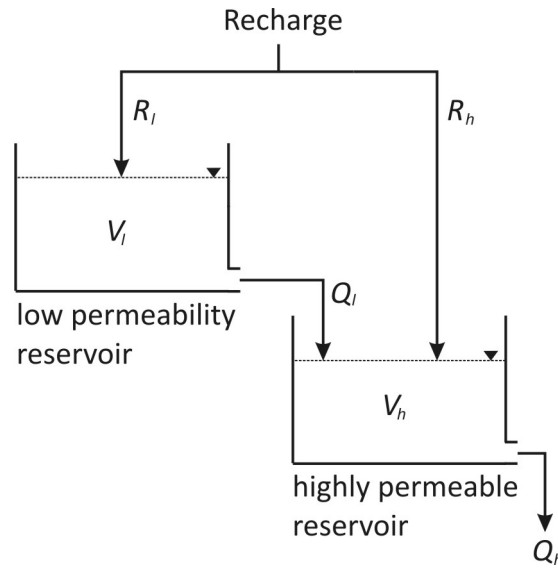


**Figure 3.1:** A two-reservoir model, which allows the simulation of the hydraulic behaviour of karst aquifers in principle.  $R_l$  recharge into the low permeability reservoir,  $R_h$  recharge into the highly permeable reservoir,  $Q_l$  flow from the low permeability reservoir into the highly permeable reservoir,  $Q_h$  outflow from the highly permeable reservoir (spring discharge).

### 3.2.1 Analytical solution

The analytical solution of eqs. (3.1) and (3.2) contains integrals involving the time-dependent recharge functions  $R_l(t)$  and  $R_h(t)$ . Appendix A provides an example how these integrals can be evaluated exactly if  $R_l(t)$  and  $R_h(t)$  are represented by “simple” functions (constant or linear) within pre-defined time intervals characterising the recharge dynamics. The beginning of each time interval corresponds to the lower limit of an integration interval and in order to facilitate the integration it was found convenient to introduce the generic symbol  $t^*$  to denote these lower limits. Based on this, the analytical solution of eqs. (3.1) and (3.2) is written as:

$$V_l(t) = V_l^* e^{-\alpha_l(t-t^*)} + \int_{t^*}^t R_l(\tilde{t}) e^{-\alpha_l(t-\tilde{t})} d\tilde{t} \quad (3.3)$$

and

$$V_h(t) = V_h^* e^{-\alpha_h(t-t^*)} + \int_{t^*}^t R_h(\tilde{t}) e^{-\alpha_h(t-\tilde{t})} d\tilde{t} +$$



$$+ \frac{\alpha_l}{\alpha_h - \alpha_l} \left[ V_l(t) - V_l^* e^{-\alpha_h(t-t^*)} - \int_{t^*}^t R_l(\tilde{t}) e^{-\alpha_h(t-\tilde{t})} d\tilde{t} \right] \quad (3.4)$$

with general initial conditions  $V_l(t^*) = V_l^*$  and  $V_h(t^*) = V_h^*$ , resp. For specific input signals the

quantities  $t^*, V_l^*, V_h^*$  and the integrals  $\int_{t^*}^t R_l(\tilde{t}) e^{-\alpha_l(t-\tilde{t})} d\tilde{t}$ ,  $\int_{t^*}^t R_h(\tilde{t}) e^{-\alpha_h(t-\tilde{t})} d\tilde{t}$

and  $\int_{t^*}^t R_l(\tilde{t}) e^{-\alpha_l(t-\tilde{t})} d\tilde{t}$  have to be determined for each integration interval.

### 3.2.2 Numerical solution

For practical applications, it is more convenient to solve the model equations using a numerical finite-difference scheme, where any type of temporal recharge distribution can easily be implemented. Solving the explicit finite-difference forms of eqs. (3.1) and (3.2) for the water volume of each reservoir yields

$$V_l(t) = \frac{1}{\alpha_l} Q_l(t) = V_l(t - \Delta t) - \Delta t \alpha_l V_l(t - \Delta t) + \Delta t R_l(t) \quad (3.5)$$

and

$$V_h(t) = \frac{1}{\alpha_h} Q_h(t) = V_h(t - \Delta t) - \Delta t \alpha_h V_h(t - \Delta t) + \Delta t (R_h(t) + \alpha_l V_l(t)) \quad (3.6)$$

where  $\Delta t$  is the time step.

#### ***Relationship between temporal recharge distribution and spring hydrograph***

For an aquifer represented by a single reservoir, the temporal recharge distribution can be calculated by solving eq. (3.5) for  $R_l(t)$ . The recession coefficient, which must first be known to apply the equation, can be obtained from the recession of the spring hydrograph  $Q_s(t)$  (Ford and Williams 2007, p. 176):

$$\alpha_l = \frac{\log Q_s(t - \Delta t) - \log Q_s(t)}{0.4343 \Delta t} \quad (3.7)$$

For the two-reservoir model considered here, rearrangement of eq. (3.6) only allows the quantification of the sum of the two flow components into the highly permeable reservoir  $I_h(t)$  from the spring hydrograph  $Q_h(t) = \alpha_h V_h(t)$ :

$$I_h(t) = R_h(t) + \alpha_l V_l(t) = \frac{1}{\alpha_h} \frac{Q_h(t) - Q_h(t - \Delta t)}{\Delta t} + Q_h(t - \Delta t) \quad (3.8)$$

The recession coefficient of the highly permeable reservoir  $\alpha_h$  relates the amplitude of the first time derivative of  $Q_h$  with the inflow-outflow difference of the highly permeable reservoir via

$$\frac{dQ_h}{dt} \approx \frac{\Delta Q_h}{\Delta t} = \alpha_h (I_h(t) - Q_h(t - \Delta t)) \quad (3.9)$$

as can be directly derived from eq. (3.8).

### 3.3 Parameter studies

In order to examine the interrelation of recharge function and spring hydrograph, spring responses to hypothetical recharge events have been simulated using the above-described two-reservoir model. In a first scenario, recharge is applied only to the highly permeable reservoir, in a second scenario only to the low permeability reservoir, and in a third scenario to both types of reservoirs. In any case, total recharge is 10 mm. Following the results of field studies (e.g. Sauter 1992, Perrin et al. 2003), the portion directly infiltrating into the highly permeable reservoir is varied from 5% to 50%. The recession coefficient of the highly permeable reservoir ( $\alpha_h$ ) is 0.5 1/d, while that of the low permeability reservoir ( $\alpha_l$ ) is 0.01 1/d. These values correspond to those found in various field studies (e.g. Forkasiewicz and Paloc 1967, Sauter 1992, Padilla et al. 1994). Initially, the low permeability reservoir contains a water volume of  $V_l = 3,200,000 \text{ m}^3$  (catchment area = 16 km<sup>2</sup>, aquifer thickness = 10 m, effective porosity = 0.02) and the water volume in the highly permeable reservoir equals  $V_h = 0 \text{ m}^3$ . The outflow from the low permeability reservoir fills the highly permeable reservoir until the volume  $V_h = Q_l / \alpha_h$  is reached (Figure 3.2). After that, inflow from the low permeability reservoir is lower than outflow at the spring, i.e.  $Q_l < Q_h$ , and  $V_h$  decreases. To avoid effects caused by the initial filling of the highly permeable reservoir, parameter studies using synthetic recharge events commence 50 days after filling of  $V_h$  started.

In addition to the spring hydrograph itself, we analyse the first and second time derivative of the discharge using the finite-difference approximation. The time step is set to 0.01 days. The accuracy of the numerical calculation was verified by comparing the numerical result with the analytical solution for the case of a dual recharge function (Appendix A).

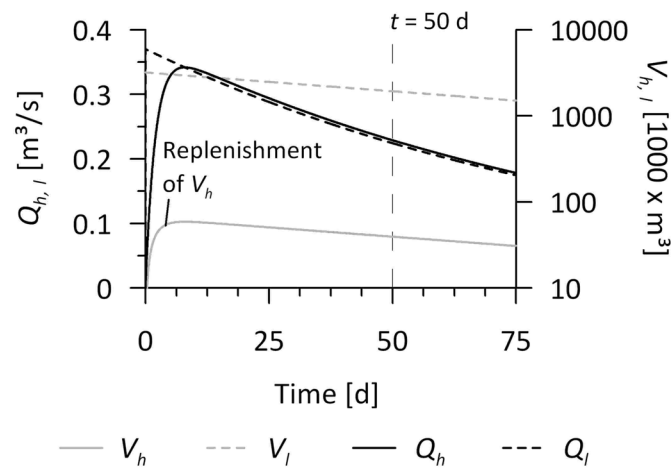


Figure 3.2: Replenishment of the highly permeable reservoir  $V_h$  and recession behaviour of the two-reservoir model. Parameter studies commence on  $t = 50$  d.

### 3.4 Results from the parameter studies

Figure 3.3 shows the effects of trapezoidal recharge into the highly permeable reservoir on the spring hydrograph  $Q_h$ . It is found that the shape of the graph of the first time derivative is very similar to that of the recharge function but skewed in some parts as a result of the effects of the recession process (eq. 3.9). The points of inflection on the rising and falling limb of the hydrograph coincide with the peak and the end of the recharge event, respectively, as shown by Király (1998, in Kovács et al. 2005). Since  $Q_h = \alpha_h V_h$ , the minimum of the spring hydrograph represents the minimum water volume in the highly permeable reservoir that is an approximation for the commencement of an intensive recharge event into the highly permeable reservoir. Until the maximum water volume in the highly permeable reservoir is reached, the first derivative of the hydrograph is positive which means that  $Q_h < I_h$ . Afterwards, the first time derivative is negative and thus  $Q_h > I_h$ . After recharge has ceased,  $Q_h$  slowly approaches the value of the inflow rate into the highly permeable reservoir, i.e.  $Q_h \rightarrow I_h = Q_l$  for  $t \rightarrow \infty$ . Thus, the long-term recession is controlled by the low permeability reservoir.

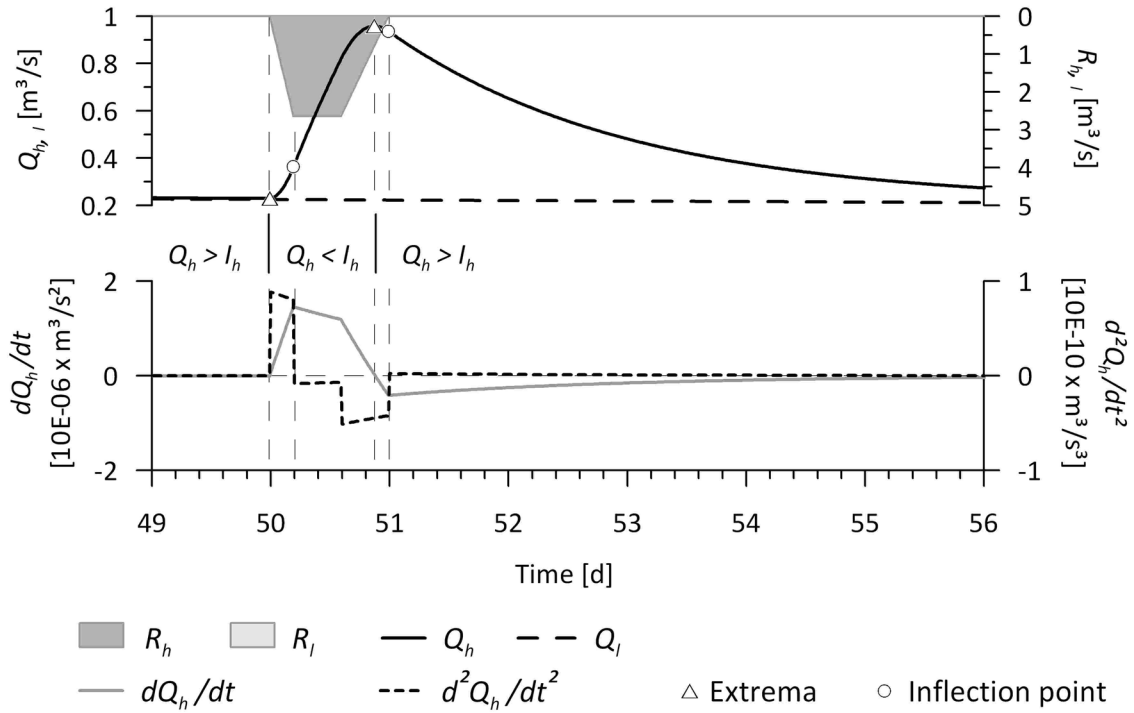


Figure 3.3: Simulation results with recharge into the highly permeable reservoir only.

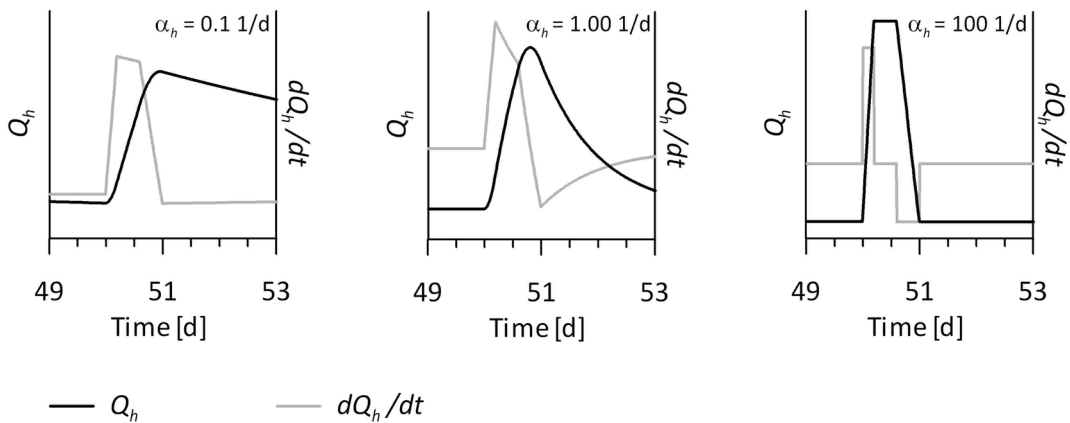


Figure 3.4: Influence of the recession coefficient  $\alpha_h$  on the spring hydrograph  $Q_h$  and its first derivative if recharge is into the highly permeable reservoir only. The corresponding recharge function is shown in Figure 3.3.

Figure 3.4 illustrates the influence of the recession coefficient of the highly permeable reservoir  $\alpha_h$  on the hydrograph and its first time derivative. It is found that the shape of the hydrograph is identical to that of the recharge function if the recession coefficient is very large ( $\alpha_h = 100$  1/d). This behaviour can be explained by eq. (3.8) because the relative weight of the first time derivative compared to  $Q_h$  decreases with increasing  $\alpha_h$ . Consequently if the recession coefficient

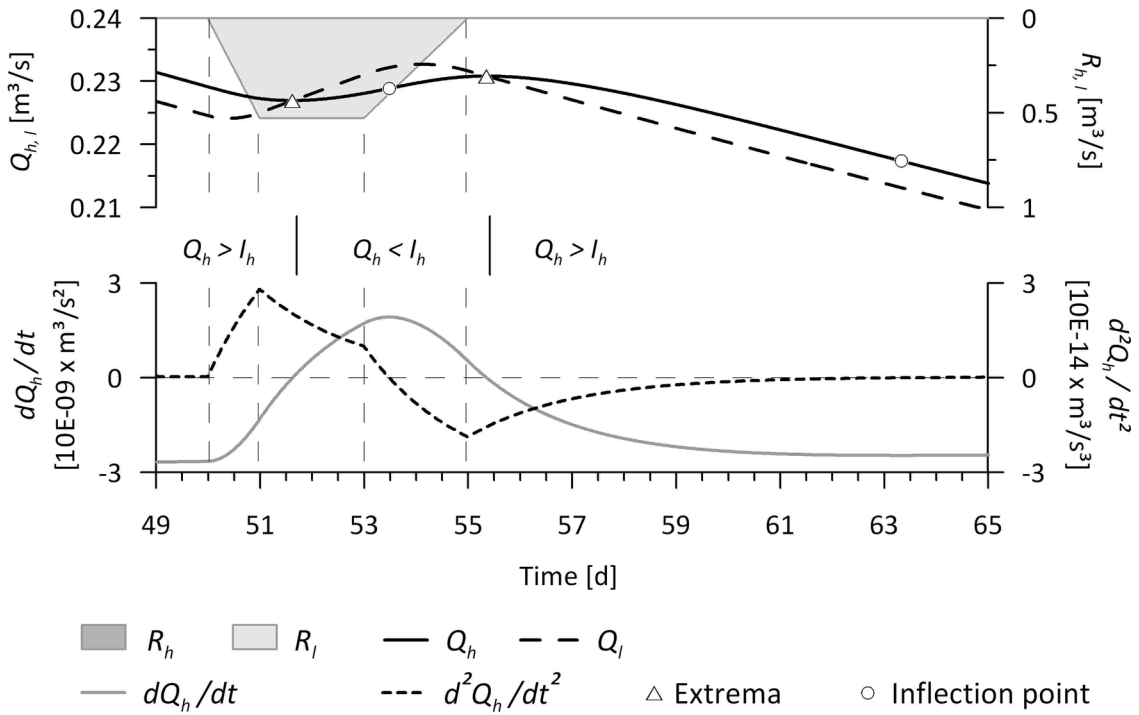


Figure 3.5: Simulation results with recharge into the low permeability reservoir only.

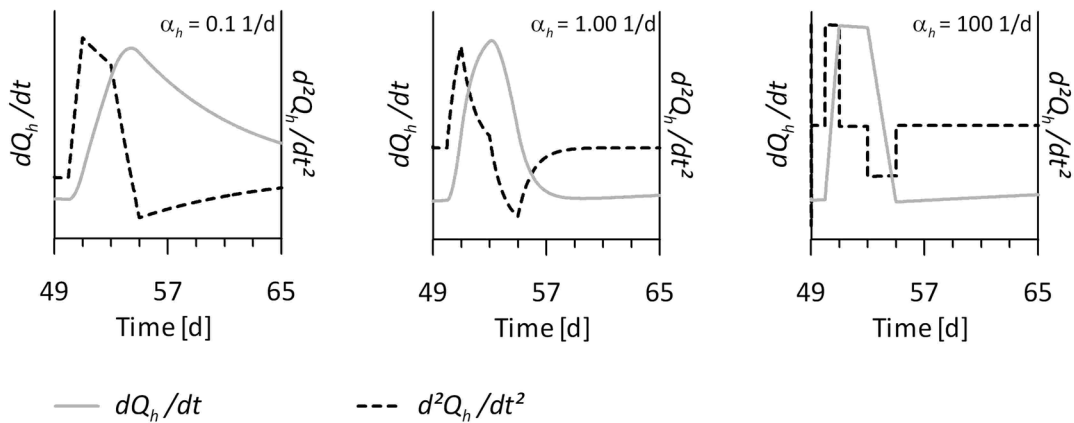


Figure 3.6: Influence of the recession coefficient  $\alpha_h$  on the first and second derivative of the spring hydrograph  $Q_h$  if recharge is into the highly permeable reservoir only. The corresponding recharge function is shown in Figure 3.5.

is very small, the shape of the first time derivative of the hydrograph is that of the recharge function. Between these extremes, the characteristics of the recharge pattern are distributed to both the hydrograph and its time derivative. If recharge is applied only to the low permeability reservoir, the shape of the first time derivative is different from that of the recharge function (Figure 3.5). Thus, the points of inflection in the hydrograph do not coincide with the maximum and the end of the recharge event. Yet, in the given example, the second time derivative of the

hydrograph reveals the properties of the recharge function. Similar to the aforementioned case, the graph can be more or less distorted, and depending on the value of  $\alpha_h$  the shape of the recharge function may resemble the first or the second time derivative of the hydrograph (Figure 3.6). It is noteworthy that the extreme points of the hydrograph shown in Figure 3.5 indicate the times when the outflow from the low permeability reservoir  $Q_l$  begins to exceed and falls below the spring hydrograph  $Q_h$ , i.e.  $Q_h < Q_l$  in the time period between hydrograph minimum and maximum.

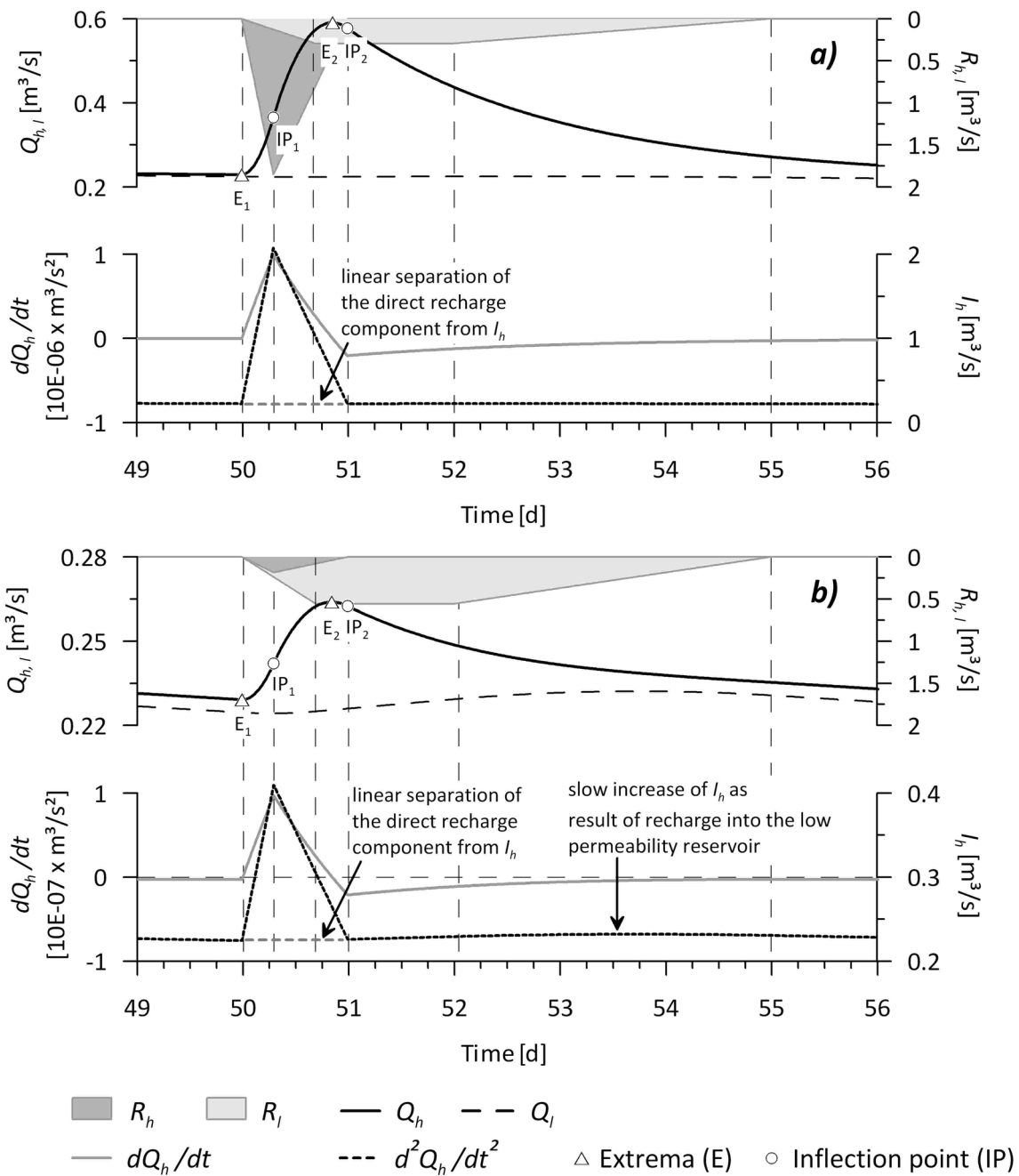


Figure 3.7: Simulation results with dual recharge function. The portion of the total recharge that is applied directly to the highly permeable reservoir amounts to 50% in a) and to 5% in b).

Figure 3.7 illustrates the effects of dual recharge into the two reservoirs. The portion of the total recharge that is applied directly to the highly permeable reservoir amounts to 50% in Figure 3.7a and to 5% in Figure 3.7b. In either case, the first derivative of the hydrograph yield the shape of the recharge function of the highly permeable reservoir. In contrast to the scenarios shown in Figures 3.5 and 3.6, the shape of the recharge function into the low permeability reservoir is difficult to obtain from the first and second time derivative because of the superposition of the dominating effects of direct recharge. The amplitude of the first time derivative after direct recharge, for example, is several orders of magnitude higher than the amplitude of the first time derivative after recharge into the low permeability reservoir (Figures 3.5 and 3.6). Thus, the short-term response of the spring appears to be mainly controlled by direct recharge into the highly permeable reservoir if the fraction of this recharge component is within the range suggested by field studies (e.g. Sauter 1992, Perrin et al. 2003). This is a direct consequence of the large difference in the recession coefficients of the two reservoirs and can be employed for the interpretation of the direct recharge component into the karst conduit system. A linear interpolation of  $I_h$  between the time of pre-event minimum  $t_{E1}$  and the time of inflection point  $t_{IP2}$  on the falling limb of the spring hydrograph, for example, provides an approximation of the direct recharge component for the parameter studies:

$$R_h \approx I_h(t) - I_h(t_{E1}) - (t - t_{E1}) \frac{I_h(t_{IP2}) - I_h(t_{E1})}{t_{IP2} - t_{E1}} \quad (3.10)$$

In the given examples, this procedure yields an estimation of nearly 100% of direct recharge for Figure 3.7a as well as for Figure 3.7b.

### 3.5 Case study

As a first application, two recharge events at the karst spring Gallusquelle (Swabian Alb, Germany) (Figure 3.8) are evaluated using the first time derivative of the spring hydrograph to calculate the temporal variation of inflow to the karst conduit system by eq. (3.8). The catchment area of spring Gallusquelle is ca. 45 km<sup>2</sup> and spring discharge  $Q_s = Q_h$  ranges between less than 0.1 m<sup>3</sup>/s and 2.5 m<sup>3</sup>/s with an annual average of approximately 0.5 m<sup>3</sup>/s. Sauter (1992) showed that the aquifer is unconfined, on average 20 m in thickness and contains a highly karstified zone. The karstified zone cuts across three different geological units consisting of bedded, marly, and massive upper Jurassic limestone. The fault zone Hohenzollern-graben (Figure 3.8) crosses the catchment from north-west to south-east and is of special interest for groundwater flow. Drilling investigations in the 1960s suggest that the catchment is bordered by

the southern fault zone of the graben. The northern fault zone is believed to be a preferential path way. A more detailed geological and hydrogeological description of the catchment is given by Sauter (1992, p. 4-27). The landscape of the catchment is characterised by dry valleys (Figure 3.8b). They are interpreted to be the result of formerly active watercourses, which dried up when the karstification level dropped below the river bottoms. Heinz et al. (2007) showed in a vulnerability case study that dry valleys act as fast infiltration path ways for wastewater in the catchment.

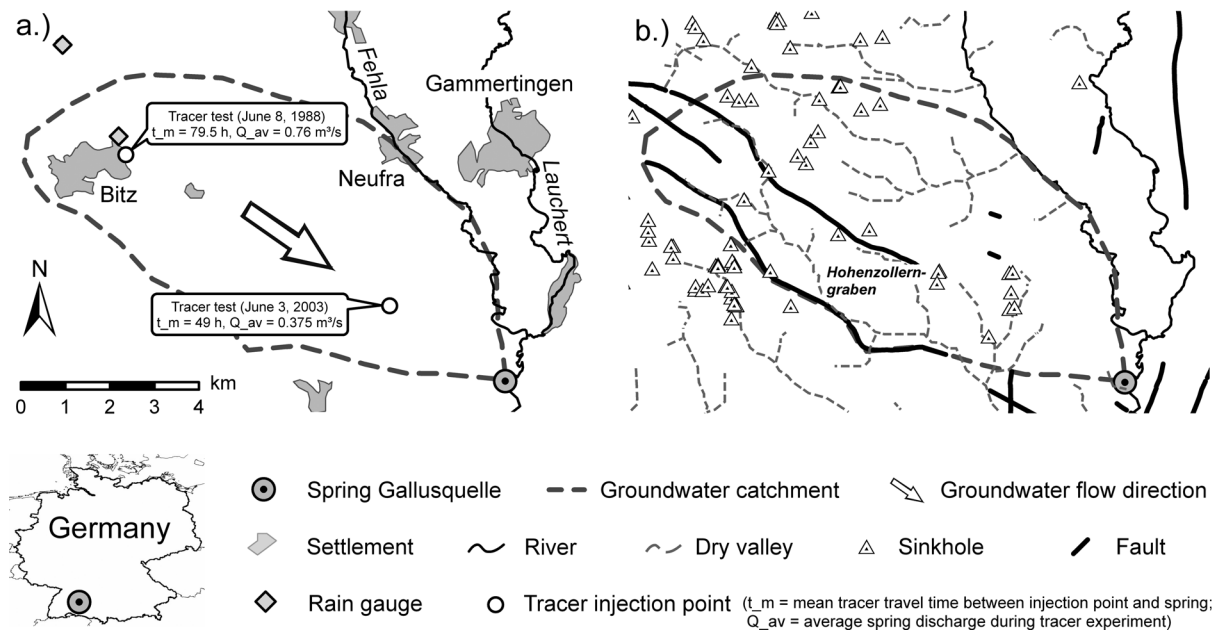


Figure 3.8: a) Location of Gallusquelle catchment (delineation according to Sauter (1992)); b) Distribution of dry valleys and sinkholes as features of direct recharge.

### 3.6 Determination of the recession coefficient for the conduit system

The only parameter required for the estimation of inflow into the conduit system is the recession coefficient of the highly permeable system of a karst aquifer (eqs. 3.8 and 3.9). Sauter (1992, p. 58) estimated a recession coefficient of  $\alpha_c = \alpha_h = 0.25$  1/d for the conduit system of the Gallusquelle catchment. His analysis is based on the estimation of recession coefficients from the spring hydrograph (eq. 3.7) for several events during two and a half years of observation. It is assumed that the highest evaluated recession coefficient corresponds to that of the conduit system.

The recession coefficient of a conduit system represented by a linear store can also be evaluated from the mean tracer travel time  $t_m$  obtained from artificial tracer tests. The mean tracer travel time is related to the conduit volume  $V_c = V_h$  via the relationship  $V_c = Q_s t_m$  with spring discharge



$Q_s = Q_h$  (Atkinson et al. 1973, Field 2002). The recession coefficient of the conduit system can be expressed as  $\alpha_c = Q_s/V_c$  and is therefore the reciprocal of the mean tracer travel time ( $\alpha_c = 1/t_m$ ). Geyer et al. (2007) conducted an artificial tracer test with an injection point at a distance of 3000 m to the spring (Figure 3.8). At an average spring discharge of 0.375 m<sup>3</sup>/s the mean tracer travel time amounted to 48.5 h yielding a water-filled conduit volume of 66,000 m<sup>3</sup> and thus a recession coefficient of  $\alpha_c = 0.5$  1/d. Sauter (1992, p. 49) reports a tracer test with a tracer injection point at a distance of 9800 m to the spring. At an average spring discharge of 0.76 m<sup>3</sup>/s peak concentration ( $\approx t_m$ ) was observed after 79.5 h yielding a water-filled conduit volume of 218,000 m<sup>3</sup> and thus a recession coefficient of  $\alpha_c = 0.3$  1/d. The difference between the estimated recession coefficients derived from the tracer tests can be explained by the difference in tracer travel distances determining tracer travel times within the conduit. Consequently, a tracer test conducted close to a spring yields a shorter tracer travel time and accordingly a higher recession coefficient than tracer tests conducted at large distances from a spring. Thus, recession coefficients calculated by recession analysis and tracer test results agree well.

### 3.7 Temporal recharge distribution from discharge events

The first recharge event examined here resulted from an intensive rainfall event during May 2003 (Figure 3.9). Water levels at the spring were measured every 10 minutes and transformed to spring discharge  $Q_s$  using a rating curve. Rainfall occurred over a time period of 16 hours with a sum of 23 mm and a maximum intensity of 6.9 mm/h. Spring discharge began to increase with a time lag of 4 hours after the maximum rainfall intensity, and after further 23.5 h maximum discharge was reached. The inflection points are estimated to occur 9.5 h and 33.3 h after discharge began to rise. The shape of first time derivative, which is believed to represent the shape of the inflow function of the highly permeable reservoir, resembles a triangle similar to those in Figure 3.7. The time derivative can be transformed to the inflow  $I_h$  using eq. (3.8). Figure 3.9 shows two results obtained with  $\alpha_h = 0.25$  1/d and  $\alpha_h = 0.5$  1/d. According with the results from the parameter studies, the shape of the curve with the higher  $\alpha_h$  is smoother and tends to be more similar to the spring hydrograph (Figure 3.4). For  $\alpha_h = 0.25$  1/d, derived from hydrograph analysis and an artificial tracer test covering the extent of the conduit system of the catchment,  $I_h$  has returned more or less to the pre-event value at the time of the inflection point on the falling limb (IP2 in Figure 3.9). This behaviour is comparable to that observed in the

above parameter studies (Figure 3.7). The total amount of direct recharge can be approximated by integration of eq. 3.10 between the time of pre-event minimum and the time of inflection point on the falling limb of the hydrograph. With the given catchment area, the direct recharge component amounts to 0.92 mm if  $\alpha_h = 0.25$  1/d and 0.45 mm if  $\alpha_h = 0.50$  1/d. Based on  $\delta^{18}O$  values in rainfall and spring water of the Gallusquelle, Sauter (1997) determined the fraction of the direct recharge component between 5% to 10%. With these values, the total amount of recharge can be estimated to range between 9.25 and 18.5 mm ( $\alpha_h = 0.25$  1/d) and between 4.5 and 9 mm ( $\alpha_h = 0.50$  1/d), which is reasonable in relation to the total amount of rainfall of 23 mm.

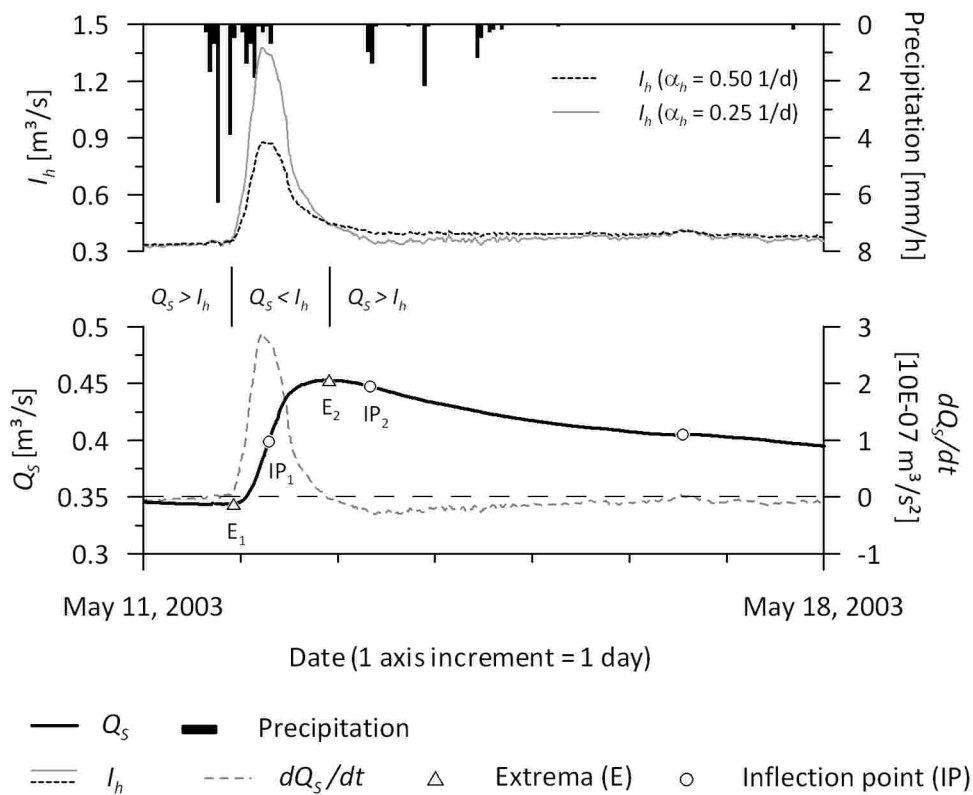


**Figure 3.9: Estimation of first derivative of spring discharge  $Q_s$  and total inflow into the conduit system after a recharge event caused by an intensive storm event.**

The second recharge event occurred after snowmelt caused by rising air temperature (Figure 3.10). As the air temperature exhibits a daily cycle with a minimum during the night (between 2 a.m. and 6 a.m.) and a maximum during the day (between 11 a.m. and 3 p.m.), it can be assumed that snowmelt, too, follows a daily cycle. The step-like shape of the rising limb of the spring hydrograph is in accordance with this idea, but the identification of the daily cycles is not straightforward. The first time derivative of the spring hydrograph, however, clearly indicates the daily cycles of recharge caused by snow melt. The maxima of the derivative are observed between 2 a.m. and 4 a.m. and the minima between 1 p.m. and 7 p.m. between March 17 and March 23,

2005. Figure 3.10 shows that  $I_h$  does not fully return to the initial value after one cycle, i.e. the cyclic behaviour is superimposed on a long-term rising trend. Thus, inflow to the highly permeable reservoir remained high. The source of this inflow can be the low permeability reservoir, which had been filled during the extended long-lasting melting period or a continuous direct recharge component.

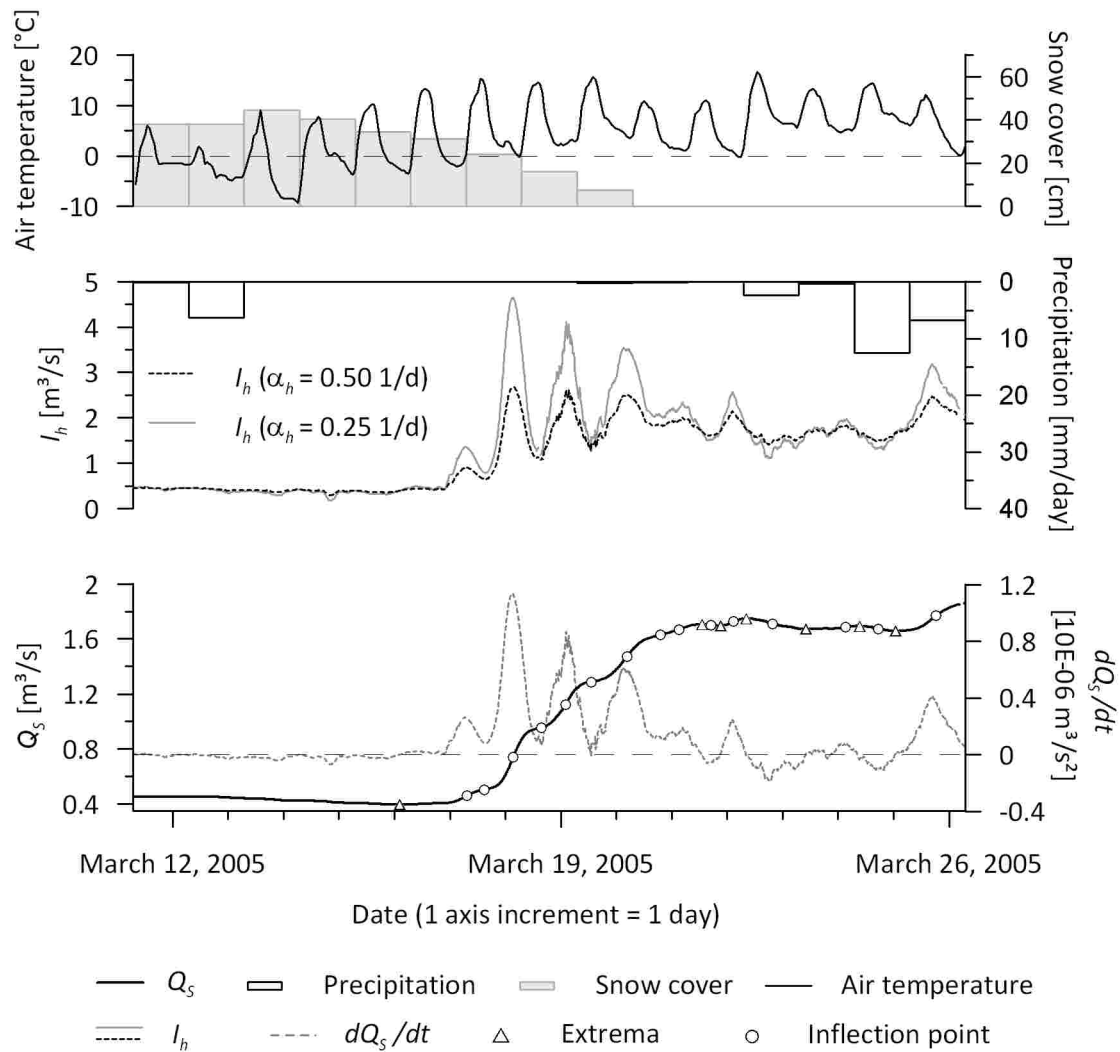


**Figure 3.10:** Estimation of first derivative of spring discharge  $Q_s$  and total inflow into the conduit system after a recharge event initiated by a snowmelt.

### 3.8 Discussion and conclusions

Our results show that time derivatives as well as extremes and inflection points of the spring hydrograph provide important information about the temporal distribution of recharge. The time derivatives reflect the temporal changes of inflow to and outflow from the reservoirs, which are determined by the recession coefficients. The recession coefficients depend on diffusivity (e.g.

Kovács et al. 2005), which controls the velocity with which a signal is transmitted through the system. For instance, a highly permeable conduit system that is entirely filled with water allows a nearly instantaneous transmission of pressure pulses to the spring and thus must have a very high recession coefficient. Field studies, e.g. by Sauter (1992), suggest that recession coefficients of karst conduit systems are one or several orders of magnitude higher than those of the fissured matrix blocks. Yet, our parameter studies demonstrate that these values are not large enough to allow a quasi-instantaneous transmission of recharge pulses. Thus, the spring hydrograph itself does not reveal the temporal recharge distribution. Instead, the first derivative of the spring hydrograph appears to be similar in shape to the recharge function of the conduit system.

The Gallusquelle case study illustrates how the temporal distribution of the direct, concentrated recharge into the conduit system can be identified using the first time derivative of the spring hydrograph. The shape of the recharge function of the conduit system identified for a recharge event caused by intense rainfall (Figure 3.9) is similar to the triangular function examined in the parameter study (Figure 3.7). According to the parameter study, it can be assumed that flow from the fissured matrix blocks, represented by the low permeability reservoir, contributes only little to the rapid response of the hydrograph. Thus, the increase of total inflow to the conduit system can mainly be attributed to direct, concentrated recharge. With this assumption a reasonable total amount of direct recharge into the conduit system is obtained, which agrees well with results obtained from the evaluation of isotope data. The methodology has further been applied to a recharge event caused by snowmelt. As a result of diurnal variations of the air temperature, a diurnal cycle of recharge into the conduit system can be expected. While this is not easily recognizable from the spring hydrograph, the evaluation of the first derivative of the spring hydrograph allows a clear identification of diurnal cycles in the recharge function. The hydrograph analysis further reveals an increasing trend superimposed on the diurnal cycles, which can be interpreted as a slow release of water recharged into the fissured matrix blocks or as continuous direct recharge component into the conduit system.

The accuracy of the determination of the amount and the temporal variation of direct recharge evidently depends on the magnitude of the recession coefficient of the conduit system. The karst conduit system manifests itself in the rapid transport of tracers. The recession coefficient of the conduit system can be obtained from tracer experiments. Tracer tests with injection points at large distances from the spring are more representative for the estimation of conduit recession coefficients because a large fraction of the entire conduit volume of an aquifer is considered. For the Gallusquelle catchment investigated here this independent estimation confirms the approximate value of the recession coefficient obtained by Sauter (1992) with long term hydrograph recession analysis. Thus, we are confident that the proposed methodology for estimation of temporal distribution of recharge is applicable to the Gallusquelle karst system. As

other field studies suggest similar recession coefficients of the conduit system (e.g. Forkasiewicz and Paloc 1967, Padilla et al. 1994), the methodology can very likely be transferred to other karst regions as well. In principle, all information needed for calculating the recharge function of the conduit system can be obtained from the spring hydrograph. Yet, if results from tracer tests are available, an independent estimation of the recession coefficient of the conduit system is advisable. It should further be noted that spring hydrographs might be affected by additional processes, such as spatially heterogeneous recharge, reversal of gradients between the different flow systems, or groundwater abstraction by pumping or evapotranspiration, none of which is taken into account in our approach. Thus, a careful inspection of measured hydrographs is required to identify any other disturbing factors that potentially impair the outcome of the analysis.

### 3.9 Appendix A

In the following, the integrals appearing in eqs. (3.3) and (3.4) are evaluated for a specific recharge pattern (Figure 3.11) to provide an example for the analytical model presented in section 2.1. Results given below were also used as a measure of comparison for the finite-difference scheme introduced in section 2.2

#### *Low permeability reservoir*

The water volume  $V_l(t)$  per unit surface area in the low permeability reservoir is given by eq. (3.3), which represents the general analytical solution of eq. (3.1). In our modelling studies, time-dependent recharge  $R_l(t)$  is estimated by a trapezoidal function:

$$R_l(t) = \begin{cases} 0 & 0 \leq t \leq t_{l1} \\ R_{le} \frac{t - t_{l1}}{t_{l2} - t_{l1}} & t_{l1} \leq t \leq t_{l2} \\ R_{le} & t_{l2} \leq t \leq t_{l3} \\ R_{le} \frac{t_{l4} - t}{t_{l4} - t_{l3}} & t_{l3} \leq t \leq t_{l4} \\ 0 & t_{l4} \leq t \end{cases} \quad (3-A1)$$

Times  $t_{l1}$  to  $t_{l4}$  with  $0 \leq t_{l1} < t_{l2} \leq t_{l3} < t_{l4}$  characterise the trapezoid as shown in the upper part of Figure 3.11. Subscript e stands for the maximum recharge as result of a precipitation event. By inserting eq. (3-A1) in eq. (3.3), the time-dependent water volume of the low permeability system  $V_l(t)$  can be expressed as:

$$V_l(t) = V_l(0)e^{-\alpha_l t} + \frac{R_{le}}{\alpha_l} \cdot \begin{cases} 0 & 0 \leq t \leq t_{l1} \\ \left[ \frac{t - t_{l1}}{t_{l2} - t_{l1}} - \frac{1 - e^{-\alpha_l(t-t_{l1})}}{\alpha_l(t_{l2} - t_{l1})} \right] & t_{l1} \leq t \leq t_{l2} \\ \left[ 1 - \frac{e^{-\alpha_l(t-t_{l2})} - e^{-\alpha_l(t-t_{l1})}}{\alpha_l(t_{l2} - t_{l1})} \right] & t_{l2} \leq t \leq t_{l3} \\ \left[ \frac{t_{l4} - t}{t_{l4} - t_{l3}} + \frac{1 - e^{-\alpha_l(t-t_{l3})}}{\alpha_l(t_{l4} - t_{l3})} - \frac{e^{-\alpha_l(t-t_{l2})} - e^{-\alpha_l(t-t_{l1})}}{\alpha_l(t_{l2} - t_{l1})} \right] & t_{l3} \leq t \leq t_{l4} \\ \left[ \frac{e^{-\alpha_l(t-t_{l4})} - e^{-\alpha_l(t-t_{l3})}}{\alpha_l(t_{l4} - t_{l3})} - \frac{e^{-\alpha_l(t-t_{l2})} - e^{-\alpha_l(t-t_{l1})}}{\alpha_l(t_{l2} - t_{l1})} \right] & t_{l4} \leq t \end{cases} \quad (3-A2)$$

$V_l(0)$  is the water volume of  $V_l(t)$  at the start of the simulation. It is introduced to simulate simple aquifer recession before groundwater recharge sets in (Figure 3.2).

### Highly permeable reservoir

According to Figure 3.11, the input signal for the highly permeable reservoir,  $R_h(t)$ , is approximated by a triangular function:

$$R_h(t) = \begin{cases} 0 & 0 \leq t \leq t_{h1} \\ R_{he} \frac{t - t_{h1}}{t_{h2} - t_{h1}} & t_{h1} \leq t \leq t_{h2} \\ R_{he} \frac{t_{h4} - t}{t_{h4} - t_{h3}} & t_{h3} \leq t \leq t_{h4} \\ 0 & t_{h4} \leq t \end{cases} \quad (3-A3)$$

with  $0 \leq t_{h1} < t_{h2} = t_{h3} < t_{h4}$ . The general analytical solution  $V_h(t)$  is given by eq. (3.4). In order to solve the integrals, it is necessary to specify a sequence of time levels consisting of the  $t_l$ 's and the  $t_h$ 's. Obviously, this can be done in many ways depending on the recharge pattern and it is

important to note that each sequence requires another strategy to successively solve the integrals in eq. (3.4). As an example, we consider the sequence  $0 < t_{h1} < t_{l1} = t_{h2} = t_{h3} < t_{h4} \leq t_{l2} \leq t_{l3} < t_{l4}$  (Figure 3.11) where the maximum recharge to the highly permeable system occurs at the onset of recharge to the low permeability reservoir. For this setting, seven cases have to be distinguished in order to evaluate eq. (3.4) according to the underlying sequence of time levels. In the following, the individual terms needed to calculate  $V_h(t)$  from eq. (3.4) are given for these cases.

Case 1:  $0 \leq t \leq t_{h1}$

Here,  $t^* = 0$ ,  $V_l^* = V_l(0)$ , and  $V_h^* = V_h(0) = 0$ .  $V_l(t)$  is given by the 1<sup>st</sup> line of eq. (3-A2). The two integrals appearing in eq. (3.4) equal 0, i.e.  $\int_0^t R_h(\tilde{t})e^{-\alpha_h(t-\tilde{t})}d\tilde{t} = 0$  and

$$\int_0^t R_l(\tilde{t})e^{-\alpha_l(t-\tilde{t})}d\tilde{t} = 0.$$

Case 2:  $t_{h1} \leq t \leq t_{l1} = t_{h2} = t_{h3}$

Now,  $t^* = t_{h1}$  and  $V_h^* = V_h(t_{h1})$  from Case 1.  $V_l(t)$  and  $V_l^* = V_l(t_{h1})$  are again obtained from the 1<sup>st</sup> line of eq. (3.2) as in Case 1. The integrals needed in eq. (3.4) are given by

$$\int_{t_{h1}}^t R_h(\tilde{t})e^{-\alpha_h(t-\tilde{t})}d\tilde{t} = \frac{R_{he}}{\alpha_h} \left[ \frac{t-t_{h1}}{t_{h2}-t_{h1}} - \frac{1-e^{-\alpha_h(t-t_{h1})}}{\alpha_h(t_{h2}-t_{h1})} \right] \text{ and } \int_{t_{h1}}^t R_l(\tilde{t})e^{-\alpha_l(t-\tilde{t})}d\tilde{t} = 0, \text{ resp.}$$

Case 3:  $t_{l1} = t_{h2} = t_{h3} \leq t \leq t_{h4}$

In this case,  $t^* = t_{h3}$  and  $V_h^* = V_h(t_{h3})$  from Case 2.  $V_l(t)$  and  $V_l^* = V_l(t_{h3})$  result from the 2<sup>nd</sup> line of eq. (3-A2). This leads to

$$\int_{t_{h3}}^t R_h(\tilde{t})e^{-\alpha_h(t-\tilde{t})}d\tilde{t} = \frac{R_{he}}{\alpha_h} \left[ 1 - e^{-\alpha_h(t-t_{h3})} \right] - \frac{R_{he}}{\alpha_h} \left[ \frac{t-t_{h3}}{t_{h4}-t_{h3}} - \frac{1-e^{-\alpha_h(t-t_{h3})}}{\alpha_h(t_{h4}-t_{h3})} \right] \text{ and}$$

$$\int_{t_{h3}}^t R_l(\tilde{t})e^{-\alpha_l(t-\tilde{t})}d\tilde{t} = \frac{R_{le}}{\alpha_l} \left[ \frac{t-t_{l1}}{t_{l2}-t_{l1}} - \frac{t_{h3}-t_{l1}}{t_{l2}-t_{l1}} e^{-\alpha_l(t-t_{h3})} - \frac{1-e^{-\alpha_l(t-t_{h3})}}{\alpha_l(t_{l2}-t_{l1})} \right]$$

Case 4:  $t_{h4} \leq t \leq t_{l2}$

Here,  $t^* = t_{h4}$  and  $V_h^* = V_h(t_{h4})$  from Case 3. The volumes  $V_l(t)$  and  $V_l^* = V_l(t_{h4})$  can again be

computed from the 2<sup>nd</sup> line of eq. (3-A2). Integration yields  $\int_{t_{h4}}^t R_h(\tilde{t})e^{-\alpha_h(t-\tilde{t})}d\tilde{t} = 0$  and

$$\int_{t_{h4}}^t R_l(\tilde{t})e^{-\alpha_h(t-\tilde{t})}d\tilde{t} = \frac{R_{le}}{\alpha_h} \left[ \frac{t-t_{l1}}{t_{l2}-t_{l1}} - \frac{t_{h4}-t_{l1}}{t_{l2}-t_{l1}} e^{-\alpha_h(t-t_{h4})} - \frac{1-e^{-\alpha_h(t-t_{h4})}}{\alpha_h(t_{l2}-t_{l1})} \right]$$

Case 5:  $t_{l2} \leq t \leq t_{l3}$

With  $t^* = t_{l2}$  we obtain  $V_h^* = V_h(t_{l2})$  from Case 4.  $V_l(t)$  and  $V_l^* = V_l(t_{l2})$  are now given by the

3<sup>rd</sup> line of eq. (3-A2). The integrals equal  $\int_{t_{l2}}^t R_h(\tilde{t})e^{-\alpha_h(t-\tilde{t})}d\tilde{t} = 0$  and

$$\int_{t_{l2}}^t R_l(\tilde{t})e^{-\alpha_h(t-\tilde{t})}d\tilde{t} = \frac{R_{le}}{\alpha_h} [1 - e^{-\alpha_h(t-t_{l2})}], \text{ resp.}$$

Case 6:  $t_{l3} \leq t \leq t_{l4}$

Now,  $t^* = t_{l3}$  and  $V_h^* = V_h(t_{l3})$  from Case 5. The 4<sup>th</sup> line of eq. (3-A2) allows to determine  $V_l(t)$

and  $V_l^* = V_l(t_{l3})$ . This results in  $\int_{t_{l3}}^t R_h(\tilde{t})e^{-\alpha_h(t-\tilde{t})}d\tilde{t} = 0$  and

$$\int_{t_{l3}}^t R_l(\tilde{t})e^{-\alpha_h(t-\tilde{t})}d\tilde{t} = \frac{R_{le}}{\alpha_h} [1 - e^{-\alpha_h(t-t_{l3})}] - \frac{R_{le}}{\alpha_h} \left[ \frac{t-t_{l3}}{t_{l4}-t_{l3}} - \frac{1-e^{-\alpha_h(t-t_{l3})}}{\alpha_h(t_{l4}-t_{l3})} \right].$$

Case 7:  $t_{l4} \leq t$

Here, we have  $t^* = t_{l4}$  and  $V_h^* = V_h(t_{l4})$  from Case 6.  $V_l(t)$  and  $V_l^* = V_l(t_{l4})$  are given by the 5<sup>th</sup>

line of eq. (3-A2). Both integrals needed in eq. (3.4) equal 0, i.e.  $\int_{t_{l4}}^t R_h(\tilde{t})e^{-\alpha_h(t-\tilde{t})}d\tilde{t} = 0$  and

$$\int_{t_{l4}}^t R_l(\tilde{t})e^{-\alpha_h(t-\tilde{t})}d\tilde{t} = 0.$$



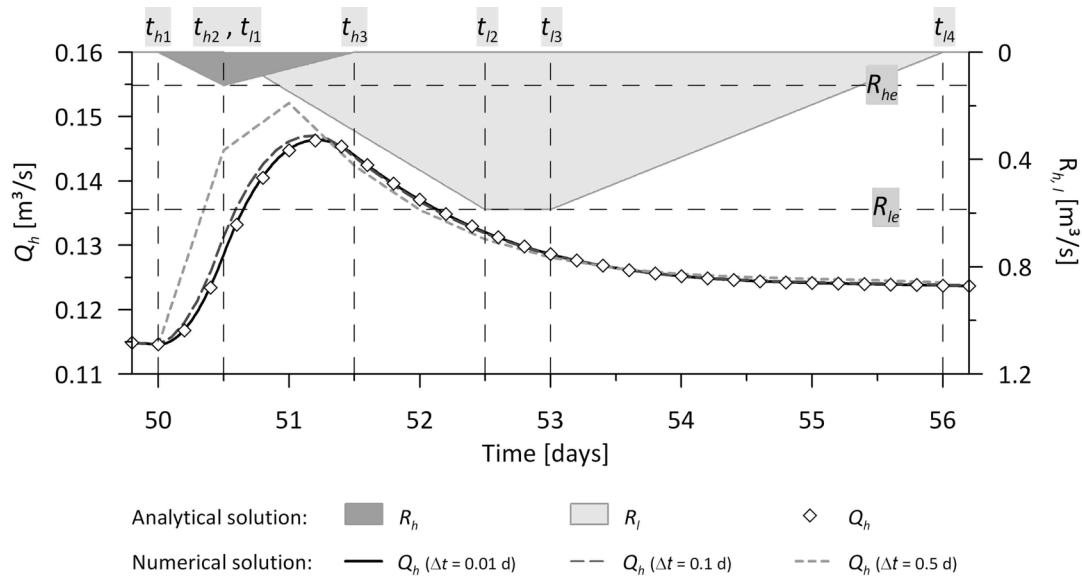


Figure 3.11: Comparison of analytical and numerical solution for the two-reservoir model.

## Acknowledgements

This work was funded by the Deutsche Forschungsgemeinschaft (DFG; German Research Foundation) under grants no. LI 727/11-1 and SA 501/24-1. Grateful acknowledgement is made to the staff of the water supply company Hermentingen / Swabian Alb.

## 3.10 References

- Atkinson, T.C., 1977. Diffuse and conduit flow in limestone terrain in the Mendip Hills, Somerset (Great Britain). *Journal of Hydrology* 35, 93-110.
- Atkinson, T.C., Smith, D.I., Lavis, J.J., Whitaker, R.J., 1973. Experiments in tracing underground waters in limestones. *Journal of Hydrology* 19, 323-349.
- Dreiss, S.J., 1983. Linear unit-response functions as indicators of recharge areas for large karst springs. *Journal of Hydrology* 61, 31-44.
- Eisenlohr, L., Király, L., Bouzelboudjen, M., Rossier, Y., 1997. Numerical simulation as a tool for checking the interpretation of karst spring hydrographs. *Journal of Hydrology* 193, 306-315.
- Field, M.S., 2002. The QTRACER2 program for tracer-breakthrough curve analysis for tracer tests in karstic aquifers and other hydrologic systems. EPA/600/R-02/001. Washington, D.C., 179 pp.
- Ford, D., Williams, P., 2007. *Karst hydrogeology and Geomorphology*. John Wiley & Sons Ltd., West Sussex, 562 pp.
- Forkasiewicz, J., Paloc, H., 1967. Le régime de tarissement de la Foux de la Vis étude préliminaire. In: *Proceedings of the Dubrovnik Symposium, October 1965, Hydrology of fractured rocks, Vol. 1*, 213-226.
- Geyer, T., Birk, S., Licha, T., Liedl, R., Sauter, M., 2007. Multi-tracer test approach to characterize reactive transport in karst aquifers. *Ground Water* 45 (1), 36-45.

- Halihan, T., Wicks, C.M., 1998. Modeling of storm responses in conduit flow aquifers with reservoirs. *Journal of Hydrology* 208, 82-91.
- Heinz, B., Birk, S., Liedl, R., Geyer, T., Straub, K., L., Bester, K., Kappler, A., 2007. Vulnerability of a karst spring to waste water infiltration (Gallusquelle, Southwest Germany). *Austrian Journal of Earth Sciences* 99, 11-17.
- Hergarten, S., Birk, S., 2007. A fractal approach to the recession of spring hydrographs. *Geophysical Research Letters* 34, L11401, doi:10.1029/2007GL030097.
- Hobbs, S.L., Smart, P.L., 1986. Characterisation of carbonate aquifers: A conceptual base. In: Graves, B.J., Lehr, J.H., Butcher, K., Crawford, N.C. (Eds.), *Proceedings of the Environmental Problems in Karst Terranes and their Solutions Conference*. Bowling Green, Kentucky, October, 28-30, 1986, 1-14.
- Jeannin, P.-Y., 2001. Modeling flow in phreatic and epiphreatic karst conduits in the Hölloch cave (Muotatal, Switzerland). *Water Resources Research* 37 (2), 191-200.
- Jeannin, P.-Y., Sauter, M., 1998. Analysis of karst hydrodynamic behaviour using global approach: a review. *Bulletin d'Hydrogéologie (Neuchâtel)* 16, 9-30.
- Jocson, J.M.U., Jenson, J.W., Contractor, D.N., 2002. Recharge and aquifer response: Northern Guam Lens Aquifer, Guam, Mariana Islands. *Journal of Hydrology* 260, 231-254.
- Jukić, D., Denić-Jukić V., 2004. A frequency domain approach to groundwater recharge estimation in karst. *Journal of Hydrology* 289, 95-110.
- Ketchum Jr., J.N., Donovan, J.J., Avery, W.H., 2000. Recharge characteristics of a phreatic aquifer as determined by storage accumulation. *Hydrogeology Journal* 8, 579-593.
- Király, L., 1998. Introduction à l'hydrogéologie des roches fissurées et karstiques, Bases théoriques à l'intention des hydrogéologues. Université de Neuchâtel, Manuscrit.
- Király, L., 2002. Karstification and Groundwater Flow. In: Gabrovšek, F. (Ed.), *Proceedings of the Conference on Evolution of Karst: From Prekarst to Cessation*. Postojna-Ljubljana, 155-190.
- Király, L., Morel, G., 1976: Etude de régularisation de l'Areuse par modèle mathématique. *Bulletin d'Hydrogéologie (Neuchâtel)* 1, 19-36.
- Kovács, A., Perrochet, P., Király, L., Jeannin, P.-Y., 2005. A quantitative method for the characterisation of karst aquifers based on spring hydrograph analysis. *Journal of Hydrology* 303, 152-164.
- Labat, D., Ababou, R., Mangin, A., 2000. Rainfall-runoff relations for karstic springs. Part I: convolution and spectral analyses. *Journal of Hydrology* 238 (3-4), 123-148.
- Lahey, B., Krothe, N.C., 1996. Stable isotopic variation of storm discharge from a perennial karst spring, Indiana. *Water Resources Research* 32 (3), 721-731.
- Maillet, E., 1905. *Essais d'hydraulique souterraine et fluviale*. Paris, 218 pp.
- Mangin, A., 1984. Pour une meilleure connaissance des systèmes hydrologiques à partir des analyses corrélatoire et spectrale. *Journal of Hydrology* 67, 25-43.
- Padilla, A., Pulido-Bosch, A., 1995. Study of hydrographs of karstic aquifers by means of correlation and cross-spectral analysis. *Journal of Hydrology* 168, 73-89.
- Padilla, A., Pulido-Bosch, A., Mangin, A., 1994. Relative importance of baseflow and quickflow from hydrographs of karst springs. *Ground Water* 32 (2), 267-277.
- Perrin, J., Jeannin, P.-Y., Zwahlen, F., 2003. Epikarst storage in a karst aquifer: a conceptual model based on isotopic data, Milandre test site, Switzerland. *Journal of Hydrology* 279, 106-124.
- Rushton, K.R., Ward, C., 1979. The estimation of groundwater recharge. *Journal of Hydrology* 41, 345-361.
- Sauter, M., 1992. Quantification and forecasting of regional groundwater flow and transport in a karst aquifer (Gallusquelle, Malm, SW. Germany). *Tübinger Geowissenschaftliche Arbeiten*, C13, 150 pp.
- Sauter, M., 1997. Differentiation of fast and slow flow components in a karst aquifer using the  $\delta^{18}\text{O}$  signature - Data analysis and modeling. In: Kranjc, A. (Ed.), *Tracer Hydrology* 97, Balkema, 435-441.
- Williams, P.W., 1983. The role of the subcutaneous zone in karst hydrology. *Journal of Hydrology* 61, 45-67.

## Chapter 4

# Multitracer test approach to characterise reactive transport in karst aquifers

Tobias Geyer<sup>1,4</sup>, Steffen Birk<sup>2</sup>, Tobias Licha<sup>1</sup>, Rudolf Liedl<sup>3</sup>, Martin Sauter<sup>1</sup>

Citation: Geyer, T., Birk, S., Licha, T., Liedl, R., Sauter, M., 2007. Multitracer test to characterize reactive transport in karst aquifers. *Ground Water* 45 (1), 36-45.

1 Geoscientific Centre, University of Göttingen, Goldschmidtstr. 3, D-37077 Göttingen, Germany

2 Institute for Earth Sciences, University of Graz, Heinrichstr. 26, A-8010 Graz, Austria

3 Institute for Groundwater Management, Dresden University of Technology, Karcherallee 8, D-01277 Dresden, Germany

4 Corresponding author - Phone: (49) 551 399398; Fax: (49) 551 399379; tgeyer@gwdg.de

## Abstract

A method to estimate reactive transport parameters as well as geometric conduit parameters from a multi-tracer test in a karst aquifer is provided. For this purpose, a calibration strategy was developed applying the two-region non-equilibrium model CXTFIT. The ambiguity of the model calibration was reduced by first calibrating the model with respect to conservative tracer breakthrough and later transferring conservative transport parameters to the reactive model calibration. The reactive transport parameters were only allowed to be within a defined sensible range to get reasonable calibration values. This calibration strategy was applied to breakthrough curves obtained from a large-scale multi-tracer test, which was performed in a karst aquifer of the Swabian Alb, Germany. The multi-tracer test was conducted by the simultaneous injection of uranine, sulforhodamine G, and tinopal CBS-X. The model succeeds to represent the tracer breakthrough curves (TBCs) of uranine and sulforhodamine G and verifies that tracer rock interactions preferably occur in the immobile fluid region, although the fraction of this region amounts to only 3.5% of the total water. However, the model failed to account for the long tailing observed in the TBC of tinopal CBS-X. Sensitivity analyses reveal that model results for the conservative tracer transport are most sensitive to average velocity and volume fraction of the mobile fluid region, while dispersion and mass transfer coefficients are least influential. Consequently, reactive tracer calibration allows the determination of sorption sites in the mobile and immobile fluid region at small retardation coefficients.

## 4.1 Introduction

Karst aquifers represent important water resources supplying an estimated 25% of the world's population with drinking water (Ford and Williams 1996, p. 6). However, these aquifers are highly vulnerable to contamination due to the fast infiltration and the rapid transport of pollutants in karst conduits. Effective strategies for the management and protection of karst water resources, therefore, must be based on reliable information about transport processes in karst conduit systems. Since boreholes are usually not directly connected to conduits, it is difficult to obtain hydraulic and geometric information on conduits from borehole testing. In contrast, surface features of karst systems, such as sinkholes and karst springs, are likely to be linked to the conduit system. Thus, tracer tests between sinkholes and karst springs provide a promising method for the quantitative characterization of conduit properties.

In early studies, Brown et al. (1969), Brown and Ford (1971), and Atkinson et al. (1973) demonstrated the potential of ground water tracing techniques to differentiate simple classes of conduit networks by ground water tracing. Later, Smart (1988) inferred a detailed structural model of a conduit system from a series of tracer tests.

The method of moments is frequently employed in the estimation of conservative tracer transport parameters (Field 2002). It yields estimates of mean tracer velocity and dispersion by evaluating the centre of mass and time-variance of a tracer breakthrough curve (TBC). However, TBCs of conservative tracers in karstified as well as fissured terranes often display strong tailings, which cannot adequately be explained by the one-dimensional (1D) advective-dispersive transport model (Maloszewski et al. 1998). This phenomenon can generally be described by diffusion between matrix and fissures (Sudicky and Frind 1982, Maloszewski and Zuber 1985, Witthüser et al. 2003) or flow channelling (Tsang and Tsang 1987, Tsang and Neretnieks 1998, Becker and Shapiro 2003). Maloszewski et al. (1992) introduced a multi-dispersion model with parallel flow paths of differing velocities and dispersivities to simulate TBCs in karstified systems. On the other hand, Field and Pinsky (2000) used a two-region non-equilibrium model with first-order mass transfer to describe the observed tailings of TBCs measured by tracer tests in karst conduits. This approach is based on tracer exchange between mobile and immobile fluid regions within the conduit and is also used to analyse tracer transport in porous media (e.g. Coats and Smith 1964, van Genuchten and Wierenga 1976), surface streams (e.g. Bencala and Walters 1983, De Smedt et al. 2005), and fractures (Raven et al. 1988). Field and Pinsky (2000) describe immobile fluid regions in karst conduits as a result of, e.g., vortices and eddies produced by conduit surface irregularities. This description was confirmed by three-dimensional (3D) computational fluid dynamics modelling (Hauns et al. 2001).

In addition to conservative transport processes, tracers and contaminants are often subject to reactive processes, which complicate the analysis of TBCs. Field and Pinsky (2000) demonstrated that the fraction of immobile water cannot be unambiguously identified by analysing a single TBC if the reactive transport parameters are unknown and vice versa. Reactive tracers, however, can provide useful information on reactive transport processes in karst conduits if multiple TBCs resulting from the simultaneous injection of both conservative and reactive tracers are analysed. Thus, based on the work by Field and Pinsky (2000), which introduced the application of the two-region non-equilibrium modelling approach to the analysis of single tracer tests in karst aquifers, the present work aims at the development of a multi-tracer test approach in order to reduce the ambiguity in model interpretation. Moreover, the methodology outlined in the following section is used to analyse a multi-tracer test conducted at a karst field site in southwest Germany.

## 4.2 Methodology

In this work, the uniaxial two-region non-equilibrium transport model implemented in the software CXTFIT2.1 (Toride et al. 1999) is used in the analysis of TBCs. The model approach assumes that the liquid phase in the conduit can be divided into a mobile and an immobile fluid region. Water in the immobile fluid region is assumed as stagnant relative to the water flowing in the mobile fluid region. Field and Pinsky (2000) provide an overview of possible immobile fluid regions in karst conduits. Thus, deposited sediments, for example, at the inside of meanders as well as dead-end passages will cause large immobile fluid regions. Furthermore, immobile fluid regions may also be a result of irregular cross sections, laminar boundary layers, and of the development of vortices and eddies, where water is not immediately displaced by plug flow along the karst conduit. The latter effect is also confirmed by Hauns et al. (2001), who simulated TBCs by different channel geometries with a three dimensional computational fluid dynamics code at laboratory scale. These authors demonstrated that substantial tracer mass is delayed in eddies and zones of slow flow and slowly released with time. This type of flow can also explain considerable tailing, which may sometimes erroneously be interpreted as matrix diffusion.

The corresponding conceptual model is illustrated in Figure 4.1. The flow velocity is highest along the centre line of the conduit and decreases towards the conduit wall. Flow in karst conduits is often turbulent, with the turbulent core separated from the conduit wall by a laminar boundary layer. However, if the laminar layer collapses due to considerable surface roughness of the walls, the conduit behaves as a completely rough pipe (White 1988, p. 164) and the mobile fluid region is in direct contact with the conduit wall. Large surface roughness in karst conduits can result from scallops, sediments on cave floors, and surface coatings (Field 2002, p. 45).

Solute transport processes considered in this work include advection, dispersion, mass transfer between mobile and immobile zones, reversible interactions between tracers and rock surfaces, e.g. sorption, and tracer degradation. The corresponding equations of the 1D two-region non-equilibrium model are (modified from Van Genuchten and Wagenet 1989, Field and Pinsky 2000):

$$\beta R \frac{\partial c_m}{\partial t} = D \frac{\partial^2 c_m}{\partial x^2} - v \frac{\partial c_m}{\partial x} - \alpha(c_m - c_{im}) - \theta_m \mu_l c_m \quad (4.1)$$

$$(1 - \beta)R \frac{\partial c_{im}}{\partial t} = \alpha(c_m - c_{im}) - \theta_{im} \mu_l c_{im} \quad (4.2)$$

with the retardation coefficient given as:

$$R = 1 + \frac{A}{V} K_a \quad (4.3)$$

and the coefficient of partitioning between mobile and immobile fluid regions:

$$\beta = \frac{\theta_m + f(R - 1)}{R} \quad (4.4)$$

where  $t$  is time,  $x$  is space coordinate,  $D$  is dispersion coefficient,  $v$  is average velocity,  $\alpha$  is first-order mass transfer coefficient,  $K_a$  is the linear distribution coefficient given as tracer mass per unit surface area of the solid phase and unit concentration in the conduit,  $A/V$  is the ratio of conduit surface area and conduit volume,  $f$  is the fraction of sorption sites that equilibrates with the mobile water, and  $c_m$  and  $c_{im}$  are the respective solute concentrations in the mobile and immobile fluid region.  $\theta_m$  and  $\theta_{im}$  are volume fractions of the mobile and immobile fluid regions, which add up to the total volumetric water content of the fully saturated conduit  $\theta = \theta_m + \theta_{im} = 1$ .  $\mu_l$  is a first-order degradation coefficient in the liquid phase of mobile and immobile fluid regions and is assumed to be equal in both regions. However, Van Genuchten and Wagenet (1989) present also analytical solutions for degradation at equal or differing rates in liquid and sorbed phases.

CXTFIT2.1 provides analytical solutions to the above equations for several types of input functions. In this work, a Dirac pulse representing an instantaneous tracer injection was used, i.e. it has been assumed that the tracer injection period is negligible compared to the observed tracer travel time.

Eq. (4.4) can be simplified for a conservative tracer by setting  $R = 1$ , thus yielding  $\theta_m = \beta$  and  $\theta_{im} = 1 - \beta$ . In this case, model calibration yields estimates for transport parameters  $v$ ,  $D$ ,  $\alpha$ , and

$\theta_m$ . As illustrated by Figure 4.1, the mass transfer between mobile and immobile fluid regions is dominated by advective processes (eddies and vortices) rather than diffusive processes (Field and Pinsky 2000, Hauns et al. 2001, Raven et al. 1988). Therefore, the mass transfer coefficient  $\alpha$  along with  $v$  and  $D$  can be assumed to be independent of physico-chemical properties of the tracers and is thus identical for all tracers. Consequently, the values of  $v$ ,  $D$  and  $\alpha$  obtained for the conservative tracer were preset when calibrating the model to the TBCs of the reactive tracers, leaving only  $R$ ,  $\beta$ , and, if the model accounts for tracer degradation,  $\mu_i$  as adjustable parameters.

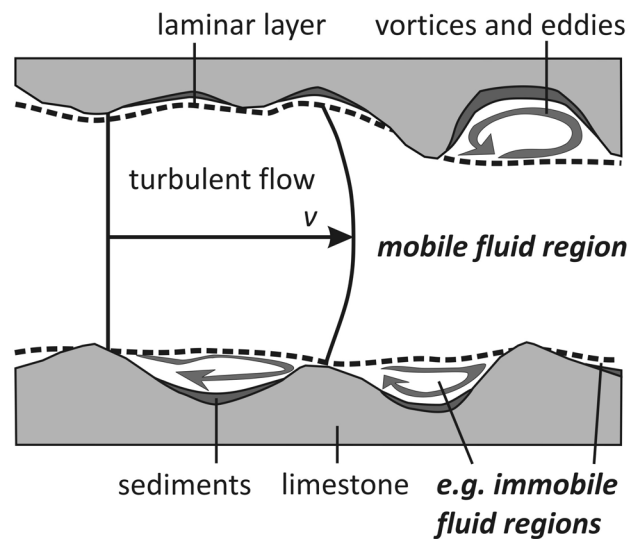


**Figure 4.1: Conceptual model of the geometry and the flow within a karst conduit.**

CXTFIT2.1 may be used for forward as well as inverse modelling. In this study, initial values for calibration of  $v$  and  $D$  are derived from centre of gravity and Chatwin method (Field 2002). Initial estimates for  $\alpha$  are generally not possible but reasonable initial estimates for  $\theta_m$  may be obtained from the ratio between mean tracer velocity and peak velocity (Field and Pinsky 2000). Reactive parameter calibration starts from conservative parameter calibration with  $\beta = \theta_m$ ,  $R = 1$ , and  $\mu_i = 0$ .

Using the resulting  $R$  and  $\beta$  obtained from the reactive tracer analysis, together with the volume fraction of mobile water  $\theta_m$  from the conservative tracer analysis, allows the calculation of the fraction of sorption sites  $f$  equilibrating with the mobile water:

$$f = \frac{\beta R - \theta_m}{R - 1} \quad (4.5)$$

Eq. (4.5) only applies to reactive ( $R > 1$ ) but not to conservative transport ( $R = 1$ ), where the parameter  $f$  is meaningless. The fraction of sorption sites  $f$  that equilibrate with the mobile water



can be used for a simple validation of the calibrated reactive transport parameters, as it can only have physically reasonable values between 0 and 1. Inserting these limits into eq. (4.4) yields the following constraints on  $\beta$ :

$$\frac{\theta_m}{R} \leq \beta \leq 1 - \frac{\theta_{im}}{R} \quad (4.6)$$

The retardation coefficient  $R$  defined by eq. (4.3) depends on the conduit surface-volume ratio  $A/V$  and the distribution coefficient  $K_a$ . Neglecting matrix-conduit exchange (Birk et al. 2005), an upper bound of the conduit volume between injection location and spring can be estimated from  $V = \bar{Q} t_m$  (e.g. Sauter 1992, Field and Nash 1997), where  $\bar{Q}$  is the mean spring discharge and  $t_m = L/v$  the mean tracer residence time ( $L =$  travel distance,  $v =$  calibrated average velocity). With known travel distance a diameter  $a$  of a cylindrical conduit can be calculated and an estimate of  $A/V = 4/a$  can be obtained. As the total conduit volume may be composed of several conduits, the actual conduit diameter  $a$  of the individual conduit is likely to be smaller. Solving eq. (4.3) for the distribution coefficient  $K_a$  and inserting the estimated  $A/V$  yields an upper bound on the actual  $K_a$ :

$$K_a \leq \frac{R-1}{A/V} \quad (4.7)$$

If independent and reliable estimates of  $K_a$  were available (e.g. from lab experiments) the above-suggested methodology could be slightly modified by solving eq. (4.3) for  $A/V$  instead of  $K_a$ , thereby providing more accurate estimates of conduit surface-volume ratios.

### 4.3 Field site

In order to test the applicability of the above-outlined methodology, a multi-tracer experiment was performed within the Gallusquelle catchment, situated on the Swabian Alb, a NE-SW striking low mountain range in southwest Germany (Figure 4.2). Sauter (1992) estimated the catchment area to be 45 km<sup>2</sup>. Dry valleys characterize the catchment's landscape. They are interpreted to be the result of formerly active water courses, which dried up when the karstification level dropped below the river bottoms. The catchment is geologically and hydrogeologically well studied including borehole investigations (drilling, slug tests), piezometric surface mapping, and previous ground water tracing (Birk et al. 2005, Sauter 1992, Sauter 1995). Drilling investigations in the 1960s suggest that the saturated karst aquifer is on average 20 m in thickness and contains a highly karstified zone, which does not follow any stratigraphical boundary and cuts across three

different geological units consisting of bedded, marly and massive Upper Jurassic limestone. The catchment is bounded by the southern fault zones of the Hohenzollerngraben in the southwest and the Fehla river in the northeast. A ground water divide in the northwest forms the northern boundary. The discharge at the spring (Gallusquelle) ranges from less than  $0.1 \text{ m}^3/\text{s}$  to  $2.5 \text{ m}^3/\text{s}$  with an annual average of approximately  $0.5 \text{ m}^3/\text{s}$ . However, some water is likely to flow below the gauging station. Estimates for this flow component range from less than  $0.05 \text{ m}^3/\text{s}$  to  $0.2 \text{ m}^3/\text{s}$  (Sauter 1992).

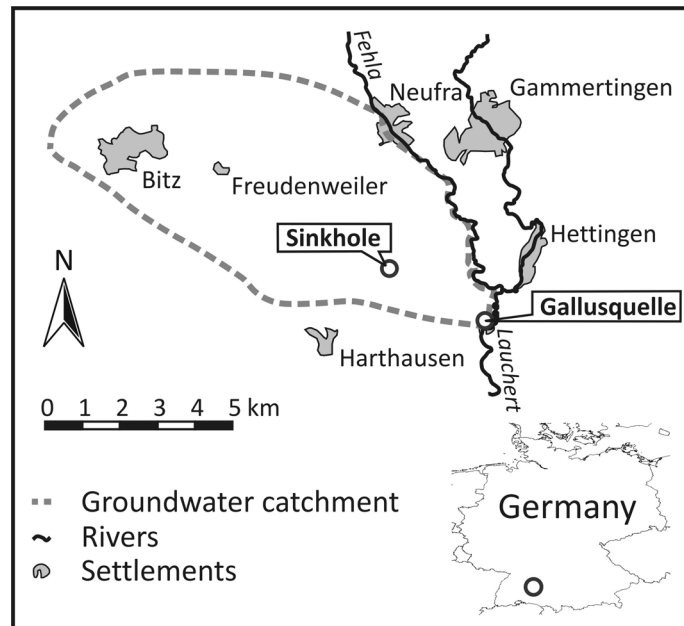


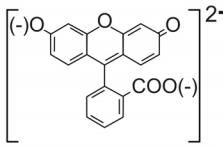
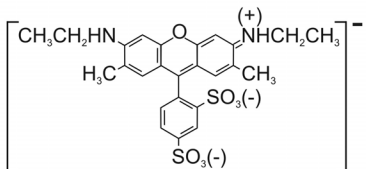
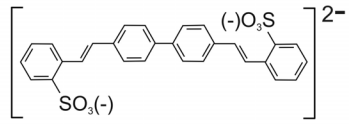
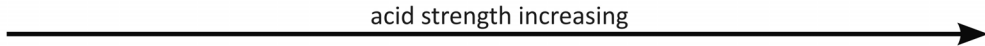
**Figure 4.2: General map of Gallusquelle catchment showing the tracer injection point (sinkhole) (from Birk et al. 2005).**

#### 4.4 Tracer selection

The selection of tracers was based on a literature review as well as the chemical structure of the tracers. Furthermore, it was presupposed that the tracers can be measured simultaneously on-site with low detection limits to get smooth TBCs with a high resolution in time and concentration. This limits the choice of tracers to certain fluorescent dyes. The number of applicable fluorescent dye tracers in ground water is small. Käss (1998) and Flury and Wai (2001) provide a global review and summary of previous work with fluorescent dye tracers. Generally, dye tracers are organic molecules with one or more ionic functional groups (e.g. sulfonic groups). Kasnavia et al. (1999) discuss the importance of interactions between fluorescent dyes and oppositely charged mineral surfaces. Their results reinforce the observation of Sabatini and Austin (1991) and Shiau et al. (1993) that, except for extreme pH conditions, fluorescent dye sorption is dominated by ion exchange rather than partitioning into organic matter. Sabatini (2000) presents sorption studies

of uranine and sulforhodamine B on natural aquifer materials. His results show that uranine, with one weak acidic negative carboxylic group, sorbs much less than sulforhodamine B, with two strong acidic negative sulfonic groups, onto positively charged limestone surfaces. Since sulforhodamine B is considered as hazardous in Germany (Behrens et al. 2001), environmental compatible fluorescent dyes with similar chemical structure were selected as reactive tracers, namely sulforhodamine G ("amidorhodamine G") with one and tinopal CBS-X with two sulfonic groups. Due to an increase in acid strength from uranine to tinopal CBS-X, retardation by ion exchange of the selected tracers with positively charged mineral surfaces increases in that order (Table 4.1). Thus, uranine is regarded as a conservative tracer, while sulforhodamine G and tinopal CBS-X must be considered reactive (Behrens 1986).

**Table 4.1: Chemical structure of the selected fluorescent dyes (modified after Behrens 1986, Field 2002).**

Name	Uranine	Sulforhodamine G	Tinopal CBS-X
Chemical formula	$C_{20}H_{10}O_5Na_2$	$C_{25}H_{26}N_2O_7S_2Na$	$C_{28}H_{20}O_6S_2Na_2$
Structural formula (salts)			
			

## 4.5 Multitracer experiment

A sinkhole 3 km northeast of the Gallusquelle was selected as tracer injection location (Figure 4.2), primarily confirmed to be connected to the spring (Birk et al. 2005). Water-table measurements in two boreholes 1.0 and 1.5 km northeast of the sinkhole suggest a thickness of the unsaturated zone in the order of 100 m.

Conservative (uranine) and reactive tracers (sulforhodamine G, tinopal CBS-X) were simultaneously injected into the sinkhole on June 3<sup>rd</sup>, 2003. Prior to tracer injection, the sinkhole was flushed with approximately 108 m<sup>3</sup> of water over a time period of nearly 6 hours to minimize the influence of the unsaturated zone. Immediately before the injection, 750 g uranine, 750 g sulforhodamine G, and 1500 g tinopal CBS-X were mixed in a 1 m<sup>3</sup> barrel. After the tracer injection, flushing was continued for another 4.5 hours with approximately 77 m<sup>3</sup> of water to force the tracer mixture into the saturated conduit system.

Tracer concentrations in spring water were measured during a time period of three weeks using a field spectrofluorometer GGUN-FL30 manufactured by the University of Neuchâtel (Schneegg 2002). The lowest measurable concentration in the spring water was 0.02 µg/L for uranine, 0.25 µg/L for sulforhodamine G, and 0.7 µg/L for tinopal CBS-X. A matrix-adjusted simultaneous calibration of the fluorometer ensured the quality of the data. Measurement intervals with the fluorometer varied between one and five minutes, depending on the observed tracer breakthrough. For calibration and sensitivity analysis, recorded concentrations were interpolated to intervals of three minutes during the entire breakthrough.

As a main result, evidence for reactive tracer transport by surface interactions is given by the retardation of the peak concentrations of the reactive tracers. The uranine peak arrived first, followed by sulforhodamine G after 25 minutes, and tinopal CBS-X after 45 minutes.

Spring discharge during the tracer breakthrough, derived from water level measurements in the stream using a water-level discharge rating curve, amounts to approximately 0.375 m<sup>3</sup>/s. Based on this discharge, the recovery during the measurement period of the conservative tracer uranine (determined with zero moment analysis) amounts to 72% with respect to the injected mass. The reactive tracers sulforhodamine G and tinopal CBS-X exhibit lower recoveries with 41% and 46%, respectively (Figure 4.3). The total recoveries of uranine and sulforhodamine G were reached at approximately 100 hours, whereas tinopal CBS-X exhibits a long flat tailing of up to 400 hours. The mass loss of the conservative tracer uranine can possibly be explained by discharge measurement errors or the aforementioned ungauged discharge below the weir. However, uranine recovery is 22% lower than in a tracer test in the same sinkhole one month earlier (Birk et al. 2005). There are several reasons explaining the different tracer recovery: (1) the accuracy of the discharge estimation is approximately ±0.02 m<sup>3</sup>/s, (2) the area surrounding the weir was cleared of weeds, which somewhat changed the discharge measurements between the tracer tests, (3) possible tracer loss in the unsaturated zone, (4) the proportion of flow below the weir likely increase with lower discharge (Sauter 1992). In order to account for the apparent mass loss of uranine, the injected mass in the model was set equal to the actual recovered mass. One likely cause for the additional losses of the reactive tracers is irreversible surface complexation (Vasudevan et al. 2001). In addition, precipitation losses of tinopal CBS-X might have occurred due to the low solubility in water in the presence of hardening agents (e.g. calcium) (Käss 1998, p. 51). To keep the model less complex, additional mass losses of the reactive tracers were accounted for by using the recovered masses as injected tracer masses. Tracer transport simulation with first-order degradation in the liquid phase of the conduit (eqs. 4.1, 4.2) was also tested. In this case, the injected mass in the model of the respective reactive tracer was corrected for, based on the percentage mass loss observed in the conservative uranine TBC.

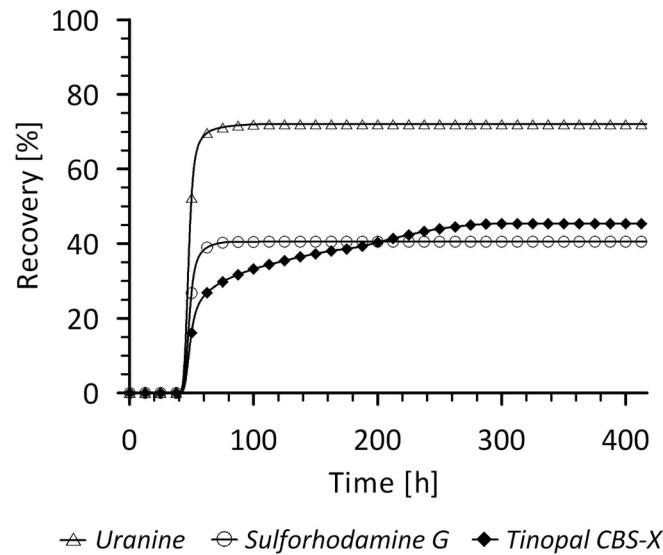


Figure 4.3: Tracer recovery with time.

## 4.6 Modelling results

Calibrating the conservative tracer model to the observed TBC of uranine yielded good agreement between measured and fitted concentrations (Figure 4.4). The resulting parameter estimates are listed in Table 4.2. With the assumed travel distance  $L$  of 3000 m between sinkhole and spring, a velocity  $v$  of  $1.71 \cdot 10^{-2}$  m/s, and a dispersion coefficient  $D$  of  $7.3 \cdot 10^{-2}$  m<sup>2</sup>/s, a Péclet number  $Pe = vL/D$  of approximately 700 is calculated. This high Péclet number clearly indicates advection-dominated transport, which agrees well with the conceptual model of rapid transport through a karst conduit. According to Jakowski and Ebhardt (1997), Péclet numbers larger than 100 are typically found within maturely karstified aquifers of the middle Swabian Alb, which the Gallusquelle catchment is part of. The resulting volume fraction of the mobile water  $\theta_m$  (96.5%) is slightly higher, and the mass transfer coefficient  $\alpha$  ( $2.5 \cdot 10^{-6}$  1/s) is slightly lower than the corresponding values reported by Field and Pinsky (2000) for tracer tests in several karst aquifers. Neglecting the flow below the gauging station, the estimated conduit volume between injection location and spring is approximately 66,000 m<sup>3</sup>, which can be transformed into a corresponding equivalent diameter of a circular conduit of  $a = 5.3$  m. This agrees well with results from an earlier single-tracer test with uranine (Birk et al. 2005).

Model calibration to the TBC of the reactive tracer sulforhodamine G also showed good agreement between measured and simulated concentrations (Figure 4.4) with respect to peak concentration and tailing. As a consequence, a retardation coefficient  $R = 1.021$  is obtained (Table 4.2). The resulting  $\beta$  lies well within the physically reasonable range defined by eq. 4.6 ( $0.9453 \leq \beta \leq 0.9659$ ) giving confidence in the validity of the model. Applying eq. 4.5 yields a

fraction of the total surface area that equilibrates with the mobile water  $f = 0.41$ . Thus, the assumption of negligible tracer-rock surface interactions in the mobile fluid region (Field and Pinsky 2000) is not justified here. Nevertheless, tracer-rock surface interactions appear to occur preferably within the immobile fluid region. Although the conduit volume fraction of the immobile fluid region  $\theta_{im}$  amounts to only 3.5%, it accounts for 59% of the total conduit surface area available for tracer-conduit surface interactions.

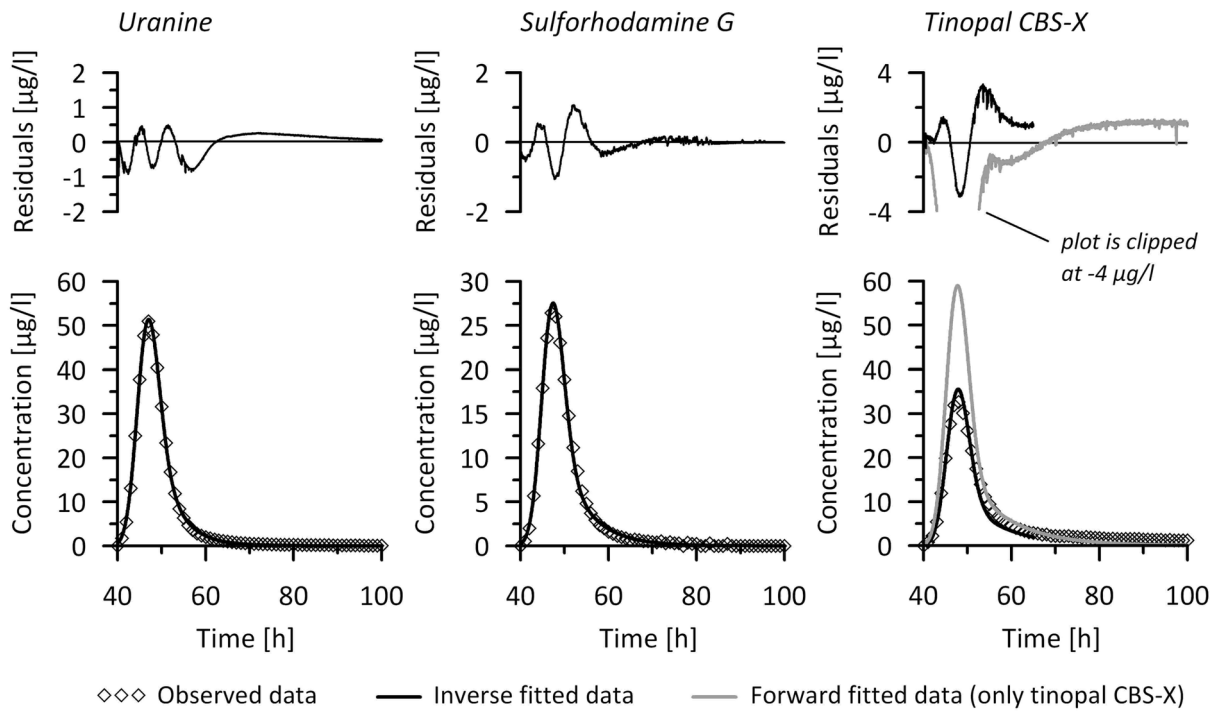


**Figure 4.4:** TBCs resulting from transport simulations based on the physical non-equilibrium model. The diamonds for observed data represent every twentieth measurement point. Residuals represent observed minus fitted concentrations. Note that for tinopal CBS-X the grey curve was fitted by manual calibration taking into account the completely recovered mass and the black curve was fitted under consideration of the recovered mass after 65 hours (see chapter modelling results).

While CXTFIT succeeded in calibrating the model to the TBCs of uranine and sulforhodamine G, the automated calibration failed to converge when applied to the TBC of tinopal CBS-X. Therefore, the model was manually calibrated (forward modelling). Attempts to calibrate the peak time and the pronounced tailing (Figure 4.3) of tinopal CBS-X failed. Thus, it was attempted to obtain the best possible match of peak time and shape of the peak breakthrough. Considering the totally recovered tracer mass, the simulated concentrations of tinopal CBS-X are significantly higher than the measured concentrations for the first 70 hours and later dropped below the measured concentrations (Figure 4.4). Thus, the model is clearly not capable of reproducing the observed tailing. In a further attempt, the observation period and accordingly the injected model mass (Table 4.2) was tentatively reduced until CXTFIT succeeded in fitting model results to the

TBC of tinopal CBS-X. This was the case for an observation period of 65 hours (Figure 4.4), suggesting that at later times the process causing the tailing becomes dominant over the processes considered in the model. Parameter estimates of the retardation factor  $R$  and the partitioning coefficient  $\beta$  resulting from manual calibration to the entire observation period and automated calibration to a time period of 65 hours are similar (Table 4.2). Note, that the coefficients of determination between both fits and the observed data are also similar. However, it should be emphasized that these estimates must be interpreted with great care, since both models fail to reproduce the tailing in the TBC of tinopal CBS-X.

**Table 4.2: Parameter estimates resulting from physical non-equilibrium modelling. Results of model calibration are displayed in italics, fixed model parameters are underlined. Note that for tinopal CBS-X the values in parentheses are obtained by truncation of the long flat tailing after 65 h of tracer observation.  $K_a$  and  $f$  are estimated from the modelling parameters according to eqs. 4.5 and 4.7.**

Tracer	Uranine	Sulforhodamine G	Tinopal CBS-X
$v$ [m/s]	1.71 <sup>-2</sup>	<u>1.71</u> <sup>-2</sup>	<u>1.71</u> <sup>-2</sup>
$D$ [m <sup>2</sup> /s]	7.31 <sup>-2</sup>	<u>7.31</u> <sup>-2</sup>	<u>7.31</u> <sup>-2</sup>
$\alpha$ [1/s]	2.51 <sup>-6</sup>	<u>2.51</u> <sup>-6</sup>	<u>2.51</u> <sup>-6</sup>
$\beta$ [-]	0.9652	0.9538	0.9300 (0.9356)
$R$ [-]	<u>1.000</u>	1.021	1.060 (1.053)
$K_a$ [m]	0	0.028	0.079 (0.070)
$f$ [-]	0	0.41	0.34 (0.38)
$\rho^2$	0.9997	0.9990	0.9912 (0.9936)
RMSE [ $\mu\text{g/l}$ ]	0.213	0.213	3.18 (1.06)
$m_m$ [g]	<u>540</u>	<u>304</u>	<u>690</u> (413)
$m$ [g]	750	750	1500

( $v$  = average velocity,  $D$  = dispersion coefficient,  $\alpha$  = mass transfer coefficient,  $\beta$  = partitioning coefficient,  $R$  = retardation factor,  $K_a$  = linear distribution coefficient,  $f$  = fraction of the surface area that equilibrates with the mobile water,  $m_m$  = tracer injection mass in the model,  $m$  = mass of tracer injected into the sinkhole,  $\rho^2$  = coefficient of determination, RMSE = root mean square error)

Nevertheless, the distribution coefficient  $K_a$  determined for tinopal CBS-X is fully in accordance with the beforehand expected reactivity trend of the tracers (acid strength), as it is between two to three times that of sulforhodamine G (Table 4.1). Comparable to sulforhodamine G, the resulting values of  $\beta$  are well within the physically reasonable range ( $0.9166 \leq \beta \leq 0.9670$ ) defined

by eq. 4.6. The corresponding fraction of the total surface area equilibrating with the mobile water  $f$  amounts to 38% for tinopal CBS-X (65h observation period), which is reasonably close to the value resulting from the analysis of the TBC of sulforhodamine G. The introduction of a first-order tracer degradation coefficient (eqs. 4.1, 4.2) to account for mass losses by the postulated surface complexation and tracer precipitation yielded almost identical results for sulforhodamine G ( $R = 1.024$ ,  $f = 0.43$ ,  $\mu_l = 0.012$  1/h). In case of tinopal CBS-X ( $R = 1.1$ ,  $f = 0.24$ ,  $\mu_l = 0.019$  1/h) the inverse calibration procedure failed again to match the tailing. The introduction of the degradation coefficient therefore would not significantly improve the simulation results in this study.

## 4.7 Sensitivity analyses

In order to examine the sensitivity of model results to parameter variations, each calibration parameter was varied within reasonable ranges around the respective calibration result. The quality of the resulting model fits was assessed by comparing the root mean square errors (RMSEs). The sensitivity analysis for the conservative tracer uranine shows that model results are highly sensitive to changes in  $\nu$  and  $\theta_m$  ( $= \beta$  for conservative transport) but less sensitive to changes in  $D$  and  $\alpha$  (Figure 4.5). It may be noted here that increasing  $\theta_m$  was restricted by the constraint  $\theta_m \leq 1$ .

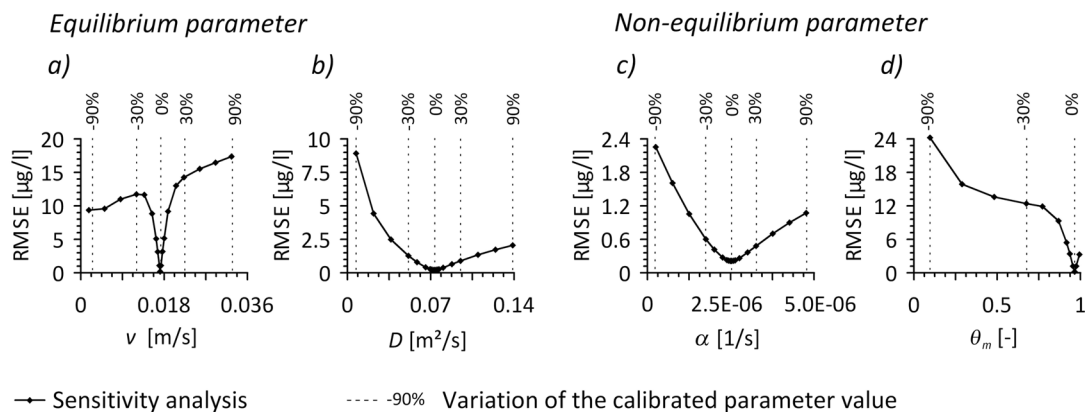
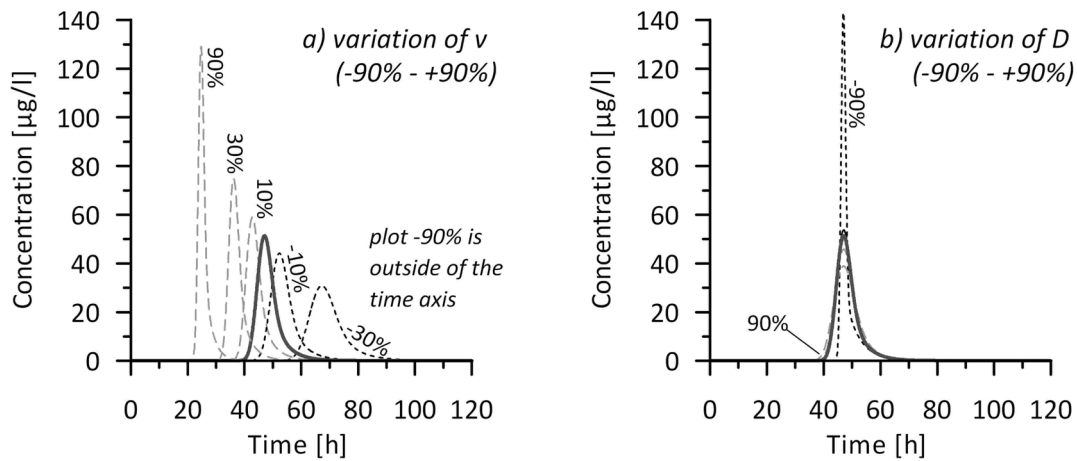


**Figure 4.5: Sensitivity analysis of the conservative transport model. The respective calibration parameter (Table 4.2) was varied between  $-90\%$  and  $90\%$ . Please note the different scales of the ordinates. The variations of  $\nu$  and  $\theta_m$  yield the largest root mean square error (RMSE). Model results are least sensitive to changes in the mass transfer coefficient  $\alpha$ . Because  $\theta_m$  is allowed to vary only between 0 and 1 the range of positive variations of this parameter is limited.**



## Equilibrium parameters of the conservative transport



## Non-equilibrium parameters of the conservative transport

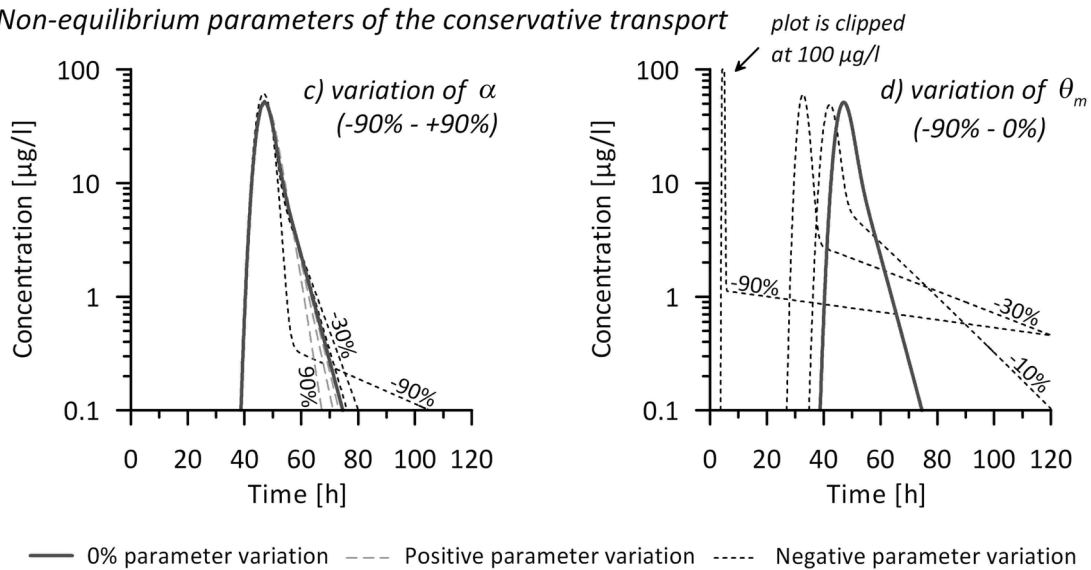


**Figure 4.6: Diagrams illustrating the effect of parameter variation for the conservative transport parameters. The illustrated steps of variations are -90, -30, -10, 10, 30, and 90% of the calibrated value (0%) (compare with Figure 4.5). Note that diagrams for the non-equilibrium parameters are plotted logarithmically on the ordinate to clarify the importance of the parameters with respect to the tail of the TBC.**

Figure 4.6 illustrates the results of the conservative transport model calibration in more detail. The variation of  $v$  results in a displacement of the entire TBC; thus, already a small displacement causes a significant rise in RMSE. In addition, an increase or decrease of  $v$  yields smaller or wider TBCs due to a shorter or longer continuation of dispersion processes. In contrast to the velocity, varying  $D$  does not shift the curve but causes a different dilution and spreading of the TBC. Varying  $\alpha$  and  $\theta_m$  influences the tailing of the TBC. Lower mass transfer coefficients (decreasing  $\alpha$ ) between the mobile and immobile fluid regions cause a longer tailing, larger mass transfer coefficients (increasing  $\alpha$ ) result in a shorter tailing. However, Figure 4.5 indicates that the quality of the model fit is much less sensitive to changes in  $\alpha$  than to changes in  $\theta_m$ . Yet, Figure

4.6c demonstrates that a very small  $\alpha$  (variation  $-90\%$ ) can produce a distinct change of shape in the TBC because the immobile fluid region releases the tracer very slowly. Figure 4.6d reveals that TBCs with a low  $\theta_m$  are characterized by (1) an increased shift of the peak concentration towards earlier times and (2) an increased tailing. The displacement of the TBC for conservative tracer transport can be explained via the relationship (modified from Field and Pinsky 2000):

$$\theta_m = \frac{v}{v_m} \approx \frac{\bar{v}}{v_p} \quad (4.8)$$

where  $v_m$  is the flow velocity in the mobile fluid region,  $\bar{v}$  the mean tracer velocity, and  $v_p$  the peak tracer velocity. Thus, assuming a fixed  $v$ , a decrease in  $\theta_m$  causes an increase in  $v_m$  and accordingly in  $v_p$ . However, adjusting the average tracer velocity  $v$  does not have the same effect on TBCs as changes in  $\theta_m$ , since  $\theta_m$  does not only influence the peak time but also the tailing of the TBC. Model calibration therefore yields unambiguous estimates of the two parameters  $v$  and  $\theta_m$ .

The sensitivity analysis of the reactive transport models (Figures 4.7, 4.8) shows that the partitioning coefficient  $\beta$  is a more important calibration parameter for both reactive tracers than the retardation factor  $R$ . The effects of varying  $\beta$  in the reactive model are similar to those discussed earlier for  $\theta_m$ . In case of  $R$ , it should be noted that model sensitivity on the retardation factor is investigated by varying the parameter  $R - 1$  as this difference is responsible for the shift in TBCs. However, varying  $R - 1$  has the same effect on the TBC as varying the average velocity  $v$  (cf. Figures 4.6a, 4.8a, and 4.8c). Thus, unambiguous values of  $\beta$  and  $R$  are only obtained if  $v$  and  $\theta_m$  are determined independently using a conservative tracer ( $\beta = \theta_m$ ,  $R = 1$ ).

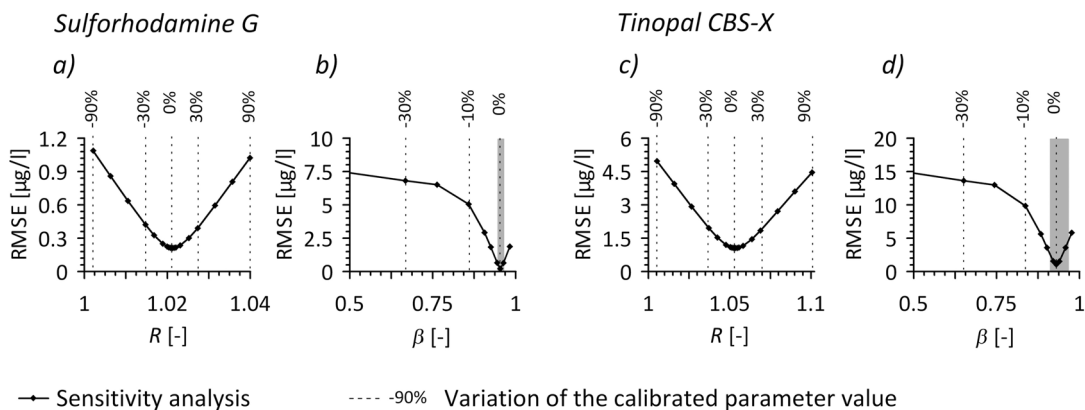


**Figure 4.7: Sensitivity analysis of the reactive transport model for sulforhodamine G and tinopal CBS-X. Because  $\beta$  is allowed to vary only between 0 and 1, the range of positive variations of this parameter is limited. Please note the different scales of the ordinates. The grey boxes in diagrams b and d indicate the possible range of  $\beta$  to accomplish the requirement for physically reasonable values of  $f$  (eq. 4.6).**

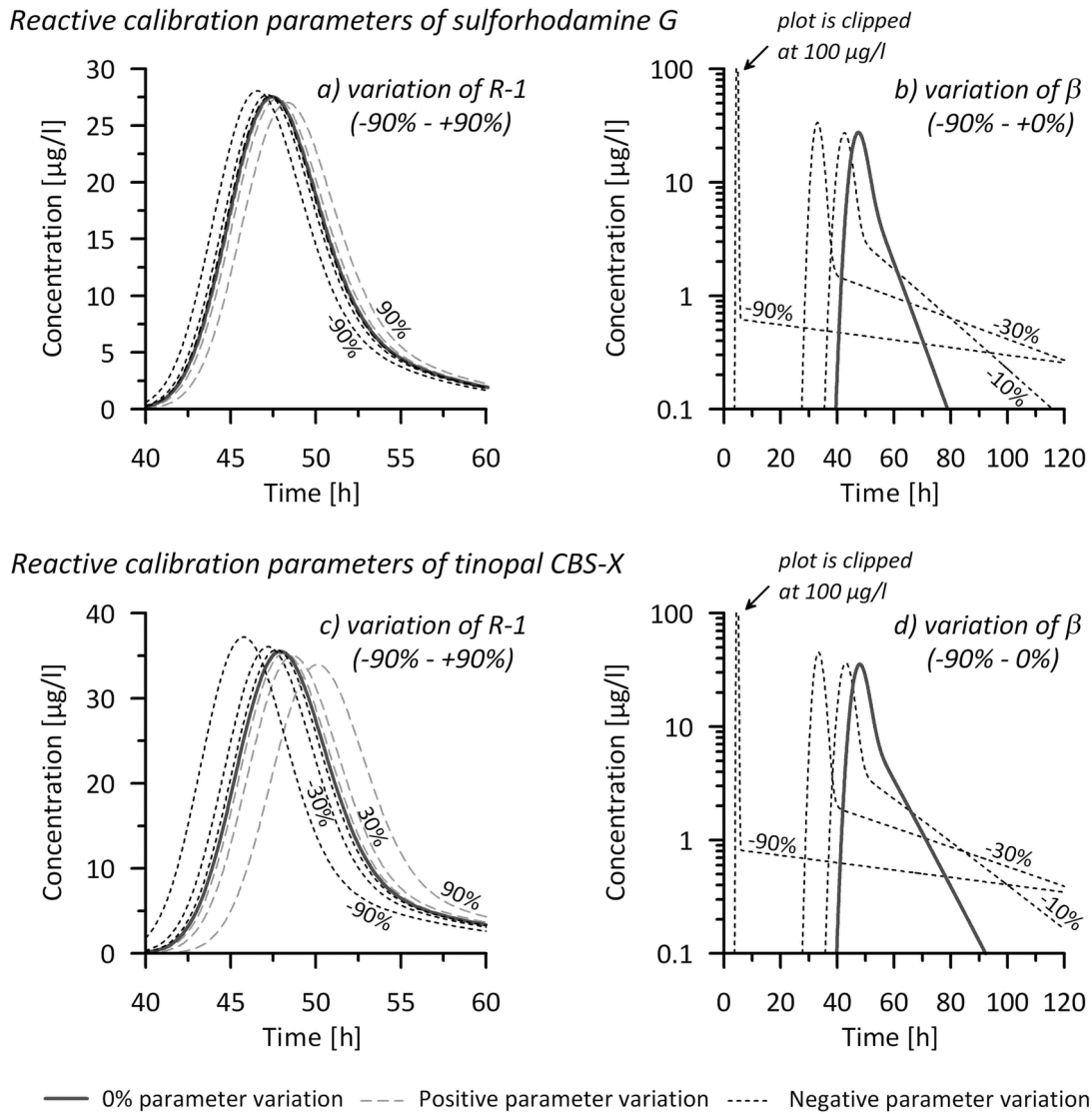


**Figure 4.8:** Diagrams that illustrate the effect of parameter variations by sensitivity analysis to the reactive TBCs. The steps of variations are  $-90$ ,  $-30$ ,  $-10$ ,  $10$ ,  $30$ , and  $90\%$  of the calibrated value ( $0\%$ ) (compare with Figure 4.7). Note that diagrams for  $\beta$  are plotted logarithmically on the ordinate to clarify the importance of the parameters with respect to the tail of the TBC.

## 4.8 Discussion and conclusions

The sensitivity analyses show that the conservative transport model responds highly sensitive and in different manner (Figure 4.6) to changes of the calibrated parameters average velocity  $v$  and the fraction of mobile water  $\theta_m$  but in different manners. Thus, model calibration provides valuable and unambiguous estimates of the two parameters, a prerequisite for the estimation of reactive transport parameters (eqs. (4.5) and (4.7)). In particular, the retardation coefficient  $R$  cannot be determined by calibrating a reactive transport model if  $v$  is unknown, and the volume fraction of the mobile water  $\theta_m$  is required for calculating the fraction of the total surface area

available for tracer-rock surface interactions  $f$ . The latter can only have physically reasonable values between 0 and 1, thus constraining the possible values of the partitioning coefficient  $\beta$ . The constraints on  $\beta$  depend on the volume fractions of the mobile and immobile fluid regions derived from the conservative tracer thus providing a method of checking the consistency of the transport models. As demonstrated by eq. (4.6) and Figure 4.7, the physically reasonable range of  $\beta$  increases with increasing  $R$ . In the present work, the reactive tracers were only slightly retarded, i.e.,  $R - 1$  was low, and thus the reasonable range of  $\beta$  is narrow. Nonetheless, the calibrated values fall into the specified range, supporting the quality of the results. In addition, the calibrated retardation coefficients  $R$  and the resulting estimates of the distribution coefficient  $K_d$  coincide with expectations based on the molecular structure of the tracers. The suggested methodology, therefore, allows a consistent interpretation of the multi-tracer experiment and yields less ambiguous parameter estimates than parameter ranges obtained from the single tracer test methodology as applied by Field and Pinsky (2000). However, the modelling approach employed here was found to be inadequate to reproduce the pronounced tailing in the TBC of tinopal CBS-X. One possible process causing this tailing might be the slow dissolution of previously precipitated tinopal CBS-X. Further research is required to confirm this hypothesis or to identify other relevant causes.

The simulation results from the multi-tracer test suggest that even in a karst system with extremely rapid transport velocities, retardation by reversible ion exchange can be observed. In the given example, retardation is very low because ion exchange mainly takes place within the immobile fluid region that contacts the conduit surface to a larger amount than the mobile fluid region (Figure 1) but accounts for only 3.5% of the total conduit water volume. Higher retardation factors may be expected with increasing conduit surface, e.g., as a result of increasing conduit roughness and thus increasing volume of the immobile fluid region. Yet, the resulting tracer recoveries show that, depending on solute chemistry, significant mass losses are possible even if the volume fraction of the immobile fluid zones is low.

## Acknowledgements

This work was funded by the Deutsche Forschungsgemeinschaft (DFG; German Research Foundation) under grants no. LI 727/10 and SA 501/17. Grateful acknowledgment is made to the staff of the water supply company Hermentingen, in particular Peter Knaus, who assisted with the logistics of the tracer test, as well as to the reviewers Dr. Bruno Arfib, Dr. Todd Halihan, Dr. Malcolm Field, and one further anonymous reviewer.

## 4.9 References

- Atkinson, T.C., Smith, D.I., Lavis, J.J., Whitaker, R.J., 1973. Experiments in tracing underground waters in limestones. *Journal of Hydrology* 19 (4), 323-349.
- Becker, M.W., Shapiro, A.M., 2003. Interpreting tracer breakthrough tailing from different forced-gradient tracer experiment configurations in fractured bedrock. *Water Resources Research* 39 (1), 1024, doi: 10.1029/2001WR001190.
- Behrens, H., 1986. Water tracer chemistry - a factor determining performance and analytics of tracers. In *Proceedings of the 5th International Symposium on Underground Water Tracing*, Institute of Geology and Mineral Exploration, Athens, Greece, 121-133.
- Behrens, H., Beims, U., Dieter, U., Dietze, G., Eikmann, T., Grummt, T., Hanisch, H., Henseling, H., Käß, W., Kerndorff, H., Leibundgut, C., Müller-Wegener, U., Rönnefahrt, I., Scharenberg, B., Schleyer, R., Schloz, W., Tilkes, F., 2001. Toxicological and ecotoxicological assessment of water tracers. *Hydrogeology Journal* 9, 321-325.
- Bencala, K.E., Walters, R.A., 1983. Simulation of solute transport in a mountain pool-and-riffle stream: a transient storage model. *Water Resources Research* 19 (3), 718-724.
- Birk, S., Geyer, T., Liedl, R., Sauter, M., 2005: Process-based interpretation of tracer tests in carbonate aquifers. *Ground Water* 43 (3), 381-388.
- Brown, M.C., Ford, D.C., 1971. Quantitative tracer methods for investigations of karst hydrology systems, with special reference to the Maligne Basin area, Canada. *Transactions of the Cave Research Group of Great Britain* 13 (1), 37-51.
- Brown, M.C., Ford, D.C., Wigley, T.M.L., 1969. Water budget studies in karst aquifers. *Journal of Hydrology* 9 (1), 113-116.
- Coats, K., Smith, B., 1964. Dead-end pore volume and dispersion in porous media. *Society for Petroleum, Engineering Journal* 4, 73-84.
- De Smedt, F., Brevis, W., Debels, P., 2005. Analytical solution for solute transport resulting from instantaneous injection in streams with transient storage. *Journal of Hydrology* 315 (1-4), 25-39.
- Field, M.S., 2002. The QTRACER2 program for tracer-breakthrough curve analysis for tracer tests in karstic aquifers and other hydrologic systems. EPA/600/R-02/001. Washington, D.C., 179 pp.
- Field, M.S., Nash, S.G., 1997. Risk assessment methodology for karst aquifers: (1) Estimating karst conduit-flow parameters. *Environmental Monitoring and Assessment* 47 (1), 1-21.
- Field, M.S., Pinsky, P.F., 2000. A two-region nonequilibrium model for solute transport in solution conduits in karstic aquifers. *Journal of Contaminant Hydrology* 44, 329-351.
- Flury, M., Wai, N.N., 2001. Dyes as tracers for vadose zone hydrology. *Reviews of Geophysics* 41 (1), 1002, doi, 10.1029/2001RG000109.
- Ford, D.C., Williams, P.W., 1996. *Karst geomorphology and hydrology*. London, Chapman & Hall.
- Hauns, M., Jeannin, P.-Y., Atteia, O., 2001. Dispersion, retardation and scale effect in tracer breakthrough curves in karst conduits. *Journal of Hydrology* 241 (3-4), 177-193.
- Jakowski, A.E., Ebhardt, G., 1997. Geohydraulic parameters in hard rocks of SW-Germany determined by tracer tests. In: Kranjc, A. (Ed.), *Tracer Hydrology* 97, 415-421. Rotterdam, Netherlands, Balkema.
- Kasnavia, T., Vu, D., Sabatini, D.A., 1999. Fluorescent dye and media properties affecting sorption and tracer selection. *Ground Water* 37 (3), 1-6.
- Käss, W., 1998. *Tracing technique in geohydrology*. Rotterdam, A.A. Balkema.
- Maloszewski, P., Benischke, R., Harum, T., Zojer, H., 1998. Estimation of solute transport parameters in a karstic aquifer using artificial tracer experiments. In: *Shallow Groundwater Systems* 18, Dillon, P., Simmers, I. (Ed.), 177-190.

- Maloszewski, P., Harum, T., Benischke, R., 1992. Mathematical modelling of tracer experiments in the karst of Lurbach system. *Steirische Beiträge zur Hydrogeologie* 43, 116-136.
- Maloszewski, P., Zuber, A., 1985. On the theory of tracer experiments in fissured rocks with a porous matrix. *Journal of Hydrology* 79 (3-4), 333-358.
- Raven, K.G., Novakowski, K.S., Lapcevic, P.A., 1988. Interpretation of field tracer tests of a single fracture using a transient solute storage model. *Water Resources Research* 24 (12), 2019-2032.
- Sabatini, A.D., 2000. Sorption and intraparticle diffusion of fluorescent dyes with consolidated aquifer media. *Ground Water* 38 (5), 651-656.
- Sabatini, A.D., T.A. Austin, T., 1991. Characteristics of rhodamine WT and fluorescein as adsorbing ground-water tracer. *Ground Water* 29 (3), 341-349.
- Sauter, M., 1992. Quantification and forecasting of regional groundwater flow and transport in a karst aquifer (Gallusquelle, Malm, SW-Germany). *Tübinger Geowissenschaftliche Arbeiten C13*, 150 pp.
- Sauter, M., 1995. Delineation of a karst aquifer using geological and hydrological data and information on landscape development. *Carbonates and Evaporites* 10 (2), 129-139.
- Schnegg, P.A., 2002. An inexpensive field fluorometer for hydrogeological tracer tests with three tracers and turbidity measurement. In: E. Bocanegra, D. Martinez, H. Massone (Eds.), *Groundwater and Human Development*, Mar Del Plata, Argentina, October 2002, 1484-1488.
- Shiau, B.-J., Sabatini, D.A., Harwell, J.H., 1993. Influence of rhodamine WT properties on sorption and transport in subsurface media. *Ground Water* 31 (6), 913-920.
- Smart, C.C., 1988. Artificial tracer techniques for the determination of the structure of conduit aquifers. *Ground Water* 26 (4), 445-453.
- Sudicky, E.A., Frind, E.O., 1982. Contaminant transport in fractured porous media: analytical solutions for a system of parallel fractures. *Water Resources Research* 18 (6), 1634-1642.
- Toride, N., Leij, F.J., van Genuchten, M.T., 1999. The CXTFIT code (version 2.1) for estimating transport parameters from laboratory or field tracer experiments. U.S. Salinity Laboratory Agricultural Research Service, U.S. Department of Agriculture Riverside, California. Research Report 137, 119 pp.
- Tsang, C.F., Neretnieks, I., 1998. Flow channelling in heterogeneous fractured rocks. *Reviews in Geophysics* 36 (2), 275-298.
- Tsang, Y.W., Tsang, C.F., 1987. Channel model of flow through fractured media. *Water Resources Research* 23 (3), 476-479.
- Van Genuchten, M.T., Wierenga, P.J., 1976. Mass transfer studies in sorbing media I, Analytical solutions. *Soil Science Society of America Journal* 40 (4), 473-480.
- Van Genuchten, M.T., Wagenet, R.J., 1989. Two-site/two-region models for pesticide transport and degradation: Theoretical development and analytical solutions. *Soil Science Society of America Journal* 53 (5), 1303-1310.
- Vasudevan, D., Fimmen, R.L., Francisco, A.B., 2001. Tracer-Grade Rhodamine WT: Structure of constituent isomers and their sorption behavior. *Environmental Science and Technology* 35 (20), 4089-4096.
- White, W.B., 1988. *Geomorphology and hydrology of karst terrains*. New York, Oxford University Press.
- Witthüser, K., Reichert, B., Hötzl, H. 2003. Contaminant transport in fractured chalk: Laboratory and field experiments. *Ground Water* 41 (6), 806-815.

## Chapter 5

### **Analysing transport of the environmental tracers $^3\text{H}$ , $^{85}\text{Kr}$ , $\text{SF}_6$ , and He in a karst system with a thick unsaturated zone**

Tobias Geyer<sup>1,3</sup>, Thomas Graf<sup>1</sup>, Jürgen Sültenfuß<sup>2</sup>, Martin Sauter<sup>1</sup>

Citation: Geyer, T., Graf, T., Sültenfuß, J., Sauter, M., 2008. Analysing transport of the environmental tracers  $^3\text{H}$ ,  $^{85}\text{Kr}$ ,  $\text{SF}_6$ , and He in a karst system with a thick unsaturated zone. In preparation for submission to a peer-reviewed journal.

<sup>1</sup> Geoscientific Centre, University of Göttingen, Goldschmidtstr. 3, D-37077 Göttingen, Germany

<sup>2</sup> Department of Oceanography, University of Bremen, Otto-Hahn-Allee, D-28359 Bremen, Germany

<sup>3</sup> Corresponding author - Phone: (49) 551 399398; Fax: (49) 551 399379; tgeyer@gwdg.de

## Abstract

The present study reveals that differences between transit times from environmental tracers in karst systems may be explained by percentage variability in the slow percolation of water through a thick unsaturated zone, i.e. diffuse recharge into fissured matrix blocks. Additionally, it is shown that mean groundwater ages within the catchment area of a karst spring are largely influenced by the contrast in hydraulic parameters of karst systems and therefore depend to a large degree on the location of sampling.

The interpretation of tracer data obtained in the catchment area of the karst spring Gallusquelle/Swabian Alb is based on a combination of lumped parameter modelling and distributive parameter modelling. Mean tracer ages at the spring obtained with lumped parameter modelling decrease in the following order:  $^3\text{H} \gg ^{85}\text{Kr} = \text{SF}_6 > ^3\text{H}/^3\text{He}$  indicating a long travel time of  $^3\text{H}$  through the unsaturated zone of a karst system. This interpretation is supported by the simulation of flow and transport in a fissured matrix block that contains a thick unsaturated zone. The simulation shows that the unsaturated zone of karst aquifers may provide an important water storage and indicate the existence of quasi-stagnant zones in the saturated porous matrix of karst aquifers. Quasi-stagnant zones result from the low hydraulic conductivity of the porous matrix in combination with the small hydraulic gradient within the saturated zone, which leads to the development of quasi-stagnant zones. Evidence of the presence of such zones in the karst system Gallusquelle is given by the large amount of radiogenic  $^4\text{He}$  indicating old groundwater components at sampled wells within the catchment area. These components could not be identified at the Gallusquelle spring which can be explained by the fact that a karst spring is fed by mobile water under a natural hydraulic gradient, whereas pumping within a karst aquifer may lead to the mobilisation of stagnant water from the porous matrix.



## 5.1 Introduction

Karst systems exhibit complex flow and transport phenomena which need to be understood to ensure the appropriate management of karst water resources (Dörfliger et al. 1999). The groundwater water storage of karst systems is mainly provided by low permeability fissured matrix blocks which are drained by highly conductive solution conduits over large distances. Recharge occurs concentrated and rapidly, for example via sinkholes and dry valleys, as well as slowly by water percolating diffusely through fissured matrix blocks (Atkinson 1977). Fast transport through the unsaturated and saturated zone is evidenced by short-term variations of isotopic and chemical composition of spring water shortly after rainfall and snowmelt events (Ashton 1966, Aquilina et al. 2006, Williams 1983), and can be studied in detail using artificial tracer tests (Birk et al. 2005, Geyer et al. 2007, Goldscheider et al. 2008). On the other hand, interpretation of environmental tracers with long-term input functions (e.g. tritium) suggests groundwater ages of several years or decades (Einsiedl 2005, Katz et al. 2004, Maloszewski et al. 2002, Selg et al. 2005). It is to note that age dating with environmental tracers does not reflect the true groundwater age. It represents the mean transit time (mean age) of a specific tracer which can substantially differ from other tracers, e.g. depending on the respective input function and the transport behaviour of tracers (Cook and Solomon 1997, Ekwurzel et al. 1994, Oster et al. 1996). Simultaneous measurement of various tracers is therefore recommended to enhance the information gained, e.g. with respect to tracer retardation (Bauer et al. 2001) and unsaturated zone processes (Zoellmann et al. 2001). The calculation of mean tracer ages from environmental tracers requires the application of mathematical models. Lumped parameter models are capable of solving transit time distributions, e.g. describing piston flow, exponential mixing, or dispersive mixing (Eriksson 1958, Nir 1964, Maloszewski and Zuber 1982). The single type of information required is the history of tracer concentration in the recharge area and a record of tracer concentration at an observation point. Spatial variations of the hydraulic parameter field, boundary conditions, and transport parameters are neglected. Due to their simplicity, lumped parameter models are often used for the interpretation of data when it is impossible to use distributed parameter models. Especially in karst systems, the application of distributed parameter models is difficult because one needs detailed knowledge about the hydraulic properties and the geometry of the conduit system which comprises typically only a small percentage of the total aquifer porosity. Such knowledge is only available in exceptional cases (Jeannin 2001) and thus, application of distributed parameter models is usually limited to strongly simplified case studies or parameter studies (e.g. Birk et al. 2005, Cook et al. 2005). Age dating with distributed parameter models may be based on particle tracking that provides point related information (between the beginning and the end of a path line) about groundwater age. Effects of dispersion and mixing processes on isotope concentrations are ignored. Goode (1996) proposed a method that determines groundwater age at any point in a

model domain. The approach is based on a transport equation that has an internal source corresponding to the rate of aging. The method can also be applied in the sense of backtracking, which yields the time remaining before a water particle leaves the aquifer ("life expectancy") (Cornaton and Perrochet 2006, Kazemi et al. 2006).

The aim of the presented work is to study the slow and diffuse transport through a karst system involving a thick unsaturated zone. The work deals therefore with the evaluation of various environmental tracers which are useful for dating young groundwater (< 50 years) and can be distinguished with respect to their mechanisms entering a karst system. Additionally, a numerical modelling study is performed in order to simulate the transit time of water in saturated/unsaturated fissured matrix blocks and to verify conclusions made from the interpretation of mean tracer ages obtained from lumped parameter modelling.

## 5.2 Methods

### 5.2.1 Environmental tracers applied in this study

#### Tritium ( $^3\text{H}$ )

The tritium ( $^3\text{H}$ ) method is the most common method for age dating of young groundwater. Because  $^3\text{H}$  is part of the water molecule, the  $^3\text{H}$  age is a measure of the transit time of water through the entire hydrogeological system, including saturated and unsaturated zones. During this passage,  $^3\text{H}$  concentrations are subjected to radioactive decay (half-life  $T_{1/2} = \ln 2 / \lambda = 12.32$  years, Lucas and Unterweger 2000) and other transport processes like dispersion and diffusion (Cook and Solomon 1997, Foster 1975). The  $^3\text{H}$  input into an aquifer system depends on the rate of groundwater recharge and concentration of  $^3\text{H}$  in precipitation. Before 1950,  $^3\text{H}$  concentration in precipitation was cosmogenic and very low (5 - 10 T.U.). As a result of nuclear weapon testing between the mid 1950s and 1963 a large amount of  $^3\text{H}$  was produced and  $^3\text{H}$  in precipitation increased by three orders of magnitude in the northern hemisphere. Since 1963, the  $^3\text{H}$  concentration has dropped significantly (Ingraham 1998). Because  $^3\text{H}$  has a relatively short half-life, the influence of the nuclear bomb peak diminished and nowadays, annual averages of  $^3\text{H}$  in precipitation do not significantly change. Therefore, age dating of recent groundwater with  $^3\text{H}$  may be difficult now. Alternative methods used in this work are based on the evaluation of the gaseous tracers Krypton-85 ( $^{85}\text{Kr}$ ), Sulfurhexafluoride ( $\text{SF}_6$ ), and Helium ( $^3\text{He}$ ,  $^4\text{He}$ ).

### **Krypton-85 ( $^{85}\text{Kr}$ )**

$^{85}\text{Kr}$  is an inert gas with a half-life of 10.76 years (Rózański and Florkowski 1979). Natural cosmogenic production of  $^{85}\text{Kr}$  occurs by spallation ( $n, \gamma$ ) reactions from stable  $^{84}\text{Kr}$ . Since 1950, activity of  $^{85}\text{Kr}$  in the atmosphere has been increasing significantly resulting from fission of uranium and plutonium in nuclear reactors (fuel rod reprocessing) and during nuclear weapon testing (Weiss et al. 1992).  $^{85}\text{Kr}$  activity in groundwater is therefore increasing and can be used for age dating of young groundwater (e.g. Bauer et al. 2001, Cook and Solomon 1997, Rózański and Florkowski 1979). In contrast to other gaseous tracers like  $\text{SF}_6$  and He, age dating with  $^{85}\text{Kr}$  is independent of recharge temperatures and excess air because only the ratio of  $^{85}\text{Kr}$  to stable Krypton is of interest. Dispersion within the aquifer leads to elevated concentrations in older water and to the underestimation of groundwater ages. For groundwater recharged after 1970, Ekwurzel et al. (1994) estimated that this effect is less than one year if a dispersivity is less than 0.5 m.

### **Sulfurhexafluoride ( $\text{SF}_6$ )**

Significant industrial production of  $\text{SF}_6$  began in the 1960s leading to a steady increase of atmospheric  $\text{SF}_6$  concentration (Maiss et al. 1996). Similar to age dating with  $^{85}\text{Kr}$ , the  $\text{SF}_6$  method assumes that soil gas above the water table is in equilibrium with the atmosphere, i.e. a rapid gas transport through the unsaturated zone (Cook and Solomon 1997). Otherwise groundwater ages are overestimated. According to Henry's Law, equilibrium concentration of  $\text{SF}_6$  depends on atmospheric pressure, temperature, and dissolved solute content that have to be known at the time of recharge (Busenberg and Plummer 2006). The addition of excess air in groundwater, e.g. air bubbles trapped during recharge, increases the  $\text{SF}_6$  concentration and leads to a younger groundwater age (Bauer et al. 2001). The percentage of excess air may be quantified by the ratio of measured Neon ( $\text{Ne}_{\text{sample}}$ ) and Neon in equilibrium with the atmosphere ( $\text{Ne}_{\text{eq}}$ ). In contrast to  $\text{SF}_6$ , it can be assumed that Ne has no other sources than the atmosphere and that concentration of Ne in the atmosphere is constant (Torgersen et al. 1979).

### **Helium ( $^3\text{He}$ , $^4\text{He}$ )**

$^3\text{He}$  is generated amongst others from radioactive decay of  $^3\text{H}$ . When  $^3\text{H}$  decays below the water table, accumulation of tritiogenic  $^3\text{He}_{\text{trit}}$  in groundwater commences and allows the calculation of an apparent water age independent of a tracer input function (Ekwurzel et al. 1994, Schlosser et

al. 1989, Weise and Moser 1987). If groundwater flow can be described by piston flow and transport parameters of  $^3\text{He}$  and  $^3\text{H}$  are identical, the  $^3\text{H}/^3\text{He}$  age is defined as (Torgersen et al. 1979):

$$^3\text{H}/^3\text{He age} = \frac{T_{1/2}}{\ln 2} \ln \left( 1 + \frac{^3\text{He}_{\text{trit}}}{^3\text{H}} \right) \quad (5.1)$$

with  $T_{1/2}$  = half life time of  $^3\text{H}$ . Because the measured  $^3\text{He}$  concentration in a water sample ( $^3\text{He}_{\text{sample}}$ ) is the sum of  $^3\text{He}$  components from different sources in an aquifer, measurement of  $^4\text{He}$  and Ne is necessary in order to identify  $^3\text{He}$  from different sources in an aquifer:

$$^3\text{He}_{\text{sample}} = ^3\text{He}_{\text{eq}} + ^3\text{He}_{\text{exc}} + ^3\text{He}_{\text{rad}} + ^3\text{He}_{\text{prim}} + ^3\text{He}_{\text{trit}} \quad (5.2)$$

The subscripts denote: eq = concentration in solubility equilibrium with the atmosphere, exc = component resulting from excess air, rad = radiogenic component originating from decay of Uranium and Thorium, prim = mantle release of  $^3\text{He}$ , and trit =  $^3\text{H}$  decay. Neglecting mantle helium ( $^3\text{He}_{\text{prim}}$ ), the tritiogenic component  $^3\text{He}_{\text{trit}}$  can be obtained with the following equations and parameters (Schlosser et al. 1989):

$$^3\text{He}_{\text{trit}} = ^3\text{He}_{\text{sample}} - \left( ^4\text{He}_{\text{sample}} \cdot ^4\text{He}_{\text{rad}} \right) \cdot R_{\text{atm}} + ^4\text{He}_{\text{eq}} \cdot R_{\text{atm}} \cdot (1 - \alpha) - ^4\text{He}_{\text{rad}} \cdot R_{\text{rad}} \quad (5.3)$$

with

$$^4\text{He}_{\text{rad}} = ^4\text{He}_{\text{sample}} - ^4\text{He}_{\text{exc}} - ^4\text{He}_{\text{eq}} \quad (5.4)$$

and

$$^4\text{He}_{\text{exc}} = (\text{Ne}_{\text{sample}} - \text{Ne}_{\text{eq}}) \cdot 0.288 \quad (5.5)$$

and the ratios:  $R_{\text{atm}} = ^3\text{He}_{\text{atm}}/^4\text{He}_{\text{atm}}$  - ratio of the atmosphere ( $= 1.38 \times 10^{-6}$ );  $R_{\text{rad}} = \text{radiogenic } ^3\text{He}_{\text{rad}}/^4\text{He}_{\text{rad}}$  - ratio ( $= 2 \times 10^{-8}$ ). The parameter  $\alpha = 0.983$  describes the helium fractionation during solution (Benson and Krause 1980). Concentrations of He and Ne in solubility equilibrium with the atmosphere ( $\text{He}_{\text{eq}}$ ,  $\text{Ne}_{\text{eq}}$ ) are calculated after Weiss (1971).

In addition to age dating with  $^3\text{He}_{\text{trit}}$ , the separation of radiogenic  $^4\text{He}_{\text{rad}}$  allows the identification of old groundwater components at a sampled location. Measurable amounts of  $^4\text{He}_{\text{rad}}$  exist in groundwater after a contact time between rock and water in the order of 1000 years (Solomon et al. 1998).

## 5.2.2 Lumped parameter modelling

The lumped parameter approach treats a flow system as an entity, i.e. spatial variations are ignored, and the flow pattern is assumed to be constant. According to Maloszewski and Zuber (1982), the relationship between concentrations of an environmental tracer at the inlet ( $C_{in}(t)$ ) and at the outlet ( $C_{out}(t)$ ) of a hydrogeological system is given by the convolution integral:

$$C_{out}(t) = \int_{-\infty}^t C_{in}(t') \exp[-\lambda(t-t')] g(t-t') dt' \quad (5.6)$$

where  $\lambda$  is the decay constant of an radioactive tracer. The term  $g(t-t')$  is a weighting function (tracer age distribution) that describes the output distribution of a tracer injected instantaneously at the inlet.  $t'$  and  $t-t'$  correspond to the entry time a tracer and the transit time. The transit time refers to the time a tracer remains in a hydrogeological system from the inlet to the outlet. At the outlet the transit time is identical to the 'tracer age' which is the time elapsed since a tracer entered a hydrogeological system (Eriksson 1971). The weighting function together with its parameters determines the lumped parameter model (Maloszewski and Zuber 1982). The piston flow model, for example, assumes that all flow lines have the same velocity, and dispersion and diffusion are negligible. It is applied to calculate the  $^3\text{H}/^3\text{He}$  age (eq. 5.1). The exponential model considers an exponential distribution of transit times of flow lines and assumes that mixing of flow lines occurs at the sampling site (Maloszewski and Zuber 2002). The only fitting parameter of both models is the mean transit time of a tracer  $t_t$  (mean tracer age). To account for diffusion between mobile water in the fissures and stagnant water in the porous matrix of karst aquifers, Einsiedl (2005) suggests the dispersion model (DM). It introduces an apparent dispersion parameter  $P_D$  that involves all discrepancies between model assumptions and the real geometry of an investigated system (Zuber 1986). Maloszewski et al. (2002) combined the dispersion model with a piston flow model to incorporate rapid tracer transport through the conduit system of a karst aquifer. The lumped parameter approach is valid for environmental tracers with constant or variable input functions. Because the tracer flux into a hydrogeological system is controlled by recharge rates, the yearly tracer input into the lumped parameter model ( $C_{in}$ ) has to be corrected, for example by a monthly weighting of tracer concentrations ( $C_m$ ) with recharge rates ( $R_m$ ) (Maloszewski and Zuber 2002):

$$C_{in} = \sum_{i=1}^{12} C_m R_m / \sum_{i=1}^{12} R_m \quad (5.7)$$

In the present work, monthly recharge rates ( $R_m$ ) are calculated with a water balance approach (Appendix B). In order to deal with a balanced groundwater storage, annual concentrations ( $C_m$ ) are calculated for the hydrological year in the area of investigation (November - October). Mean tracer ages for different tracer age distributions were calculated with the software FLOWPC (Maloszewski and Zuber 2002). The quality of the simulation result ( $err$ ) with FLOWPC is obtained by the square root of differences between the  $i$ -th observed  $C_{obs}$  and the  $i$ -th modelled data  $C_{out}$ , divided by the number of observed data  $n$ .

$$err = \left[ \sum_{i=1}^n (C_{obs(i)} - C_{out(i)})^2 \right]^{1/2} / n \quad (5.8)$$

### 5.3 Field site

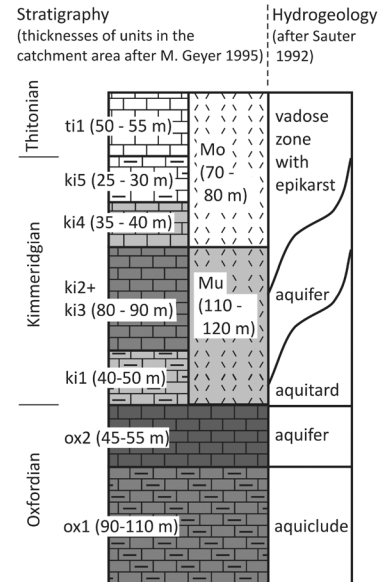
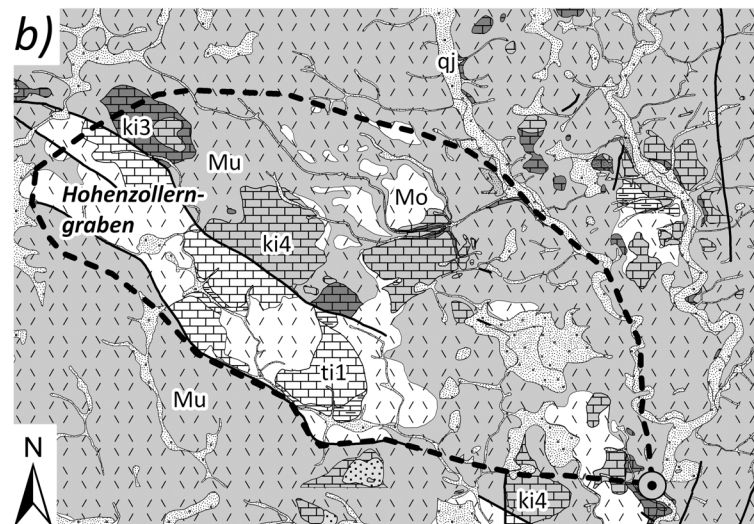
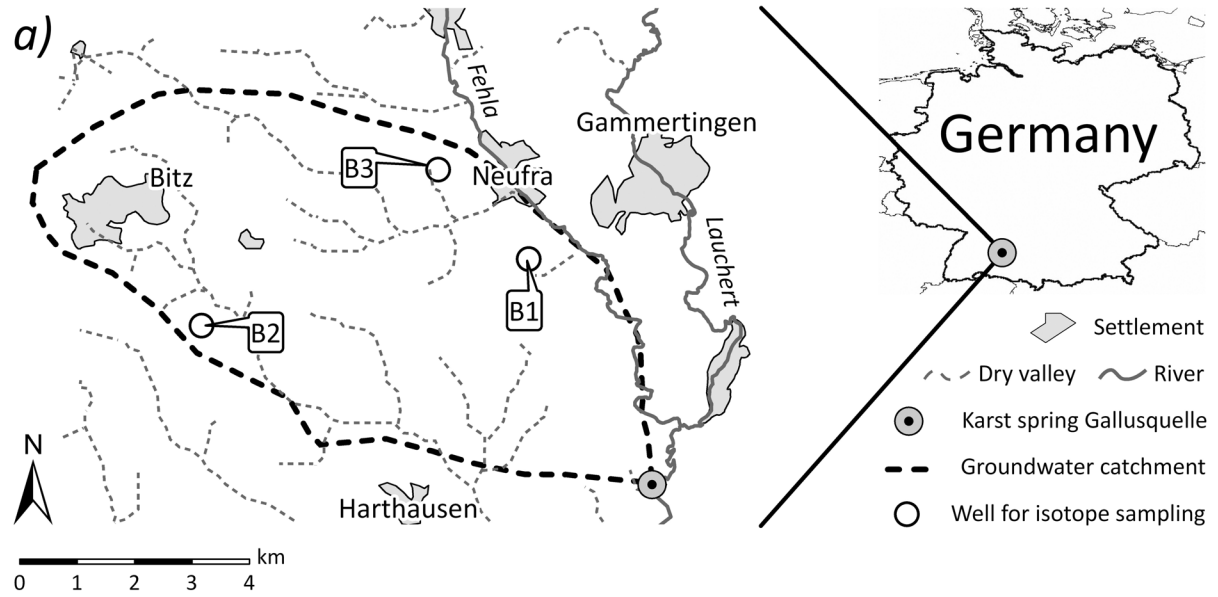
Environmental tracer data were collected at the Gallusquelle spring catchment (Figure 5.1). It is situated on the Swabian Alb, a northwest-southeast striking long mountain range in South Germany. The catchment area has a site of ca. 40 to 45 km<sup>2</sup> (Villinger 1977, Sauter 1992). The landscape is characterised by dry valleys, which intersect the gentle hilly area (700 - 900 m a.s.l.) made of Upper Jurassic carbonate rocks. Dry valleys are interpreted as the result of formerly active water courses, which dried up when the karstification level dropped below the river bottoms. The base of the karst aquifer does not follow any stratigraphical boundary. It cuts across a sequence of massive, marly, and well bedded limestones (Figures 5.1, 5.2) that dips gently southeast by 1.2° (Sauter 1992). The Gallusquelle spring originates on the continuation of the northwest-southeast striking Hohenzollern-graben. Hydraulic characteristics of the graben are not well known. Tunnelling work in the 60s suggests that the southern fault zone of the graben acts as a sealing front and forms therefore the southern catchment boundary. The northeastern catchment boundary is formed by the Fehla river. In the northwest a groundwater divide forms the boundary (Sauter 1992).

Hydraulic parameters of the aquifer vary depending on scale of investigation and method employed. Sauter (1992, p. 54-58) determined the hydraulic conductivity and porosity of the fissured system on catchment scale using a Darcy-based gradient approach and spring recession analysis. The values obtained were 10<sup>-4</sup> - 10<sup>-5</sup> m/s and 1% - 2%, respectively. The water filled conduit volume of the aquifer is ca. 200000 m<sup>3</sup> which has been determined with an artificial tracer experiment (discharge during tracer test = 0.76 m<sup>3</sup>/s) covering the extent of the conduit system in the catchment area (Geyer et al. 2008, Münzing 1988). Considering a thickness of the phreatic zone of between 15 m and 50 m (Sauter 1992, p. 58) leads to a conduit porosity

between 0.01% and 0.03%. In contrast to extensive investigations of the fissured and conduit system only limited information is available regarding hydraulic parameters of the porous matrix. Weiß (1987) measured porosities and hydraulic conductivities of core samples of the Upper Jurassic limestone sequence of the Franconian Alb, which is the geological continuation of the Swabian Alb to the northeast. Effective porosities for the bedded facies of limestones (Malm delta) varied between 0% and 12% with a mean of 4% and may be even larger for the massive facies. The average hydraulic conductivity is  $10^{-8}$  -  $10^{-9}$  m/s.

### Dynamics of the Gallusquelle aquifer

Daily discharge of the spring is recorded since 1955 and ranges between less than  $0.1 \text{ m}^3/\text{s}$  and  $2.7 \text{ m}^3/\text{s}$  with an annual average of  $0.5 \text{ m}^3/\text{s}$ . Recharge was estimated for the period between 1965 and 1990 by Sauter (1992, p. 33-43). For this study the estimation is extended to the period from 1955 to 2005 (Figure 5.2, Appendix B) in order to provide weights for tracer input concentrations according to eq. (6). Monthly recharge rates show seasonal variations with low rates during summer when evapotranspiration is high and high recharge rates during winter/spring after heavy rainfall events and snow melts. The seasonal cycle is also apparent in the spring discharge curve. The peaks of the recharge curve coincide with flood peaks of the discharge curve indicating fast and concentrated recharge through the thick unsaturated zone of the karst system. Geyer et al. (2008) showed that the discharge of the Gallusquelle spring began to rise 4 hours after a rainfall event. The rise of spring discharge can be interpreted as the arrival of fast recharged water at the groundwater table. The thickness of the unsaturated zone of the catchment area averages 100 m. The resulting flow velocity of the fast recharge component through the unsaturated zone is 25 m/h. Based on  $\delta^{18}\text{O}$  in precipitation and spring water, Sauter (1997) determined the fraction of the fast recharge component on total recharge between 5% and 10%. Flow velocities in the conduit system were observed to be up to 140 m/h using artificial tracer tests (Sauter 1992, p. 49). Diffuse recharge and/or slow release of water from the fissured matrix blocks is evidenced by the long-time recession of the discharge curve. Applying spring hydrograph recession analysis, a recession coefficient of 0.0018 1/d for the fissured system of the aquifer was estimated (Sauter 1992). The reciprocal of the recession coefficient leads to a mean transit time of mobile water of 1.5 years (hydraulic age). This value agrees well with the mean transit time of mobile water determined from the ratio of the volume of water in fissures and the volumetric flow rate (average recharge from 1955 to 2006 = 395 mm). Considering a porosity of the fissured system between 1% and 2% gives a mean transit time of mobile water of 0.4 - 2.5 years.



**Quaternary**

- Unconsolidated sediments - gravel, sand, loam

**Tertiary**

- Obere Meeresmolasse (OMM) - sand

**Upper Jurassic**

- |   |   |  |
|---|---|--|
| <ul style="list-style-type: none"> <li>Hangende Bankkalke (ti1) - well bedded limestone</li> <li>Felsenkalke (ki2 + ki3) - bedded limestone</li> <li>Lacunosamergel (ki1) - marl</li> </ul> | <ul style="list-style-type: none"> <li>Zementmergel (ki5) - lime-marlstone</li> <li>Oberer Massenkalk (Mo) - massive limestone</li> <li>Wohlgeschichtete Kalke (ox2) - well bedded limestone</li> </ul> | <ul style="list-style-type: none"> <li>Liegende Bankkalke (ki4) - thinly bedded limestone</li> <li>Unterer Massenkalk (Mu) - massive limestone</li> <li>Impressamergel (ox1) - marl</li> </ul> |
|---|---|--|

Geological map is based on data from (author(s), year, scale, geological map):  
 Geyer, M., Franz, M. (1995): GK1:25000, Blatt 7720 Albstadt; Koerner, U., Geyer, M. (1997): GK1:25000, Blatt 7820 Winterlingen  
 Gwinner, M. (1973): GK1:25000, Blatt 7721 Gammertingen; Golwer, A. (1978): GK1:25000, Blatt 7821 Veringenstadt

**Figure 5.1: a) Location of the Gallusquelle catchment (delineation according to Sauter (1992)), b) Geological map and stratigraphical overview of the Upper Jurassic in the area of investigation.**



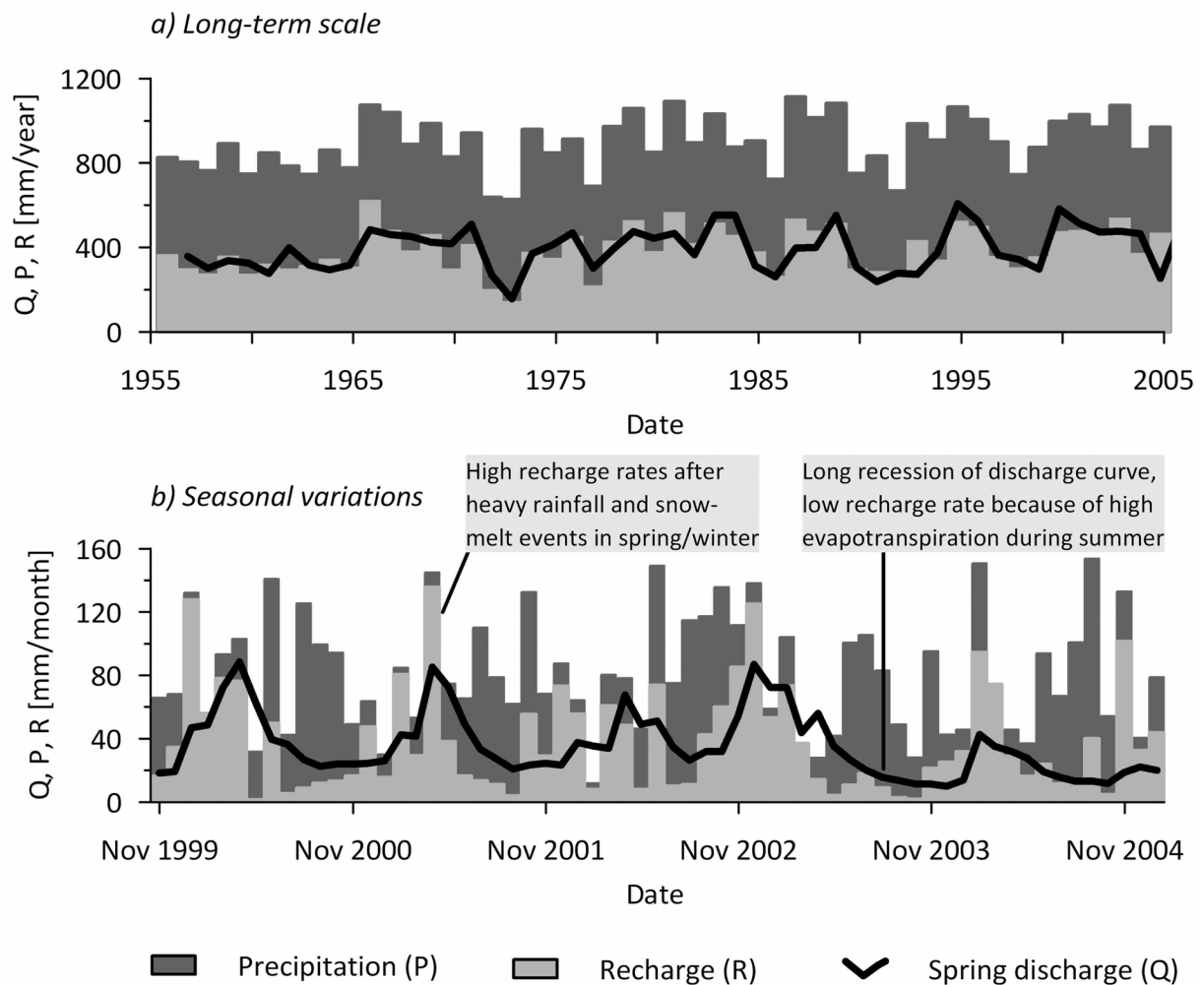


Figure 5.2: Dynamics of spring discharge, recharge, and precipitation on a) long-term scale and b) seasonal time scale.

## 5.4 Environmental tracer data in precipitation, atmosphere, and groundwater

$^3\text{H}$ ,  $^3\text{He}$ ,  $^4\text{He}$ , Ne,  $\text{SF}_6$ , and  $^{85}\text{Kr}$  samples were collected from the Gallusquelle spring in August 2003, April 2004, and September 2004 (Table 5.1). In addition, earlier measurements of  $^3\text{H}$  from Bertleff (1986) and LGRB (Geological Survey of Baden-Württemberg) are used for the calculation of the mean  $^3\text{H}$  age with the lumped parameter approach.  $^3\text{He}$ ,  $^4\text{He}$ , and Ne samples were also collected from two water supply wells (B1, B2) and an observation well (B3) in the catchment area (Figure 5.1). Water supply wells are screened within the massive limestone formation (Massenkalk, Mu, Mo) across the saturated and the unsaturated zone (Table 5.2). Pumping rates fluctuate and are less than 0.2 l/s throughout the year. The screen of well B3 is placed 60 m below the water table within a sequence of marls with bedded limestones (Lacunosamergel formation, ki1).

**Table 5.1: Measured tracer concentrations at sampling sites in the Gallusquelle catchment area.**

Sample site	Date	Discharge [m <sup>3</sup> /s]	<sup>3</sup> H [T.U.]	<sup>3</sup> He [ccSTP/kg]	<sup>4</sup> He [ccSTP/kg]	Ne [ccSTP/kg]	Storage time* [years]	<sup>85</sup> Kr [dpm/ml]	SF <sub>6</sub> [pmol/l]
Spring	13.08.2003	0.180±0.25	13.58±0.49	6.50E-11	4.60E-05	1.94E-04	0.87	64.5±3.6	1.8±0.2
Spring	29.04.2004	0.300±0.25	12.64±0.48	6.43E-11	4.56E-05	1.98E-04	0.18	68.4±2.9	1.8±0.3
Spring	07.09.2004	0.165±0.25	13.57±0.59	6.33E-11	4.57E-05	1.98E-04	0.55	68.1±2.4	1.9±0.2
B1	29.04.2004	-	12.27±0.46	7.33E-11	5.06E-05	2.18E-04	0.19	-	-
B1	09.09.2004	-	13.19±0.85	7.11E-11	4.95E-05	2.10E-04	0.55	-	-
B2	29.04.2004	-	3.04±0.28	1.16E-10	7.87E-05	2.73E-04	0.18	-	-
B2	09.09.2004	-	3.32±0.33	1.13E-10	7.71E-05	2.63E-04	0.55	-	-
B3	28.04.2004	-	12.17±0.47	1.23E-10	1.44E-04	2.20E-04	0.18	-	-
B3	08.09.2004	-	12.44±0.90	1.29E-10	1.68E-04	2.24E-04	0.55	-	-

\* Storage time of water samples for analysis of He and Ne

**Table 5.2: Characteristics of sampling sites in the Gallusquelle catchment area.**

Sample site	Spring	B1	B2	B3
Surface level [m a.s.l.]	633	759	738	784
Water level [m a.s.l.]	633	103,3 (04.07.2002)	79,1 (14.12.2002)	98,8 (08.09.2004)
Borehole depth [m]	-	160	91	160
Screened section [m]	-	97-160	77-89	154-160

Samples for He and Ne were filled in 40 ml copper tubes and pinched off with clamps to prevent gas exchange with the atmosphere. Water for <sup>3</sup>H analysis was collected in 500 ml glass bottles. Analyses of He, Ne and <sup>3</sup>H are described in detail by Sültenfuß et al. (2008). Analysis of <sup>85</sup>Kr

required 10 l gas obtained by on-site degassing of spring water.  $^{85}\text{Kr}$  activity was measured by gas proportional counting according to Loosli et al. (1980). Water samples for analysis of  $\text{SF}_6$  were filled underwater in 500 ml glass bottles and preserved in metal boxes filled with water of the sampling site. Analyses of  $\text{SF}_6$  were performed with electron-capture gas chromatography (Maiss et al. 1996).

Average monthly  $^3\text{H}$  concentration in precipitation was obtained from the stations Stuttgart, Konstanz, and Garmisch of the GNIP (Global Network of Isotopes in Precipitation, International Atom Energy Agency) for the period 1961 - 2005 (Figure 5.3). The stations are located at distances ranging between 60 km to 150 km from the area of investigation. Because of the lack of sufficient data near the catchment area,  $^3\text{H}$  in precipitation of the station Ottawa (Canada) is used for the period 1955 - 1961. Specific activity of  $^{85}\text{Kr}$  in atmosphere is provided from the station Schauinsland (80 km west of the catchment area) of the BFS (Federal Office for Radiation Protection, Germany) for the period 1976 - 2005. Before 1976, activity of  $^{85}\text{Kr}$  in northern hemisphere is documented by Rózański and Florkowski (1979) and Solomon et al. (1998). Evaluation of  $\text{SF}_6$  is based on the air curve for the northern hemisphere provided by the USGS (United States Geological Survey). Equilibrium concentrations of gaseous tracers He, Ne, and  $\text{SF}_6$  are estimated for an elevation of 700 m and a salinity of 0.5‰. The parameters reflect the mean height of the groundwater table and the salinity of the groundwater in the catchment area.

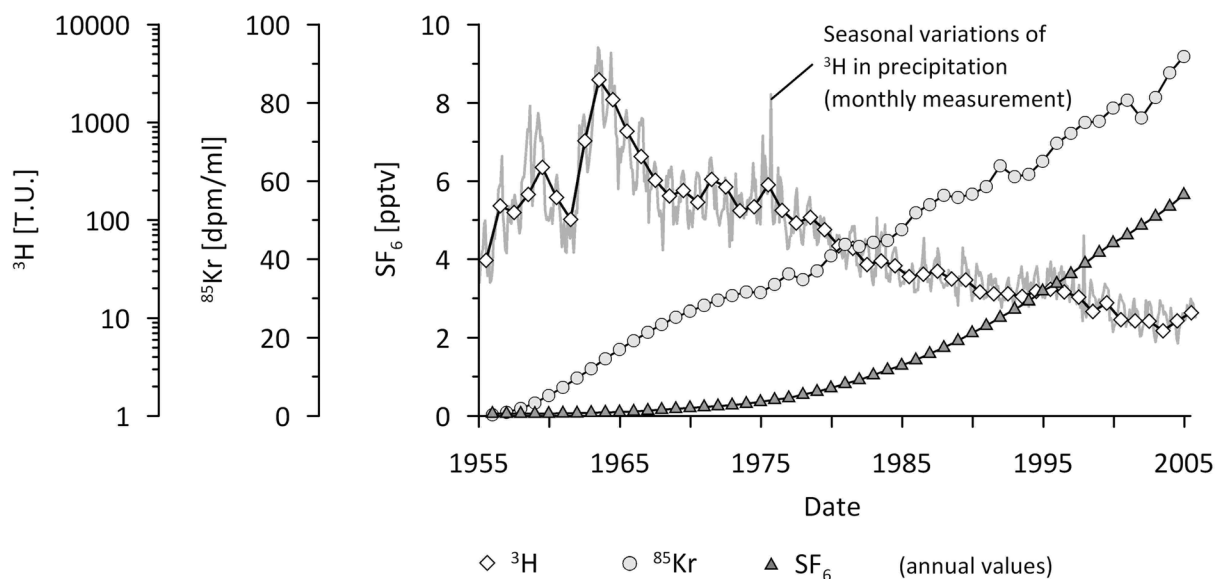
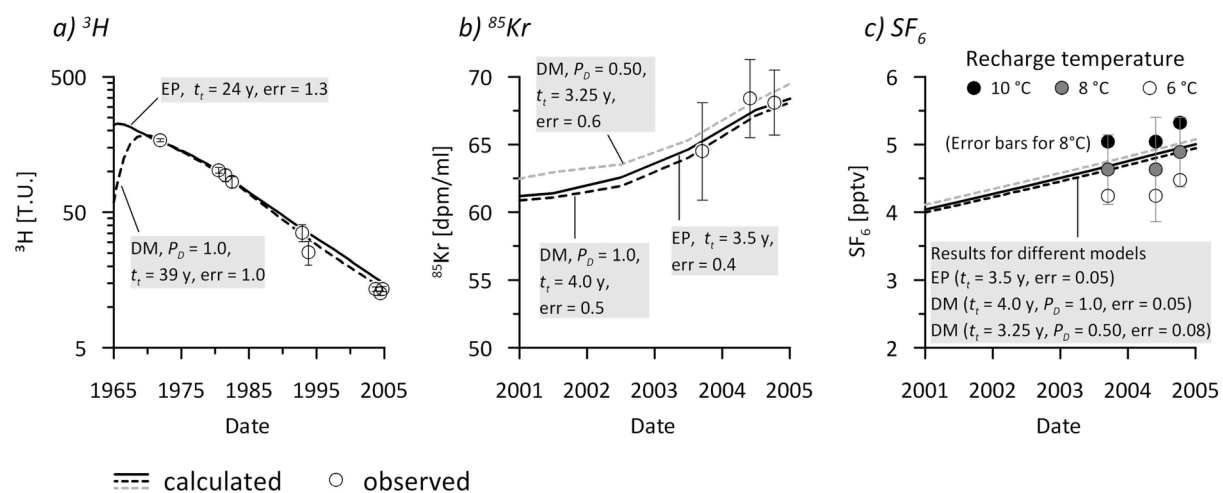


Figure 5.3: Input functions of environmental tracers employed in this study.

## 5.5 Interpretation of environmental tracers with the lumped parameter approach

The best fit to observed  $^3\text{H}$  data is achieved with the dispersion model employing a mean  $^3\text{H}$  age of 39 years and a dispersion parameter  $P_D$  of 1.0 (Figure 5.4). The exponential model with a mean  $^3\text{H}$  age of 24 years (as single fitting parameter) produces a reasonable fit, too. Therefore, a mean  $^3\text{H}$  age of more than 20 years can be considered. In contrast, mean  $^{85}\text{Kr}$  age for various lumped parameter models ranges between only 3 and 4 years, i.e. the type of weighting is not sensitive to the short transit time of  $^{85}\text{Kr}$ . Similar mean tracer ages are obtained for  $\text{SF}_6$  considering a recharge temperature of  $8.5^\circ\text{C}$ . The recharge temperature is higher than the average annual air temperature ( $6.5^\circ\text{C}$ ) in the area of investigation but close to the temperature of spring water ( $8.7^\circ\text{C}$  -  $9.1^\circ\text{C}$  between January 2003 and December 2004, measurement interval 10 minutes). The temperature of spring water reflects the mean temperature of water in the phreatic zone (100 m below surface). The recharge temperature estimated with  $\text{SF}_6$  therefore indicates that water percolates slowly through the unsaturated zone and equilibrates with the geothermal gradient. However, it has to be noted that the model sensitivity to recharge temperature is not large. For example, a recharge temperature equivalent to the annual average air temperature ( $6.5^\circ\text{C}$ ) would lead to a mean  $\text{SF}_6$  age of 5 years applying the exponential model.



**Figure 5.4: Mean tracer ages for a)  $^3\text{H}$ , b)  $^{85}\text{Kr}$ , and c)  $\text{SF}_6$  estimated by various lumped parameter models.**

The  $^3\text{H}/^3\text{He}$  age (eq. 5.1) is ca. 1 year for spring water considering the same recharge temperature as for  $\text{SF}_6$  (Table 5.3). Air contamination during sampling may explain the estimated  $^3\text{H}/^3\text{He}$  age of zero for spring water on 07.09.2004. Besides, only little variation of He are found between sampling dates on a sampling site reflecting stable sampling conditions. Calculated  $^3\text{H}/^3\text{He}$  ages within the catchment area differ greatly suggesting a complex groundwater age pattern in the Gallusquelle catchment.

Concentrations of  $^3\text{He}$  and  $^4\text{He}$  components in well B1 are similar to those found in spring water and indicate a young groundwater component with a  $^3\text{H}/^3\text{He}$  age of  $<2$  years. In contrast, samples of well B2 contained a large amount of  $^3\text{He}_{\text{trit}}$  leading to a  $^3\text{H}/^3\text{He}$  age of more than 20 years for the young groundwater component. Measured  $^3\text{H}$  in well B2 ( $\approx 3$  T.U.) ranges below atmospheric  $^3\text{H}$  concentrations of the last 50 years implying an old groundwater component recharged before 1950. This finding is supported by the presence of  $^4\text{He}_{\text{rad}}$  which refers to a long contact time of groundwater with the surrounding rock. Well B3 was used as an injection point for an artificial tracer test with the fluorescent dye uranine in 1990. The tracer was injected together with 650 l of water but has never been detected at the spring. During isotope sampling in April 2004 and September 2004, the pumped water was still coloured green from the fluorescent dye (uranine) injected in 1990. About 700 liters of water were pumped from the observation well before each sampling. The calculated  $^3\text{H}/^3\text{He}$  age is 17 - 18 years. It indicates that the groundwater equilibrated with the gas phase in 1987, which is a good approximation for the time of artificial tracer injection. It demonstrates the reliability of the  $^3\text{H}/^3\text{He}$  dating technique. The large amount of  $^4\text{He}_{\text{rad}}$  found in well B3 may be explained by an old groundwater component that mixed with young groundwater, e.g. injected water. Together with the retrieved artificial tracer it indicates the existence of stagnant zones in the Gallusquelle aquifer.

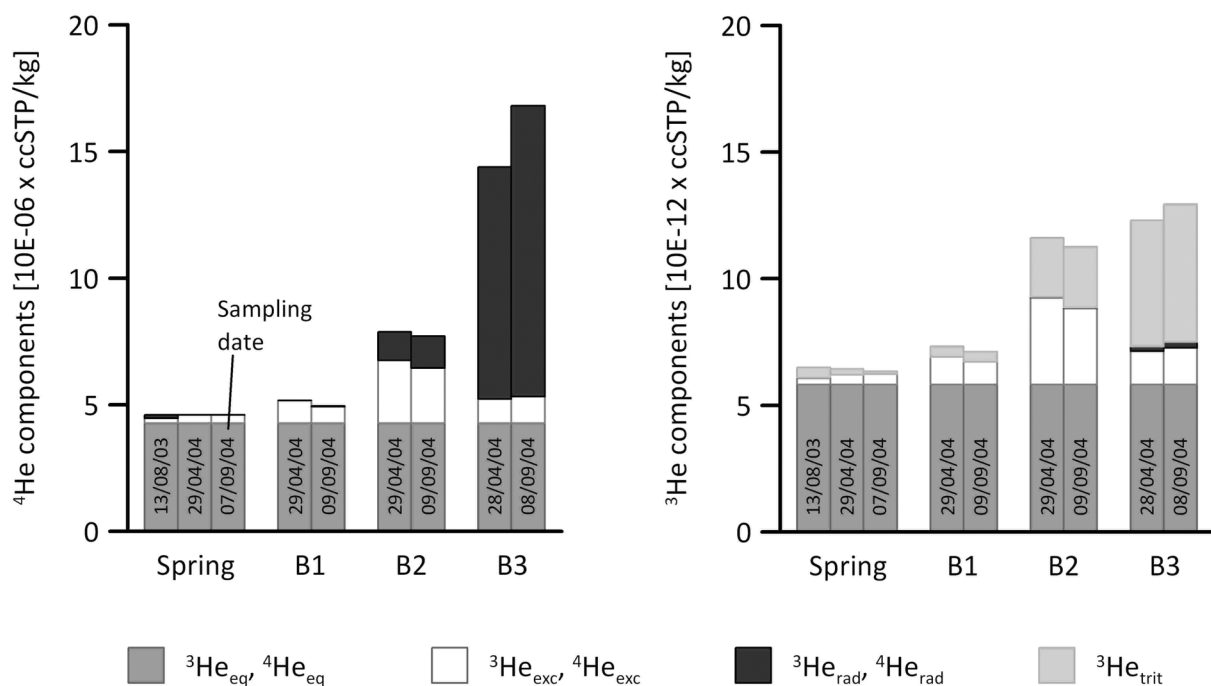


**Figure 5.5: Separation of  $^3\text{He}$  and  $^4\text{He}$  components from measured He concentrations for different sampling sites (Table 5.1).**

Massmann et al. (2008) estimated the percentage of the old water component in groundwater from the ratio of (1) the sum of measured  $^3\text{H}$  and  $^3\text{He}_{\text{trit}}$  (eq. 5.3) in a water sample and (2)  $^3\text{H}$  in

precipitation for the time of recharge (sample date minus  $^3\text{H}/^3\text{He}$  age). The sum of  $^3\text{H}$  and  $^3\text{He}_{\text{trit}}$  of water samples of well B2 adds up to 12 - 13 T.U. for 1979 and 1980 (Table 5.3). For these years,  $^3\text{H}$  in precipitation (weighted with eq. 5.7) ranged between 50 T.U. and 80 T.U. leading to an old groundwater component of 0.8 (80%). For the spring and well B1,  $^3\text{H} + ^3\text{He}_{\text{trit}}$  in water samples is much higher than  $^3\text{H}$  in precipitation for the time of recharge, i.e.  $^3\text{H}$  in percolating water near the groundwater table is higher than  $^3\text{H}$  in precipitation at the same time. Because  $^3\text{H}$  concentration in precipitation decreases, these findings can be explained by the slow percolation of water through the thick unsaturated zone. In case of well B3,  $^3\text{H} + ^3\text{He}_{\text{trit}}$  in water samples and  $^3\text{H}$  in precipitation for the time of recharge agree well suggesting only a young groundwater component which is in contrast to the large amount of  $^4\text{He}_{\text{rad}}$ . A possible interpretation may be a small percentage of the old groundwater component.

**Table 5.3: Calculated  $^3\text{H}/^3\text{He}$  ages and  $^3\text{H} + ^3\text{He}_{\text{trit}}$  in water samples at the sampling sites in the Gallusquelle catchment area.**

Sample site	Date	$^3\text{He}/^3\text{H}$ age* [years]	$^3\text{H} + ^3\text{He}_{\text{trit}}$ ** [T.U.]	Year*** of recharge according to $^3\text{He}/^3\text{H}$ age	$^3\text{H}$ in precipitation**** in year* of recharge [T.U.]	Ratio between $^3\text{H} + ^3\text{He}_{\text{trit}}$ in water samples and $^3\text{H}$ in precipitation in year of recharge
Spring	13.08.2003	1.2 ( <i>1.6</i> )	14.6	2002	9.3	1.6
Spring	29.04.2004	1.1 ( <i>1.2</i> )	13.4	2003	7.4	1.8
Spring	07.09.2004	0.0 ( <i>0.2</i> )	13.6	2004	9.4	1.4
B1	29.04.2004	2.2 ( <i>2.2</i> )	13.9	2002	9.3	1.5
B1	09.09.2004	1.5 ( <i>1.9</i> )	14.4	2003	7.4	1.9
B2	29.04.2004	24.9 ( <i>25.4</i> )	12.4	1979	79.9	0.2
B2	09.09.2004	23.7 ( <i>24.2</i> )	12.9	1980	54.3	0.2
B3	28.04.2004	17.1 ( <i>17.3</i> )	32.0	1987	30.0	1.1
B3	08.09.2004	17.5 ( <i>17.7</i> )	33.9	1987	30.0	1.1

(\* $^3\text{He}/^3\text{H}$  ages for recharge temperatures of 8.5°C and 6.5°C (*italic*), \*\*measured  $^3\text{H}$  (Table 5.2) and  $^3\text{He}_{\text{trit}}$  (eq. 5.3) in a water sample, \*\*\*hydrological year (November - October), \*\*\*\*corrected with recharge rate according to eq. (5.7))

## 5.6 Simulation of life expectancy of water in a fissured matrix block

The evaluation of environmental tracers sampled in the groundwater catchment of the Gallusquelle spring reflects slow and diffuse mass transport in the karst aquifer and indicates the importance of the unsaturated zone for interpretation of groundwater ages. Let us therefore consider a 2D vertical model (software: FEFLOW5.3, Diersch 2006) which simulates flow and transport through the saturated and unsaturated zone of a fissured matrix block (Figure 5.6). The vertical profile is assumed to represent the course of a streamline in a 2D horizontal model to the point of drainage (e.g. conduit system). Transport of groundwater from the conduit system to the spring is neglected because artificial tracer tests indicate that the transport time is just a few days (Geyer et al. 2007).

Because there is no information about the geometry of fissured matrix blocks, it should be emphasised that the intention of distributed modelling is not to calibrate the numerical model with observed field data, but rather to study saturated/unsaturated flow in heterogeneous media and its influence to groundwater ages. The rectangular model domain (120 m × 120 m) is composed of quadrilateral elements (235366 elements) with a size of 0.25 m and is refined near the spring and the model boundaries. Fissures are simulated within the model domain as local areas (fissure length = 120 m, fissure width = 0.5 m) with higher hydraulic conductivities than the surrounding porous matrix (Figure 5.6). Hydraulic conductivities are in the range of those found for the Gallusquelle aquifer (chapter 3). Unsaturated flow simulation is based on Richards' equation and respective parameters are described via the Van Genuchten (1980) parametric model. Van Genuchten parameters  $\alpha$  and  $n$  are taken from Roulier et al. (2006) (porous matrix) and from Finsterle et al. (2002) (fissures). The porosity for the flow as well as for the transport problem is set at 5% across the entire model domain. Longitudinal and transversal dispersion are fixed at 1 m and 0.01 m, respectively. The diffusion coefficient is  $1.57 \times 10^{-5} \text{ cm}^2/\text{s}$  which is characteristic for  $^3\text{H}$  in water at  $10^\circ\text{C}$  (Cook and Solomon 1997). Boundary conditions for flow are first kind (Dirichlet) at the outlet (head = 20 m) and of second kind (Neumann) at the domain top (recharge = 365 mm/year). Recharge is uniformly distributed across the entire top of model in order to simulate "diffuse recharge" in karst aquifers.

Water ages can be estimated directly at any location in the model domain according to Goode (1996). The approach is based on a transport equation that assumes an internal source, corresponding to the rate of aging. The value of the source is given by the porosity. Simulation is performed in the sense of backtracking, i.e. the flow field is reversed, and the boundary conditions are adapted (Diersch 2006). The mass at the outlet boundary is set to be zero (boundary condition of first kind). At any position in the model domain, the time required for a water molecule to reach the outlet is simulated corresponding to the "life expectancy of water"

(Cornaton and Perrochet 2006), i.e. the life expectancy of water on the outlet is zero. The frequency curve of the life expectancy at the recharge boundary corresponds to the transit time distribution of water flowing from the top of the model domain to the outlet. The mean transit time is estimated from a first moment analysis of the transit time distribution.

Simulation was performed in several steps. First, a quasi-steady state flow field was calculated with a transient flow simulation. The simulated flow field was then used as initial flow condition for a transient flow and transport problem. Initial concentration of zero was assumed throughout the entire model domain. After 15000 days of transient simulation, the mode was changed to a steady flow and transport simulation. Transient simulations were performed with adaptive time stepping with a maximum time step size of 0.075 days and a maximum rate for changing the time step size of 1.05.

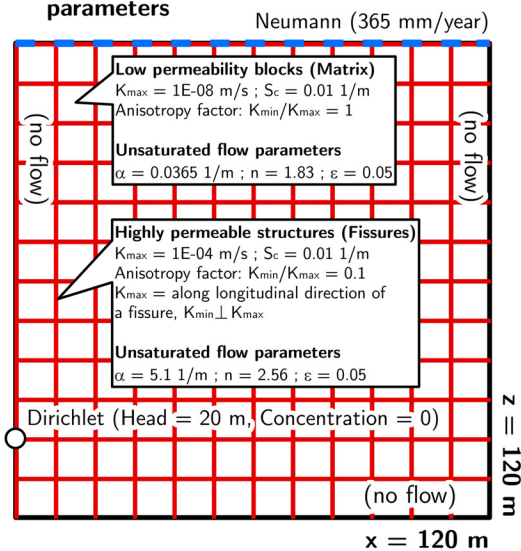
## 5.7 Results of numerical flow and transport simulation

As shown in Figure 5.6, the life expectancy of water is directly reflected in the distribution of flow velocities and position of boundary conditions in the model domain. It is lowest in saturated horizontal fissures, which exhibit the highest flow velocities, and increases with distance to the outlet. Low flow conditions in the saturated porous matrix as well as in fissures, which do not participate in the circulation of water, lead to the establishment of quasi-stagnant zones with very long life expectancies of water. The position of the groundwater table within vertical fissures is lower than in the surrounding porous matrix producing an undulating water table. The thickness of the unsaturated zone amounts to 94 - 100 m and the flow direction is vertical. Horizontal fissures do not play any role which can be attributed to the kind and position of boundary conditions. Life expectancy of water in vertical fissures is smaller than in surrounding matrix blocks. However, the contrast of life expectancy of water in the unsaturated zone is more uniform than in the saturated zone because of the given Van Genuchten Parameters for unsaturated flow. They involve that the contrast of unsaturated hydraulic conductivities between the porous matrix (nearly saturated) and the fissures (moderate saturated) is much smaller than the contrast between the saturated hydraulic conductivities of both zones. The mean transit time of water recharged on the top of the model domain and discharged at the outlet amounts to 15.8 years. The maximum simulated mean transit time from the recharge boundary to the outlet is 40 years, and therefore significantly lower than the life expectancy of water in the saturated porous matrix ( $\approx 1400$  years). This is due to low flux rates through the low permeability porous matrix and to the position of the outlet, which is directly connected to the fissures. In the model, the saturated porous matrix contributes therefore only little to the mean transit time of water determined at the outlet. On the other hand, assuming a pumping well only screened within the saturated porous

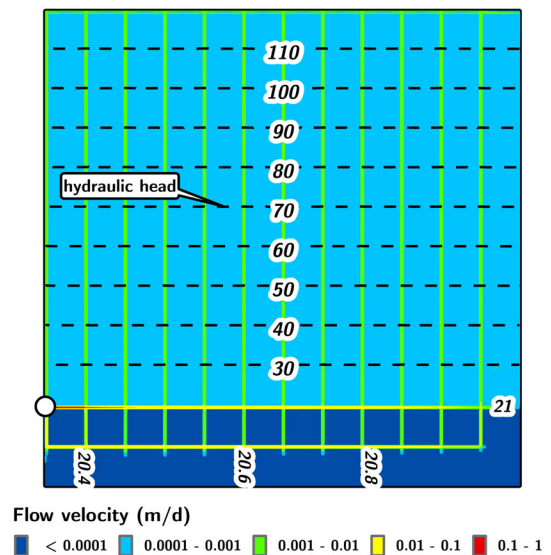


matrix would lead to a completely different result because stagnant water within the porous matrix is mobilised during pumping. Additionally, samples obtained from a pumping well screened within the fissures and the porous matrix would give a mixing water of a young and an old groundwater component as for example found by  $^3\text{H}/^3\text{He}$  dating on the catchment area of the Gallusquelle spring (chapter 5.3).

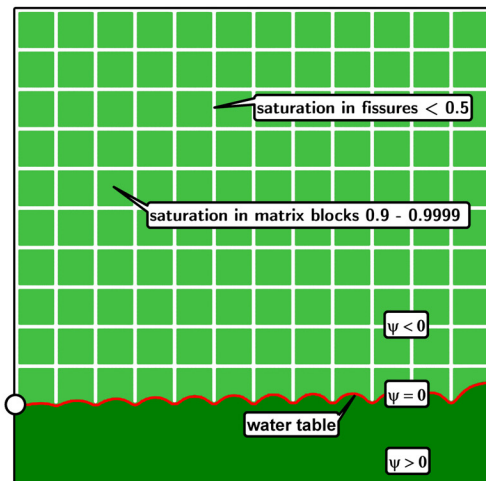
a) Model geometry, model boundaries, parameters



b) Hydraulic heads (m) and flow velocities (m/day)



c) Saturation and water table



d) Life expectancy of water in the model domain (days)

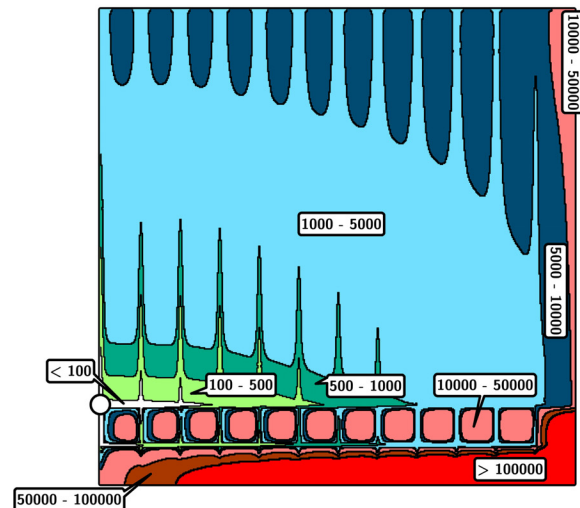


Figure 5.6: Flow and transport simulation (2D vertical model) in a fissured matrix block with diffuse recharge and a drainage point (e.g. conduit system). a) Model geometry, model boundaries, and hydraulic parameters ( $K_{\max}$ ,  $K_{\min}$  = hydraulic conductivity (maximum, minimum),  $S_c$  = confined storage coefficient,  $\varepsilon$  = porosity,  $n$  and  $\alpha$  = Van Genuchten parameters); b) Hydraulic heads and flow velocities; c) Saturation ( $\psi$  = pressure head,  $\psi > 0$  saturated medium,  $\psi < 0$  unsaturated medium); d) Distribution of life expectancy of water in the model domain.

The influence of the recharge rate on the mean transit time of water was calculated by reducing the recharge rate by 50%. For this case the mean transit time of water increases to 30.5 years. In order to calculate travel time of water through a thick unsaturated zone, a second model domain with a vertical extension of only 30 m was set up. All other parameters are identical to the 120 m x 120 m model domain (recharge 365 mm). The thickness of the unsaturated zone for the 30 m x 120 m model varies between 5 and 10 m. The mean transit time is estimated to be 4.5 years (1630 days) which denotes that under the given model conditions, travel time of water through 90 m of unsaturated zone is approximately 10 years.

## 5.8 Discussion and conclusions

As shown in this study, evaluation of environmental tracers in the catchment area of a karst spring may lead to different results depending on (1) the input function of environmental tracers and (2) the sampling location.  $^3\text{H}$  and  $^{85}\text{Kr}$  are the simplest environmental tracers to use for the interpretation of young groundwater ages. Both tracers travel conservatively through a hydrological system and calculated mean tracer ages are not affected by recharge temperatures and excess air. However, in the case of the Gallusquelle karst spring estimated mean ages for both tracers differ by more than 20 years. A number of studies describe the importance of diffusion for transport in fissured systems (Cook et al. 2005, Foster 1975, Maloszewski and Zuber 1985) which may explain differences between mean ages of different tracers. Additionally, different input mechanisms of  $^3\text{H}$  and  $^{85}\text{Kr}$  have to be taken into account.  $^3\text{H}$  is part of the water molecule and enters a karst system via precipitation. Consequently, the mean  $^3\text{H}$  age estimated for a sampling location comprises travelling of  $^3\text{H}$  through the unsaturated zone and the saturated zone. In contrast, the mean  $^{85}\text{Kr}$  age is a measure for the time since the water sample was recharged, i.e. when  $^{85}\text{Kr}$  enters the saturated zone. Therefore, a large difference between both tracer ages may indicate a slow percolation of water through the unsaturated zone. Age dating with  $\text{SF}_6$  leads to a mean tracer age equal to  $^{85}\text{Kr}$  and verifies the result accordingly.

In contrast to  $^{85}\text{Kr}$ ,  $\text{SF}_6$ , and  $^3\text{H}$ , the  $^3\text{H}/^3\text{He}$  method provides an estimate for an apparent water age in the saturated zone independent from a tracers input function.  $^3\text{H}/^3\text{He}$  age of spring water is 2 - 3 years less than the mean  $^{85}\text{Kr}$  age. A number of reasons may explain this small difference, for example, (1) diffusive loss of  $^3\text{He}$  across the groundwater table (Schlosser et al. 1989), (2) the  $^3\text{H}/^3\text{He}$  method reflects the lowest seasonal water table position (Cook and Solomon 1997), and (3) the  $^{85}\text{Kr}$  method overestimates groundwater ages because soil gas concentration above the water table is lower than atmospheric concentrations (Cook and Solomon 1995).

In order to verify a long travel time of water through the unsaturated zone, we simulated flow and transport through a two-dimensional vertical section of a fissured matrix block. In a first approach, hydraulic parameters of the fissures and the porous matrix are distributed in a rectangular pattern and simulation of flow and transport is steady state. Both assumptions do not reflect the real nature, thus further research is necessary in order to simulate field responses of transient tracers, such as  $^3\text{H}$  and  $^{85}\text{Kr}$ , through saturated/unsaturated heterogeneous media. However, the simulation results provide an estimate idea about the spatial distribution of transit times and life expectancy of water in different parts of fissured matrix blocks under steady state conditions. A considerable travel time of water through a thick unsaturated zone is simulated. It may explain large differences in mean ages for tracer with different input functions in karst systems with slow recharge through fissured matrix blocks ("diffuse recharge"). The travel time of water through fissured matrix blocks rises by lowering the total recharge rate. Considering that in karst systems recharge is distributed into a rapid component recharging directly the conduit system (e.g. via vertical shafts) and a slow diffuse component, leads to the conclusion that with an increasing rapid recharge component the travel time of the slow recharge component rises, i.e. the range of travel times through the unsaturated zone increases.

The lowest life expectancy of water flowing through fissured matrix blocks is to be expected in saturated fissures resulting from the high hydraulic conductivity of the saturated fissures. In contrast, lowest flow velocities and therefore nearly stagnant conditions are simulated for the saturated porous matrix. The presence of such zones in the karst system Gallusquelle is evidenced by a large amount of radiogenic  $^4\text{He}$  in water samples from wells located within the catchment area of the spring. Additionally,  $^3\text{H}/^3\text{He}$  age dating revealed that water samples from wells within the catchment area contained a young groundwater component which varied strongly depending on the location of sampling, e.g. the position of the well screen. It was also found that the young groundwater component of the wells was older than the  $^3\text{H}/^3\text{He}$  age estimated for spring water. This is because karst springs are connected to a highly permeable conduit system which may obtain recent water via rapid recharge and drains mobile water from fissured matrix blocks under a natural hydraulic gradient. It may explain that in the case study of the Gallusquelle spring mean ages of gaseous tracer are in the range of the hydraulic age of water in fissures determined from spring recession analysis. In contrast, pumping wells are usually located within fissured matrix blocks and pumping leads to the mobilisation of otherwise more or less stagnant water within the porous matrix which represents the main volume of karst aquifers.

## 5.9 Appendix B

### *Estimation of recharge using a water balance approach*

Recharge rates are estimated using a water balance approach. Similar to the concept of Sauter (1992), it accounts for canopy storage, snow storage, and soil-moisture storage before recharging the underlying limestone (Figure 5.7). Precipitation is distributed into canopy storage (interception) and direct throughfall that reaches the surface without interacting with the canopy. Maximum canopy capacity ( $SC$ ) is estimated as a function of (1) the leaf area index ( $LAI$ ), (2) the percentual vegetation cover ( $CV$ ), and (3) the maximum height of water on leaf area surface ( $HC$ ).  $LAI$  and vegetation cover for different types of vegetations are defined for certain stages of development during a year (according to the land use table of Schulla and Jasper 2007). Potential evaporation from canopy storage  $E_p$  (interception loss) is assessed according to the method of Penman (1948). It requires net radiation which is derived from measured sunshine duration and the maximum possible sunshine duration of a day for the given geographical latitude according to DVWK (1996). Actual evaporation from canopy  $E_c$  occurs at the potential rate only if sufficient water is stored ( $E_c = E_p$ ). Otherwise, evaporation loss amounts to the height of water on canopy ( $E_c = CC$ ). Evaporation from canopy storage reduces the potential evapotranspiration from soil storage ( $ET_p$ ). Drainage from canopy storage begins, when the maximum canopy storage capacity  $SC$  is exceeded. At negative air temperatures ( $T$ ) water arriving at the surface is stored as snow, which allows a temporal redistribution of water entering the soil storage. The release of water from snow storage to soil storage is controlled by a degree day factor ( $DD$ ) that has to be calibrated, e.g. with snow depth under consideration of a snow density (in this study  $100 \text{ kg/m}^3$ ). Evapotranspiration from soil storage and soil moisture balance is calculated according to Sauter (1992). Soil moisture is controlled by the parameters field capacity ( $FC$ ), root constant ( $RC$ ), and wilting point ( $WP$ ) (Lerner et al. 1990). Actual evapotranspiration from soil storage ( $ET_A$ ) proceeds at the potential rate (Haude 1955) if soil moisture is above the root constant. Below the root constant and above the wilting point, the potential evapotranspiration is reduced by the ratio between the present and the maximum soil moisture available to plants. Groundwater recharge occurs if field capacity is exceeded. Based on the observation that well hydrographs show a response to precipitation events even if there is a soil moisture deficit during summer. Rushton and Ward (1979) introduced a rapid recharge ( $TRR$ ) component to simulate bypasses via macro pores and desiccation cracks in the soil. It is activated if threshold of infiltration intensity into the soil storage is exceeded. Daily air temperature, air humidity, wind speed, and sunshine duration for calculation of evapotranspiration were provided from weather stations of the DWD (Germany National Meteorological Service) within or close to the catchment area (maximal distance 30 km).

Sauter (1992) calibrated the model with the observed spring discharge for periods of equal groundwater storage. These periods were derived from well hydrographs in the Gallusquelle catchment and are also used for model calibration in this study. The model results (Figure 5.2) are similar to those presented by Sauter (1992) who simulated recharge for the period 1965 - 1990 and performed also a number of sensitivity analyses varying field capacity, interception capacity, and the rapid recharge component.

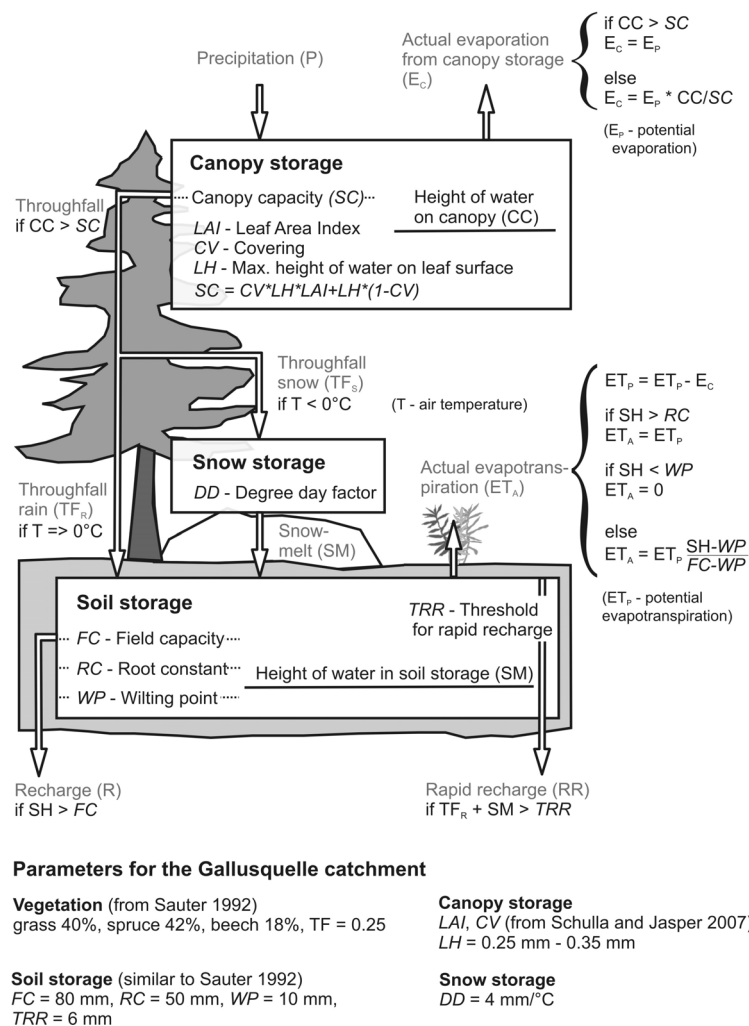


Figure 5.7: Water balance model for calculation of recharge (modified from Sauter 1992).

## Acknowledgements

This work was funded by the Deutsche Forschungsgemeinschaft (DFG; German Research Foundation) under grants SA 501/17 and SA 501/24-1. Grateful acknowledgment is made to the staff of the water supply company Hermentingen / Swabian Alb, in particular Peter Knaus, Thomas Wessner, and Hubert Schaarschmidt. We wish to thank the LGRB (Landesamt für Geologie, Rohstoffe und Bergbau; Baden-Württemberg, Germany) for supplying of data of  $^3\text{H}$

before the year 2000. Hydroisotop/Schweitenkirchen is thanked for sampling and measurement of  $^{85}\text{Kr}$ . We also thank Spurenstofflabor H. Oster for measurement of  $\text{SF}_6$ . Furthermore we would like to acknowledge the provision of time series of krypton-85 in atmosphere and tritium in precipitation by BFS (Federal Office for Radiation Protection, Germany) and GNIP/IAEA (Global Network of Isotopes in Precipitation, International Atom Energy Agency), respectively.

## 5.10 References

- Aquilina, L., Ladouche, B., Dörfliger, N., 2006. Recharge processes in karstic systems investigated through the correlation of chemical and isotopic composition of rain and spring-waters. *Applied Geochemistry* 20, 2189-2206.
- Ashton, K., 1966. The analysis of flow data from karst drainage systems. *Transactions of the Cave Research Group of Great Britain* 7 (2), 161-203.
- Atkinson, T.C., 1977. Diffuse and conduit flow in limestone terrain in the Mendip Hills, Somerset (Great Britain). *Journal of Hydrology* 35, 93-110.
- Bauer, S., Fulda, C., Schäfer, W., 2001. A multi-tracer study in a shallow aquifer using age dating tracers  $^3\text{H}$ ,  $^{85}\text{Kr}$ , CFC-113 and  $\text{SF}_6$  – indication for retarded transport of CFC-113. *Journal of Hydrology* 248, 14-34.
- Benson, B.B., Krause Jr., D., 1980. Isotopic fractionation of helium during solution: A probe for the liquid state. *Journal of Solution Chemistry* 9 (12), 895-909.
- Bertleff, B., 1986. Das Strömungssystem der Grundwässer im Malm-Karst des West-Teils des süddeutschen Molassebeckens. *Abhandlungen des Geologischen Landesamtes Baden-Württemberg Heft 12*, 271 pp.
- Birk, S., Geyer, T., Liedl, R., Sauter, M., 2005. Process-based interpretation of tracer tests in carbonate aquifers. *Ground Water* 43 (3), 381-388.
- Busenberg, E., Plummer, L.N., 2006. Potential use of other atmospheric gases. In: IAEA (Ed.): *Use of chlorofluorocarbons in hydrology – A guidebook*, 183-190.
- Cook, P.G., Love, A.J., Robinson, N.I., Simmons, C.T., 2005. Groundwater ages in fractured rock aquifers. *Journal of Hydrology* 308, 284-301.
- Cook, P.G., Solomon, D.K., 1995. Transport of atmospheric gases to the water table: Implications for groundwater dating with chlorofluorocarbons and krypton 85. *Water Resources Research* 31 (2), 263-270.
- Cook, P.G., Solomon, D.K., 1997. Recent advances in dating young groundwater: chlorofluorocarbons,  $^3\text{H}/^3\text{He}$  and  $^{85}\text{Kr}$ . *Journal of Hydrology* 191, 245-265.
- Cornaton, F., Perrochet, P., 2006. Groundwater age, life expectancy and transit time distributions in advective-dispersive systems: 1. Generalized reservoir theory. *Advances in Water Resources* 29 (9), 1267-1291.
- Diersch, H.-J.G., 2006. An efficient method for computing groundwater residence times. In: *Wasy Software FEFLOW: White Papers Volume 1*, 139-148.
- Dörfliger, N., Jeannin, P.-Y., Zwahlen, F., 1999. Water vulnerability assessment in karst environments: a new method of defining protection areas using a multi-attribute approach and GIS tools (EPIK method). *Environmental Geology* 39 (2), 165-176.
- DVWK, 1996. Ermittlung der Verdunstung von Land- und Wasserflächen. *Merkblätter* 238, 135 pp.
- Einsiedl, F., 2005. Flow system dynamics and water storage of a fissured-porous karst aquifer characterized by artificial and environmental tracers. *Journal of Hydrology* 312, 312-321.
- Ekwurzel, B., Schlosser, P., Smethie Jr. W.M., Plummer, L.N., Busenberg, E., Michel, R.L., Weppernig, R., Stute, M., 1994. Dating of shallow groundwater: Comparison of the transient tracers  $^3\text{H}/^3\text{He}$ , chlorofluorocarbons, and  $^{85}\text{Kr}$ . *Water Resources Research* 30 (6), 1693-1708.
- Eriksson, E., 1958. The possible use of tritium for estimating groundwater storage. *Tellus X*, 472-478.

- Eriksson, E., 1971. Compartment models and reservoir theory. *Annual Review of Ecology and Systematics* 2, 67-84.
- Finsterle, S., Fabryka-Martin, J.T., Wang, J.S.Y., 2002. Migration of a water pulse through fractured porous media. *Journal of Contaminant Hydrology* 54, 37-57.
- Foster, S.S.D., 1975. The chalk groundwater tritium anomaly-a possible explanation. *Journal of Hydrology*, 159-165.
- Geyer, T., Birk, S., Licha, T., Liedl, R., Sauter, M., 2007. Multi-tracer test approach to characterize reactive transport in karst aquifers. *Ground Water* 45 (1), 36-45.
- Geyer, T., Birk, S., Liedl, R., Sauter, M., 2008. Quantification of temporal distribution of recharge in karst systems from spring hydrographs. *Journal of Hydrology* 348, 452-463.
- Goldscheider, N., Meiman, J., Pronk, M., Smart, C., 2008. Tracer tests in karst hydrogeology and speleology. *International Journal of Speleology* 37 (1), 27-40.
- Goode, D.J., 1996. Direct simulation of groundwater age. *Water Resources Research* 32 (2), 289-296.
- Haude, W., 1955. Bestimmung der Verdunstung auf möglichst einfache Weise. *Mitteilungen des Deutschen Wetterdienstes* 11.
- Ingraham, N.L., 1998. Isotopic variations in precipitation. In: Kendall, C., McDonnell, J.J. (Eds.): *Isotope tracers in catchment hydrology*. Elsevier Science B.V., Amsterdam, Netherlands, 87-118.
- Jeannin, P.-Y., 2001. Modeling flow in phreatic and epiphreatic karst conduits in the Hölloch cave (Muotatal, Switzerland). *Water Resources Research* 37 (2), 191-200.
- Kazemi, G.A., Lehr, J.H., Perrochet, P., 2006. *Groundwater age*. John Wiley and Sons, New Jersey, USA, 325 pp.
- Lerner, D.N., Issar, A.S., Simmers, I., 1990. *Groundwater recharge: a guide to understanding and estimating natural recharge*. International contributions to hydrogeology 8, 345 pp.
- Loosli, H.H., Heimann, M., Oeschger, H., 1980. Low-level gas proportional counting in an underground laboratory. *Radiocarbon* 22 (2), 461-469.
- Lucas, L.L., Unterweger, M.P., 2000. Comprehensive review and critical evaluation of the half-life of  $^3\text{H}$ . *Journal of Research of the National Institute of Standards and Technology* 105 (4), 511-533.
- Maiss, M., Steele, L.P., Francey, R.J., Fraser, P.J., Langenfelds, R.L., Trivett, N.B.A., Levin, I., 1996. Sulfur hexafluoride - A powerful new atmospheric tracer: *Atmospheric Environment* 30 (10-11), 1621-1629.
- Maloszewski, P., Stichler, W., Zuber, A., Rank, D., 2002. Identifying the flow systems in a karstic-fissured-porous aquifer, the Schneelpe, Austria, by modelling of environmental  $^{18}\text{O}$  and  $^3\text{H}$  isotopes. *Journal of Hydrology* 256, 48-59.
- Maloszewski, P., Zuber, A., 1982. Determining the turnover time of groundwater systems with the aid of environmental tracers: 1. Models and their applicability. *Journal of Hydrology* 57, 207-231.
- Maloszewski, P., Zuber, A., 1985. On the theory of tracer experiments in fissured rocks with a porous matrix. *Journal of Hydrology* 79, 333-358.
- Maloszewski, P., Zuber, A., 2002. Manual on lumped-parameter models used for the interpretation of environmental tracer data in groundwaters. In: Yurtsever, Y. (ed.): *Use of isotopes for analyses of flow and transport dynamics in groundwater systems*. IAEA-UIAGS/CD 02-00131, IAEA Vienna. 2002, 1-50.
- Massmann, G., Sültenfuß, J., Dünnbier, U., Knappe, A., Taute, T., Pekdeker, A., 2008. Investigation of groundwater residence time during bank filtration in Berlin: a multi-tracer approach. *Hydrological Processes* 22 (6), 788-801.
- Münzing, K., 1988. Markierungsversuch 746. Gutachten 4763-1/88 BL1. Geologisches Landesamt Baden-Württemberg.
- Nir, A., 1964. On the interpretation of tritium age measurements of groundwater. *Journal of Geophysical Research* 69 (12), 2589-2595.
- Oster, H., Sonntag, C., Münnich, K.O., 1996. Groundwater age dating with chlorofluorocarbons. *Water Resources Research* 32 (10), 2989-3001.

- Penman, H.L., 1948. Natural evaporation from open water, bare soil and grass. *Proceedings of the Royal Society of London. A* 193, 120-145.
- Roulier, S., Baran, N., Mouvet, C., Stenemo, F., Morvan, X., Albrechtsen, H.-J., Clausen, L., Jarvis, N., 2006. Controls on atrazine leaching through a soil-unsaturated fractured limestone a Brévilles, France. *Journal of Contaminant Hydrology* 84, 81-105.
- Rózański, K., Florkowski, T., 1979. Krypton-85 dating of groundwater. IAEA-SM-228/51, 949-961.
- Rushton, K.R., Ward, C., 1979. The estimation of groundwater recharge. *Journal of Hydrology* 41, 345-361.
- Sauter, M., 1992. Quantification and forecasting of regional groundwater flow and transport in a karst aquifer (Gallusquelle, Malm, SW. Germany). *Tübinger Geowissenschaftliche Arbeiten C13*, 150 pp.
- Sauter, M., 1997. Differentiation of fast and slow flow components in a karst aquifer using the  $\delta^{18}\text{O}$  signature - Data analysis and modeling. In: Kranjc, A. (Ed.): *Tracer Hydrology 97*, Balkema, 435-441.
- Schlosser, P., Stute, M., Sonntag, C., Münnich, K.O., 1989. Tritogenic  $^3\text{He}$  in shallow groundwater. *Earth and Planetary Science Letter* 94, 245-256.
- Schulla, J., Jasper, K., 2007. Modell description WASIM (Water Balance Simulation Model) – ETH, 181 pp.
- Selg, M., Heinz, J., Mair, C., Bauer, M., 2005. Die Altersstruktur des Kluft-und Karstgrundwassers im Oberjura der Schwäbischen Alb und deren Bedeutung für den anhaltenden Atrazinaustrag. *Berichte Naturforschende Gesellschaft zu Freiburg i. Br.* 95/1, 1-45.
- Solomon, D.K., Cook, P.G., Sanford, W.E., 1998. Dissolved gases in subsurface hydrology. In: Kendall, C., McDonnell, J.J. (Eds.): *Isotope tracers in catchment hydrology*, Elsevier Science B.V., Amsterdam, Netherlands, 291-318.
- Sültenfuß, J., Rhein, M., Roether, W., 2008. The Bremen Mass Spectrometric Facility for the measurement of helium isotopes, neon, and tritium in water. *International Symposium on Quality Assurance for Analytical Methods in Isotope Hydrology*, IAEA Proceedings, IAEA-CN 119-7, Vienna, in press.
- Torgersen, T., Clarke, W.B., Jenkins, W.J., 1979. The tritium/helium-3 method in hydrology. *Isotope Hydrology 1978*, IAEA-SM-228/49, Vienna, 917-930.
- Van Genuchten, M., 1980. A closed-form equation for predicting the hydraulic conductivity of unsaturated soils. *Soil Science Society of America Journal* 44 (5), 892-898.
- Villinger, E., 1977. Über Potentialverteilung und Strömungssysteme im Karstwasser der Schwäbischen Alb (Ob. Jura, SW-Deutschland). *Geologisches Jahrbuch C18*, 92 pp.
- Weise, S., Moser, H., 1987. Groundwater dating with helium isotopes. In: *Isotope techniques in water resources development*, IAEA-SM-299/44, Vienna, 105-126.
- Weiss, R.F., 1971. Solubility of helium and neon in water and seawater. *Journal of Chemical and Engineering Data* 16 (2), 235-241.
- Weiss, W., Sartorius, H., Stockenburger, H., 1992. Global distribution of atmospheric  $^{85}\text{Kr}$ , a database for the verification of transport and mixing models. In: *Isotopes of noble gases as tracers in environmental studies*, IAEA, Vienna, 29-62.
- Weiß, E.G., 1987. Porositäten, Permeabilitäten und Verkarstungserscheinungen im Mittleren und Oberen Malm der südlichen Frankenalb. *Dissertation, University of Erlangen-Nürnberg*, 211 pp.
- Zoellmann, A., Kinzelbach, W., Fulda, C., 2001. Environmental tracer transport ( $^3\text{H}$  and  $\text{SF}_6$ ) in the saturated and unsaturated zones and its use in nitrate pollution management. *Journal of Hydrology* 240, 187-205.
- Zuber, A., 1986. On the interpretation of tracer data in variable flow systems. *Journal of Hydrology* 86 (1-2), 45-57.



# Chapter 6

## General conclusions and perspectives

Karst aquifers are highly heterogeneous groundwater systems with a strong anisotropic character. Regulation and sustainable management of karst water resources therefore requires the development of specific methods in order to characterise these systems adequately and to give predictions, e.g. about possible effects of industrial waste disposals and of intensive exploitation. Here an important role is played by mathematical models, which allow to simulate flow and transport phenomena of a hydrogeological system depending on the degree of abstraction of the real system. The major difficulty with simulation of karst aquifers lies in finding data required for the modelling of such a complex flow system (Sauter et al. 2006). This work fills the gap between model requirements for simulation of karst hydraulics and field data provision to a certain extent. It deals with the identification of flow and transport processes in karst aquifers, which is of importance, for example, to develop characterisation techniques (e.g. Birk et al. 2005) and vulnerability concepts (e.g. Brosig et al. 2007).

Evaluation of spring responses ("global methods") is an appropriate method to obtain integral hydraulic and geometric parameters of karst aquifers on catchment scale (e.g. Kovács et al. 2005). However, spring responses are influenced by the recharge mechanism that has to be known for the evaluation of these signals. Recharge in karst systems may be highly heterogeneous in time and space. Direct recharge into the conduit system can be very rapid and concentrated. It leads to the rise of discharge of karst springs within a few hours after a storm event although the unsaturated zone of karst systems may comprise more than one hundred meters. In the author's opinion, the physical process of rapid percolation of water through the unsaturated zone of a karst system is still not well understood, making it difficult to simulate this process with physical-based models. Yet, typical karst spring hydrographs cannot be simulated without applying rapid recharge.

### ***Quantification of recharge from spring hydrographs***

Based on this lack, a time-continuous approach for the determination of the temporal distribution of recharge from spring hydrographs is presented, which does not require any information about the characteristics of the unsaturated zone (chapter 3, Geyer et al. 2008). The approach is solely based on time derivative(s) of spring hydrographs and recession coefficient(s) of an aquifer. It

employs aquifers as reservoirs, which maintain water from recharge and generate discharge related to their physical characteristics. The first time derivative of the discharge curve of a reservoir reflects the temporal distribution of inflow to and outflow from the reservoir. The velocity with which a recharge signal is transmitted through the reservoir is controlled by its recession coefficient. At this, the recession coefficient is a physically based parameter describing the diffusivity (ratio of transmissivity and storage) and the geometrical properties of the reservoir. The behaviour of karst springs can, in principle, be simulated using a serial two-reservoir model, which considers the fissured matrix blocks as a low permeability reservoir, and the conduit system as a highly permeable reservoir. Based on this concept, a numerical solution is provided that can easily be applied to calculate the inflow into the conduit system of a karst aquifer. Parameter studies with the two-reservoir model reveal that the early hydrograph response of karst springs is clearly dominated by direct recharge into the conduit system even if the fraction of this component is only a few percent of total recharge. This behaviour can be attributed to the large contrast between recession coefficients of conduit system and fissured matrix blocks. It allows the separation of direct recharge into the conduit system from a spring hydrograph. The only parameter required for the separation procedure is the recession coefficient of the highly conductive conduit system of a karst aquifer. The methodology has been applied to quantify recharge into the conduit system of the Gallusquelle catchment (Swabian Alb, Germany) after a storm event. The separation of the direct recharge component is in agreement with information from an independent isotope study. The recession coefficient of the conduit system of the Gallusquelle aquifer was estimated by long-term spring hydrograph recession analysis. It corresponds to the recession coefficient (reciprocal of mean tracer travel time) obtained from an artificial tracer experiment covering the extent of the catchment area, i.e. there is a direct link between tracer transport in karst conduits and spring recession analysis.

The applicability of the presented numerical approach depends to a large degree on the available time step size for the discharge curve, which should be small, and the recession coefficient  $\alpha_c$  of the conduit system of a karst aquifer that is typically large. For example, the discharge  $Q$  of a reservoir  $V$  is the product of  $V$  and  $\alpha_c$ . Consequently, if the time step size is larger than  $1/\alpha_c$ , the reservoir would lose more water than it yields, what is not possible. Furthermore, it should be noted that spring hydrographs might be affected by additional processes that are not considered in the applied two-reservoir model, for example, reversal of gradients between the fissured matrix and the conduit system or groundwater abstraction by pumping wells. Thus, a careful inspection of measured spring hydrographs is required to identify any other disturbing factors that potentially impair the outcome of the analysis. In order to study these processes it is suggested to apply hybrid models that account for storage in the conduit system.

*The presented approach was used to calculate direct recharge into the conduit system of a karst aquifer. Furthermore parameter studies with the serial two-reservoir model showed that the second time derivative of a spring hydrograph involves information about the temporal distribution of slow recharge into fissured matrix blocks. However, this information may be difficult to obtain from real spring hydrographs when direct recharge superimposes spring hydrograph responses. Provided that boreholes are within fissured matrix blocks, a more appropriate method to calculate diffuse recharge in karst aquifers would be to analyse water level fluctuations in boreholes as suggested, for example, by Healy and Cook (2002).*

### ***Potential use of artificial tracer tests for characterisation of karst conduit systems***

Another major difficulty in karst modelling is the representation of the geometry of a karst conduit system. As shown by some authors and in this work, too, artificial tracer tests provide useful information about the total volume of a conduit system (e.g. Birk et al. 2005). However, limited information is gained about its geometry, for example, does the total conduit volume result from a strongly localised single conduit or from an extended conduit network? A reasonable approach to obtain an integral parameter about the conduit geometry is to estimate surface/volume ratios of karst conduits. Liedl et al. (1998) demonstrated that variations of water temperature after recharge events on a karst spring may be used to characterise the geometry of a conduit system, because the temperature can be thought of as a reactive tracer that interacts with the conduit surface. The basic idea was transferred to artificial tests, i.e. artificial tracers that interact with the conduit surface were applied. *It can be anticipated that the calculation of the conduit surface/volume ratios from artificial tracer tests would require extensive laboratory work in order to quantify the reactive process(es) between artificial tracers and aquifer material in detail. First of all, it requires the characterisation of the conduit surface that interacts with an artificial tracer, e.g. is the conduit surface coated and if so by which material (e.g. iron oxides, clay minerals)?* This information was only sparsely available for this work. Nevertheless, this work contributes to the issue of tracer/surface interactions in karst conduits to a crucial extent (chapter 4, Geyer et al. 2007). It deals with the question how far reactive transport of applicable artificial tracers in karst conduits can be identified at all. Therefore, a large-scale multitracer test with three different reactive tracers was performed between a sinkhole and a karst spring (Gallusquelle/Swabian Alb). The tracers (uranine, sulforhodamine G and tinopal CBS-X) separated along the flow path according to their acid strengths, which can clearly be attributed to the interaction of the tracers with the conduit surface (chapter 4). Significant retention of the sulforhodamine G and tinopal CBS-X is demonstrated as the recoveries of these tracers is much lower than that of uranine which is regarded as a nearly conservative tracer in this study. The two-region nonequilibrium transport model CXTFIT2.1 (Toride et al. 1999) was used for

calibration of conservative and reactive transport parameters from the tracer experiment. A calibration strategy was introduced which reduces the ambiguity of model calibration of the reactive tracers crucially. At this, the reactive transport parameters were allowed to fall only into specific ranges. The model succeeds in representing the measured tracer breakthrough curves (TBCs) of uranine and sulforhodamine G. It could be shown that tracer rock interactions preferably occur in immobile fluid regions of a karst conduit even though the fraction of these regions (from the total water filled conduit volume) is very small. However, the model failed to account for the observed TBC of tinopal CBS-X. A possible reason for this might be precipitation and dissolution processes of tinopal CBS-X during transport that are, however, not included in the presented model approach. The simulation of these processes would require the definition of additional calibration parameters and is therefore likely to increase the ambiguity of the results. The application of tinopal CBS-X as a process tracer to study tracer/surface interactions can therefore not be recommended.

### ***Flow and transport in a karst aquifer***

In general, flow in karst aquifers can be separated into fast and concentrated flow through solution enlarged karst conduits and slow and diffuse flow through fissures matrix blocks. At this, the intergranular matrix can be considered to be a quasi-stagnant water reservoir. As shown in chapters 4 and 5 of this work, the flow behaviour is also apparent in the transport of solutes. It is demonstrated that artificial tracer tests are a useful technique to determine conservative as well as reactive parameters for solute transport in karst conduits (chapter 4) whereas evaluation of environmental tracers provide a method to obtain information about water flow and mass transport through the whole catchment area (chapter 5).

For example, a tracer transit time of 48 h was calculated from an artificial tracer test performed in the catchment area of the Gallusquelle spring (Swabian Alb). The tracer was injected into a sinkhole 3000 m upstream of the observation point (spring). In contrast, interpretation of environmental tracers in water samples from the Gallusquelle spring suggested mean tracer ages of several years resulting from slow transport through the fissured matrix of the karst aquifer. The modelled mean ages of various environmental tracer obtained from spring water differed in the following order:  $^3\text{H} \gg ^{85}\text{Kr} = \text{SF}_6 > ^3\text{H}/^3\text{He}$ . It is to note that mean ages of the gaseous tracers  $^{85}\text{Kr}$  and  $\text{SF}_6$  are a measure for the time since the tracers enter the saturated zone from the atmosphere, and the  $^3\text{H}/^3\text{He}$  method provides an estimate of the groundwater age based on the accumulation of  $^3\text{He}$  when  $^3\text{H}$  decays below the water table. In contrast to these methods, age dating with  $^3\text{H}$  comprises travelling of  $^3\text{H}$  through the saturated and the unsaturated zone of a karst system because  $^3\text{H}$  is part of the water molecule and enters a karst system via precipitation.

A large difference between  $^3\text{H}$  and the other measured tracers (which show similar groundwater ages) may therefore indicate a slow percolation of water through the unsaturated zone of a karst system. The interpretation is supported by distributive parameter modelling (two-dimensional, FEFLOW5.3, Diersch 2006) of flow and transport in a fissured matrix block that contains a thick unsaturated zone (chapter 5). The simulation provides an insight into the time required for a water molecule to reach the outlet ("life expectancy") at any position in the model domain. It is shown that the unsaturated zone may provide an important water storage in karst aquifers. By far the greatest life expectancies were simulated in the saturated porous matrix which refers to the low hydraulic conductivity in combination with the small hydraulic gradient in these parts of the simulated fissured matrix block. Presence of such zones in the karst system Gallusquelle is evidenced by a large amount of radiogenic  $^4\text{He}$  at sampled wells within the catchment area. These components could not explicitly be identified at the Gallusquelle spring. This may be explained by the fact that a karst spring is fed by mobile water under a natural hydraulic gradient, whereas pumping leads to the mobilisation of stagnant water from the porous matrix.

*The tracer studies at the catchment of the Gallusquelle spring clarify the importance of triple porosity (conduit - fissures - matrix) concepts for transport in karst aquifers. Large contrasts between mean tracer ages obtained at the Gallusquelle spring were attributed to the different mechanisms by which the tracers enter the karst system. However, it should also be noted that transport processes, for example, diffusion between mobile water in the fissures and stagnant water in the porous matrix, may explain differences between mean transit times obtained at a sampling site for various environmental tracers. Mixing of old groundwater with direct recharge may occur in the conduit system that drains fissured matrix blocks over large distances. Further research is therefore required in order to determine the underlying processes that environmental tracers are dominated by when travelling through karst systems. To accomplish this goal parameter studies with mathematical models cooperating with the triple porosity-concept seem to be an appropriate method. Additionally, the application of multitracer studies on various field sites would be necessary in order to transfer conclusions made from a single test site, such as the Gallusquelle spring.*

### **Further perspectives**

The characterisation of karst aquifers with a single method is fraught with a number of problems which arise from the facts: (1) all techniques are limited to a certain scale, (2) most techniques concern only a part of the karst aquifer (tracer tests - conduit system, small-scale pumping tests - fissured matrix blocks), and (3) global methods are not controlled experiments. In order to allow a proper characterisation of karst aquifers the combination of various methods is therefore required.

Distributive models coupling different flow systems may be one promising approach to combine information gained from various field techniques. However, this approach requires the realistic integration of the conduit system into the model, which represents still a challenge in karst hydrogeology. Forward modelling of flow/transport of synthetic karst aquifers with various conduit geometries, and the later comparison of the results with real data may be capable to indicate the pattern of a conduit system of a real karst aquifer ("pattern matching") (Figure 2.4). At this, the development of synthetic karst systems should be supported by the simulation of karst genesis with appropriate modelling approaches (Dreybrodt et al. 2005), for example, to determine the distribution of diameters of conduit systems.

In addition to the existing field methods, the conduction of large-scale, long-term pumping tests might allow a unique scale-continuous characterisation of the hydraulic characteristics of karst aquifers by a single controlled field experiment. Due to the fact that the pumping well is connected with the draining conduit system, the evaluation of a large scale pumping test would lead to results covering the hydraulic characteristics of the conduit system as well as of the matrix system. A large scale-pumping test would be therefore suitable for investigating the exchange process between matrix- and conduit system on regional scale. Additionally, in practice used methods for characterisation of karst aquifers could be validated for their correctness (Figure 6.1).

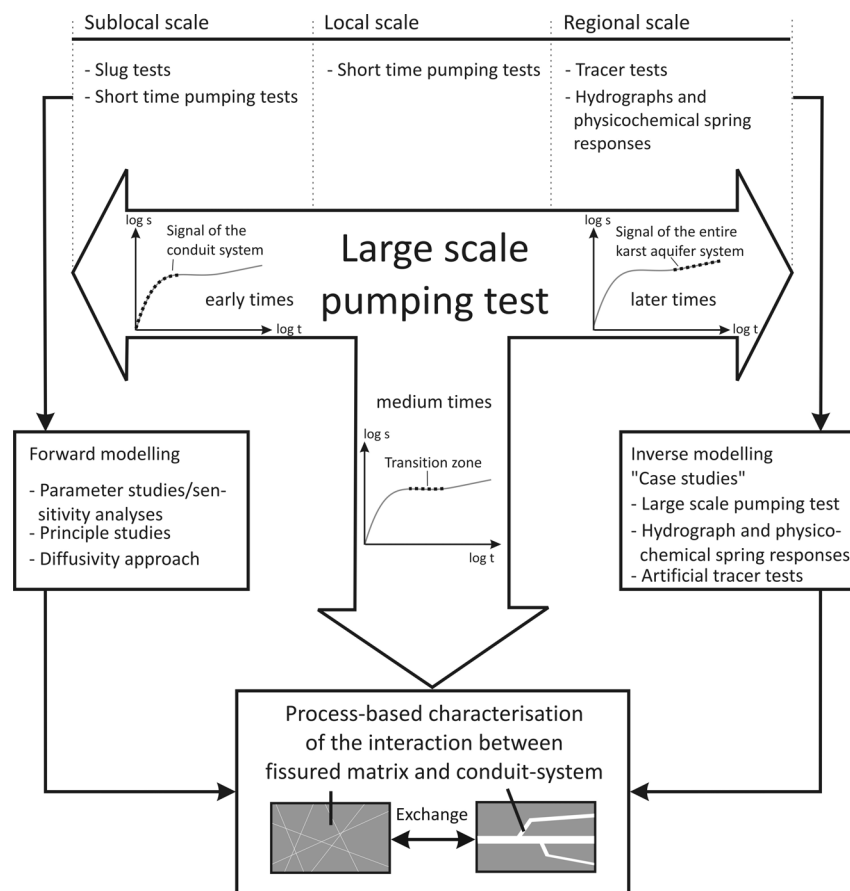


Figure 6.1: Concept for characterisation of karst aquifers by large-scale pumping tests.

## 6.1 References

- Birk, S., Geyer, T., Liedl, R., Sauter, M., 2005. Process-based interpretation of tracer tests in carbonate aquifers. *Ground Water* 43 (3), 381-388.
- Brosig, K., Geyer, T., Subah, A., Sauter, M., 2007. Travel time based approach for the assessment of vulnerability of karst groundwater: the transit time method. *Environmental Geology* 54 (5), 905-911.
- Diersch, H.-J.G., 2006. FEFLOW5.3 - Finite element subsurface flow and transport simulation - User's manual. WASY GmbH, 200 pp.
- Dreybrodt, W., Gabrovsek, F., Romanov, D., 2005. Processes of speleogenesis: a modeling approach. *Carsologica* 4, ZRC Publishing, Ljubljana, 376 pp.
- Geyer, T., Birk, S., Licha, T., Liedl, R., Sauter, M., 2007. Multi-tracer test approach to characterize reactive transport in karst aquifers. *Ground Water* 45 (1), 36-45.
- Geyer, T., Birk, S., Liedl, R., Sauter, M., 2008. Quantification of temporal distribution of recharge in karst systems from spring hydrographs. *Journal of Hydrology* 348, 452-463.
- Healy, R.W., Cook, P.G., 2002. Using groundwater levels to estimate recharge. *Hydrogeology Journal* 10, 91-109.
- Kovács, A., Perrochet, P., Kiraly, L., Jeannin, P.-Y., 2005. A quantitative method for the characterisation of karst aquifers based on spring hydrograph analysis. *Journal of Hydrology* 303, 152-164.
- Liedl, R., Renner, S., Sauter, M., 1998. Obtaining information on fracture geometry from heat flow data in karst systems. *Bulletin d'Hydrogéologie (Neuchâtel)* 16, 143-153.
- Sauter, M., Kovács, A., Geyer, T., Teutsch, G., 2006. Modellierung der Hydraulik von Karstgrundwasserleitern - Eine Übersicht. *Grundwasser* 3/2006, 143-156.
- Toride, N., Leij, F.J., van Genuchten, M.T., 1999. The CXTFIT code (version 2.1) for estimating transport parameters from laboratory or field tracer experiments. U.S. Salinity Laboratory Agricultural Research Service, U.S. Department of Agriculture Riverside, California. Research Report, 137, 119 pp.

# Appendix C

List of all publications authored or co-authored by me and related to the present work.

## Books/Journals (Peer-reviewed)

**Geyer, T.**, Birk, S., Liedl, R., Sauter, M., 2008. Quantification of temporal distribution of recharge in karst systems from spring hydrographs. *Journal of Hydrology* 348, 452-463.

Heinz, B., Birk, S., Liedl, R., **Geyer, T.**, Straub, K.L., Bester, K., Kappler, A., 2007. Vulnerability of a karst spring to waste water infiltration (Gallusquelle, Southwest Germany). *Austrian Journal of Earth Sciences* 99, 11-17

**Geyer, T.**, Birk, S., Licha, T., Liedl, R., Sauter, M., 2007. Multi-tracer test approach to characterize reactive transport in karst aquifers. *Ground Water* 45 (1), 36-45.

Brosig, K., **Geyer, T.**, Subah, A., Sauter, M., 2007. Travel time based approach for the assessment of vulnerability of karst groundwater: the transit time method. *Environmental Geology* 54 (5), 905-911.

Massmann, C., Birk, S., Liedl, R., **Geyer, T.**, 2006. Identification of hydrogeological models: application to tracer test analysis in a karst aquifer. In: Bierkens, M.F.P., Gehrels, J.C., Kovar, K. (Eds.), *Calibration and reliability in groundwater modelling: From uncertainty to decision making*. IAHS Publication 304, 59-64.

Sauter, M., Kovács, A., **Geyer, T.**, Teutsch, G., 2006. Modellierung der Hydrodynamik von Karstgrundwasserleitern - Eine Übersicht. *Grundwasser* 11 (3), 143-156.

Birk, S., **Geyer, T.**, Liedl, R., Sauter, M., 2005. Process-based interpretation of tracer tests in carbonate aquifers. *Ground Water* 43 (3), 381-388.

## In preparation

**Geyer, T.**, Graf, T., Sültenfuß, J., Sauter, M., 2008. Analysing transport of the environmental tracers  $^3\text{H}$ ,  $^{85}\text{Kr}$ ,  $\text{SF}_6$ , and He in a karst system with a thick unsaturated zone.

## Extended abstracts

Heinz, B., Birk, S., Liedl, R., **Geyer, T.**, Straub, K.L., Bester, K., Kappler, A., 2006. Vulnerability of a Karst spring to waste water infiltration. *All about karst and water - Decision making in a sensitive environment*, International Conference Vienna October 2006, 283-289.

**Geyer, T.**, Licha, T., Sauter, M., Birk, S., Liedl, R., 2005. Process-based multi-tracer test modelling in a karstic system. *Proc. 5th International Conference on Calibration and Reliability in Groundwater Modelling*, The Hague (Scheveningen), The Netherlands, 6 – 9 June 2005, 189-193.

Massmann, C., Birk, S., Liedl, R., **Geyer, T.**, 2005. Identification of hydrogeologic models: application to tracer test analysis in a karst aquifer. *Proc. 5th International Conference on Calibration and Reliability in Groundwater Modelling*, The Hague (Scheveningen), The Netherlands, 6 – 9 June 2005, 9-14.



## Abstracts

Cook, A., **Geyer, T.**, Shook, G., Butler, J.J., Whitemore, D., Kluitenberg, G., 2006. Focused recharge in a semi-arid riparian zone. *Eos Trans. AGU*, 87(52), Fall Meet. Suppl., Abstract H11A-1222.

Sauter, M., **Geyer, T.**, Kovács, K., Teutsch, G., 2006. Modelling karst groundwater hydraulics at catchment basis – An overview –. *Eos Trans. AGU*, 87(52), Fall Meet. Suppl., Abstract H42C-01.

**Geyer, T.**, Birk, S., Sültenfuß, J., Sauter, M., 2006. Untersuchungen zur Altersstruktur des Grundwassers eines verkarsteten Aquifers auf der Grundlage von  $^3\text{H}/\text{He}$ -Messungen. In: Voigt, H.-J., Kaufmann-Knoke, R., Jahnke, Ch., Herd, R. (Eds.), *Indikatoren im Grundwasser, Kurzfassungen der Vorträge und Poster, Tagung der FHDGG*, 24. bis 28. Mai 2006. Schriftenreihe der Deutschen Geologischen Gesellschaft, Heft 33, ISBN 3-932537-39-4, 137.

Birk, S., **Geyer, T.**, Liedl, R., Sauter, M., 2006. Methodischer Ansatz zur Charakterisierung von Karstgrundwasserleitern. In: Voigt, H.-J., Kaufmann-Knoke, R., Jahnke, Ch., Herd, R. (Eds.), *Indikatoren im Grundwasser, Kurzfassungen der Vorträge und Poster, Tagung der FHDGG*, Cottbus, 24. bis 28. Mai 2006. Schriftenreihe der Deutschen Geologischen Gesellschaft, Heft 33, ISBN 3-932537-39-4, 51.

**Geyer, T.**, Birk, S., Heinz, B., Liedl, R., Sauter, M., 2006. Process-based characterisation of flow and recharge properties in karst aquifers by combined analysis of hydraulic and physico-chemical spring responses. *Geophysical Research Abstracts*, Vol. 8, 07285, 2006.

Heinz, B., Birk, S., Kappler, A., Liedl, R., **Geyer, T.**, Straub, K.L., Bester, K., 2006. Consequences of waste water seepage for the water quality of a karst spring. *Geophysical Research Abstracts*, Vol. 8, 05992, 2006.

Birk, S., **Geyer, T.**, Liedl, R., Sauter, M., 2005. Towards an integrated approach to the characterization of karst aquifers. *Geological Society of America Abstracts with Programs* 37 (7), 33.

**Geyer, T.**, Birk, S., Licha, T., Liedl, R., Sauter, M., 2005. Reactive multi-tracer test in a karst system. *Geophysical Research Abstracts*, Vol. 7, 08189, 2005.

Birk, S., **Geyer, T.**, Liedl, R., Sauter, M., 2004. Coupled discrete-continuum representation of dual karst flow systems. *Geological Society of America Abstracts with Programs* 36 (5), 106.

**Geyer, T.**, Birk, S., Licha, T., Liedl, R., Sauter, M., 2004. Prozessbasierte Charakterisierung von Karströhrensystemen anhand von Multitracer-tests. In: Schiedek, T., Kaufmann-Knoke, R., Eberhardt, G. (Eds.), *Hydrogeologie regionaler Aquifersysteme, Kurzfassungen der Vorträge und Poster, Tagung der Fachsektion Hydrogeologie in der DGG*, Darmstadt, 19. bis 23. Mai 2004. Schriftenreihe der Deutschen Geologischen Gesellschaft, Heft 32, ISBN 3-932537-04-1, 37.

## Reports

Birk, S., **Geyer, T.**, Liedl, R., Sauter, M., 2006. Prozessbasierte Charakterisierung der dualen Abfluss- und Transporteigenschaften von Karstgrundwasserleitern. Abschlussbericht, DFG-Projekte LI 727/10 und SA 501/17, 45 pp.

Birk, S., **Geyer, T.**, Liedl, R., Sauter, M., 2004. Prozessbasierte Charakterisierung der dualen Abfluss- und Transporteigenschaften von Karstgrundwasserleitern. Zwischenbericht, DFG-Projekte LI 727/10 und SA 501/17, 34 pp.

# Tobias Geyer

---

## PERSÖNLICHE DATEN

geboren am 27. Februar 1978  
in Zeulenroda/Thüringen  
Familienstand ledig  
Staatsangehörigkeit deutsch

---

## AUSBILDUNG

seit 2003 **Georg-August-Universität Göttingen**  
*Promotionsstudium am Geowissenschaftlichen Zentrum Göttingen, Abteilung Angewandte Geologie*

10/1996 - 08/2002 **Friedrich-Schiller-Universität Jena**  
*Diplomstudium an der Chemisch- Geowissenschaftlichen Fakultät, Institut für Geowissenschaften, abgeschlossen mit der Note: 1,2*  
Prüfungsfächer: Angewandte Geologie, Allgemeine Geologie, Geoinformatik, Geochemie  
Thema der Diplomarbeit: Prozessmodellierung des natürlichen Wetlands am ehemaligen Flussspatbergwerk Straßberg/Harz

---

## ERFAHRUNG

seit 2003 **Georg-August-Universität Göttingen**  
*Wissenschaftlicher Mitarbeiter am Geowissenschaftlichen Zentrum Göttingen, Abteilung Angewandte Geologie (Abteilungsleiter: Prof. Dr. M. Sauter)*  
Einzugsgebietshydrogeologie von Festgesteinsgrundwasserleitern.

05/2006 - 08/2006 **Kansas Geological Survey, The University of Kansas, USA**  
*Forschungsassistent in der Abteilung Geohydrologie ("Geohydrology") unter Betreuung von Dr. Jim Butler*  
Untersuchungen zur hydraulischen Interaktion: Flussbett - alluvialer Grundwasserleiter.

08/2002 - 12/2002 **Friedrich-Schiller-Universität Jena**  
*Wissenschaftlicher Mitarbeiter am Institut für Geowissenschaften, Abteilung Hydrogeologie (Abteilungsleiter Prof. Dr. M. Sauter)*  
Ausstattung zweier grossskaliger Einzugsgebiete mit hydrogeologischer Messtechnik.